
FLOW DYNAMICS
OF
BLUFF BODIES

ANIRUDH N. RAO

A THESIS SUBMITTED TO MONASH UNIVERSITY IN FULFILMENT
OF THE REQUIREMENTS FOR THE DEGREE OF

DOCTOR OF PHILOSOPHY

DEPARTMENT OF MECHANICAL & AEROSPACE ENGINEERING

MONASH UNIVERSITY

OCTOBER 2012

**Monash University
Monash Research Graduate School**

Declaration for thesis based or partially based on conjointly published or unpublished work

General Declaration

In accordance with Monash University Doctorate Regulation 17/ Doctor of Philosophy and Master of Philosophy (MPhil) regulations the following declarations are made:

I hereby declare that this thesis contains no material which has been accepted for the award of any other degree or diploma at any university or equivalent institution and that, to the best of my knowledge and belief, this thesis contains no material previously published or written by another person, except where due reference is made in the text of the thesis.

This thesis includes **two** original papers published in peer reviewed journals and **three** publications accepted for publication. The core theme of the thesis is bluff body flow dynamics. The ideas, development and writing up of all the papers in the thesis were the principal responsibility of myself, the candidate, working within the Department of Mechanical and Aerospace Engineering under the supervision of **Prof. Mark C. Thompson** and **Prof. Kerry Hourigan**.

The inclusion of co-authors reflects the fact that the work came from active collaboration between researchers and acknowledges input into team-based research.

In the case of Chapter 2, 3, 4, 5 and 6, my contribution to the work involved the following:

Thesis chapter	Publication title	Publication status	Nature and extent of candidate's contribution
2	On the three-dimensionality of a spinning cylinder in freestream	Accepted	Conceived ideas, initiated the paper, performed numerical simulations, analysed the data, wrote the manuscript (70.00%)
3	The flow past a circular cylinder translating at different heights above a wall	Accepted	Conceived ideas, initiated the paper, performed numerical simulations, analysed the data, wrote the manuscript (80.00%)
4	Flows past rotating cylinders next to a wall	Published	Conceived ideas, initiated the paper, performed numerical simulations, analysed the data, wrote the manuscript (70.00%)
5	Dynamics and stability of the wake behind tandem cylinders sliding along a wall	Accepted	Conceived ideas, initiated the paper, performed numerical simulations, analysed the data, wrote the manuscript (80.00%)
6	Transition to chaos in the wake of a rolling sphere	Published	Initiated the paper, performed numerical simulations, analysed the data, wrote the manuscript, revised the manuscript (65.00%)

I have not renumbered sections of submitted or published papers in order to generate a consistent presentation within the thesis.

Candidate: Anirudh Rao
October 2012

Take the risk of thinking for yourself.

*Much more happiness, truth, beauty and
wisdom will come to you that way.*

Christopher E. Hitchens, 2010.

Abstract

A computational study investigating the flow past bluff bodies in the low Reynolds numbers range ($Re \leq 750$) is presented. Two- and three-dimensional investigations are performed to investigate various flow transitions that occur when canonical bluff bodies such as circular cylinders and spheres are placed near a planar boundary, rotated or a combination of the two effects.

Control parameters such as α , the non-dimensionalised rotation rate, defined as the ratio of the tangential velocity on the body surface to the oncoming fluid velocity, and gap height G/D , the distance between the body and the wall (G) non-dimensionalised by the diameter D , are extensively used together with the Reynolds number. For these investigations, α is varied between ± 3 , where positive values correspond to prograde rotation and negative values correspond to retrograde rotation. The gap height is varied from $G/D = \infty$ for bodies in freestream to $G/D \simeq 0$ for bodies near a wall.

A spectral element based solver is used to solve the Navier-Stokes equations in two- and three-dimensions. Computational domains are constructed so that the evaluated flow parameters, such as the force coefficients and the shedding frequency, are accurate to an error of less than 1%. Spatial resolution studies are performed to obtain a trade-off between accuracy and computational time. For all investigations, the results vary by less than 0.5% with respect to the domain with the highest resolution.

The first of these studies investigates the onset of various three-dimensional modes in the wake of a rotating cylinder in freestream as the rotation rate is varied for $\alpha \leq 2.5$ and $Re \leq 400$. Two transitions are considered in this study; the first being the transition to periodic flow where vortex shedding occurs. As the rotation rate was increased, the onset of periodic flow was delayed and altogether suppressed for $\alpha \geq 2.1$. The second transition considered is the transition to three-dimensionality using a technique known as linear stability analysis. For rotation rates $\alpha \leq 1$, the onset of the three-dimensional modes occurs in the unsteady regime, and is identical to that observed for a non-rotating cylinder, although the rotation rate delays the onset of transition to higher Reynolds numbers. For higher rotation rates, the three-dimensional scenario becomes increasingly complex, where three new modes bifurcate from the unsteady base flow and two new modes bifurcate from the steady base flow. The spatio-temporal characteristics and the physical mechanism leading to the instability of these modes are discussed.

A second study investigates the flow dynamics for a circular cylinder translating along a wall at different gap heights. From the two-dimensional computations, the force coefficients and the shedding frequencies were quantified. At large spacings, $G/D \gtrsim 0.28$, the transition to three-dimensionality was observed on the unsteady base flow, while below this gap height, the three-dimensional transition occurred in the steady regime at Reynolds numbers lower than the transition to periodic flow. Simulations were further carried out to determine the variation of the transitional Reynolds numbers for cylinders rolling along a wall. For forward rolling cases, the transition to unsteady flow occurred at increasingly low Reynolds numbers, while reverse rolling delayed the onset of periodic flow to higher Reynolds numbers and periodic flow was suppressed for $\alpha \leq -1.5$. Linear stability analysis indicated that the onset of three-dimensional flow was lowered as the rotation rate was increased to higher positive values of α , while three-dimensionality was suppressed for negative rotation rates of $\alpha \leq -2$. For the cylinder sliding along a wall ($\alpha = 0$), stability analysis at higher Reynolds numbers in the unsteady state shows multiple modes unstable to spanwise perturbations. The three-dimensional simulations indicate that the flow eventually becomes chaotic, possibly due to the interaction between the various modes.

The second study was further extended to investigate the flow past multiple bodies near a wall. The additional control parameter for this study was the separation distance S/D , where S is the distance between the cylinders and Reynolds number, while the rotation rate was fixed at $\alpha = 0$. For cylinders at very small and very large separations, the flow features were identical to that of the singular cylinder. As Reynolds number was increased, unsteady flow was detected at close spacings, which led to an increase in the drag coefficient on the downstream cylinder. Stability analysis showed similar trends for the limiting cases, while for intermediate spacings, the flow first became unstable, and then restabilised at slightly higher Reynolds number. This flow further became unstable at higher Reynolds number. Three-dimensional simulations over a range of separations show the flow transitioning to a chaotic state akin to the singular cylinder.

The final study investigated the wake of a forward rolling sphere for $Re \leq 500$. At $Re \simeq 140$, vortex shedding occurred by the formation of hairpin vortices which moved away from the wall and convected downstream. A secondary transition involving the loss of planar symmetry occurred at $Re \simeq 192$, where the hairpin vortices were displaced laterally along the wake centreline, giving a sinuous structure to the wake when viewed from above. Beyond this transition, the lateral oscillations exhibited a $7 : 3$ resonance with the hairpin vortex shedding. As Reynolds number was increased, the flow progressively became more disorganised and chaotic. At the highest tested Reynolds number of 500, the wake was spatio-temporally chaotic, while retaining its sinuous structure.

Acknowledgements

Firstly, I would like to thank Professors Mark C. Thompson and Kerry Hourigan, for their guidance and supervision during my candidature. Prof. Mark's erudition and articulate way of interpreting complex flow phenomenon combined with Prof. Kerry's critical reasoning and enthusiasm for research has been integral to my development as a researcher.

I would like to thank the staff at the Department of Mechanical and Aerospace Engineering, Monash University for providing me with the office space and other resources to complete this work. Financial support provided through a Monash Departmental Scholarship and ARC grants is gratefully acknowledged. For the extensive use of computational and storage facilities, I would like to thank the Monash e-Research Centre (MeRC), Victorian Life Sciences Computation Initiative (VLSCI), and National Computational Infrastructure (NCI). I would also like to thank Mr. Philip Chan for his assistance and for being very accommodative with my persistent requests for more computational time on the Monash Sun Grid.

For their collaboration on various projects, I would like to thank Dr. Thomas Leweke and Dr. Justin Leontini. Dr. Justin's assistance and co-operation on several occasions deserves special mention.

To the past and present members of the FLAIR group, thank you for the support and advice on various topics over my candidature. To my colleagues and friends in the department, thank you for making my postgraduate experience an enjoyable one. I would also like to thank the team at Monash Motorsport for giving me an opportunity to work on the championship winning FSAE car. These made my time here very special and will always cherish the friendship with you all.

I would like to thank my family; Mum, Dad and Nana, for their unwavering love, support and encouragement. To some special friends; Mr. Jonathan Nebauer, Ms. Angkana Wangvanitchakorn and Mr. Navid Shaghanian, thank you for your moral support, strength and for the amazing times we have had over this period.

Finally, to all those who have supported me and contributed in some way along this journey, thank you very much.

Publications related to the thesis

A. RAO, B.E. STEWART, M.C. THOMPSON, T. LEWEKE & K. HOURIGAN 2010 Wake Transitions of Rolling and Sliding Cylinders and Spheres. *IUTAM Symposium on Bluff Body Wakes and Vortex-Induced Vibrations (BBVIV-6)*, Capri, Italy, **212**, 357–360.

A. RAO, B.E. STEWART, M.C. THOMPSON, T. LEWEKE & K. HOURIGAN 2011 Flows past rotating cylinders next to a wall. *Journal of Fluids and Structures*, **27**, 668 – 679.

A. RAO, M.C. THOMPSON, T. LEWEKE & K. HOURIGAN 2011 Transition to lateral asymmetry in the wake of a rolling sphere. *European Nonlinear Oscillations Conference*, Rome, Italy.

A. RAO, P.-Y. PASSAGGIA, H. BOLNOT, M.C. THOMPSON, T. LEWEKE & K. HOURIGAN 2012 Transition to chaos in the wake of a rolling sphere. *Journal of Fluid Mechanics* **695**, 135–148.

A. RAO, M.C. THOMPSON, T. LEWEKE & K. HOURIGAN 2012 The flow past a circular cylinder translating at different heights above a wall. *Journal of Fluids and Structures*, (accepted).

A. RAO, J. LEONTINI, M.C. THOMPSON, T. LEWEKE & K. HOURIGAN 2012 On the three-dimensionality of a spinning cylinder in freestream. *Journal of Fluid Mechanics*, (accepted).

A. RAO, M.C. THOMPSON, T. LEWEKE & K. HOURIGAN 2012 Dynamics and stability of the wake behind tandem cylinders sliding along a wall. *Journal of Fluid Mechanics*, (accepted).

Nomenclature

A list of nomenclature used throughout the thesis is included here.

Symbol	Description
A	Projected frontal area, amplitude
C_D	Coefficient of drag, $F_D/(0.5\rho U^2 A)$
C_{DD}	Coefficient of drag on the downstream cylinder
C_{DU}	Coefficient of drag on the upstream cylinder
\bar{C}_D	Mean drag coefficient
C_L	Coefficient of lift, $2F_L/(0.5\rho U^2 A)$
\bar{C}_L	Mean lift coefficient
$C_{x,y,z}$	Coefficient of force in x, y, z
D	Diameter
f	frequency of shedding
F_D	Drag force
F_L	Lift force
G	Distance between the cylinder and the wall
n	Index
N	Number of internal node points per macroelement
N_θ	Number of Fourier planes in the azimuthal direction
r	Radial cylindrical polar coordinate
rms	Root Mean Square
Re	Reynolds number
Re_c	Critical Reynolds number for transition
S	Separation distance between the cylinders
St	Strouhal number

Continued on the next page.

Continued from previous page.

Symbol	Description
St_{3D}	Strouhal number in the spanwise direction
$St_{x,y,z}$	Strouhal number in x, y, z
t	Time (dimensional)
T	Period of oscillation, Period of sampling
$T_{\lambda_{pref}}$	Half the period of the global instability mode
Δt	Timestep
U	Velocity of the freestream
u	Cartesian streamwise velocity
v	Cartesian transverse velocity
w	Cartesian spanwise velocity
x	Cartesian streamwise coordinate
y	Cartesian transverse coordinate
z	Cartesian spanwise coordinate, Axial cylindrical polar coordinate
Symbol (Greek)	
α	Non-dimensionalised rotation rate, $D\omega/(2U)$
β, k	Non-dimensional spanwise wave number
Γ	Circulation
ω	Angular velocity
θ	Azimuthal cylindrical polar coordinate
λ	Wavelength
λ_c	Critical wavelength at the onset of the instability
λ_{pref}	Wavelength with the maximum growth rate
μ	Fluid viscosity, Floquet multiplier
ν	Kinematic viscosity, μ/ρ
ρ	Fluid density
σ	Growth rate of the instability or the Floquet exponent
σ_∞	Inviscid growth rate
$\sigma_{inviscid}$	Growth growth from the inviscid theory of Bayly (1988)

Continued on the next page.

Continued from previous page.

Symbol	Description
τ	Non-dimensionalised time, tU/D
Ψ	Streamfunction
$\Psi_{\lambda_{pref}}$	Measure of the streamfunction with an orbital period, $T_{\lambda_{pref}}$
Symbol (Miscellaneous)	
\S	Thesis section

Contents

1	Introduction	1
1.1	Review of literature	1
1.1.1	The flow past bluff bodies in freestream	1
1.1.2	The flow past multiple circular cylinders in freestream	3
1.1.3	The flow past a spinning circular cylinder in freestream	4
1.1.4	The flow past bluff bodies near a wall	7
1.1.4.1	The flow past a cylinder near a wall	7
1.1.4.2	The flow past multiple cylinders near a wall	9
1.1.4.3	The flow past a sphere near a wall	10
1.2	Aims of this study	11
1.3	Problem overview	12
1.4	Structure of the thesis	14
2	Flow past a spinning cylinder in freestream: Three-dimensional effects	15
2.1	Overview	15
2.2	Three-dimensional flow features of a spinning cylinder in freestream	16
3	Flow past a circular cylinder translating at different gap heights to a wall	47
3.1	Overview	47
3.2	Flow dynamics of a cylinder translating parallel to a wall	48
4	Flow past a cylinder rolling along a wall	67
4.1	Overview	67
4.2	Flow dynamics of a rolling cylinder near a wall	68
5	Flow past tandem cylinders sliding along a wall	83
5.1	Overview	83
5.2	Flow dynamics of tandem cylinders sliding along a wall	84

6	The sinuous mode in the wake of a rolling sphere	111
6.1	Overview	111
6.2	Transition to chaotic flow in the wake of a rolling sphere	112
7	Conclusions	129
7.1	Conclusions	129
7.2	Future directions	132

Chapter 1

Introduction

The flow past two different bluff bodies at various distances from a plane wall is investigated by two- and three-dimensional numerical simulations. In this chapter, we briefly review relevant previous studies and then describe the key aims of this body of work. In section 1.1.1, the classical studies on the wake dynamics of a circular cylinder in freestream are discussed, and this is extended to multiple cylinders in tandem in section 1.1.2. Previous studies on the wake dynamics of a rotating cylinder are discussed in section 1.1.3. The next section deals with the flow dynamics of cylinders in close proximity to a wall. A brief review on the wake dynamics of a sphere moving near a wall is presented in section 1.1.4.3. Following this, the aims of this study are defined in section 1.2, and the flow problems investigated here are described in section 1.3. The structure of this thesis is presented in 1.4.

1.1 Review of literature

In this section, we review some of the key studies conducted on bluff body flows in freestream and near a wall. However, since detailed specific literature reviews have been presented in the journal articles forming subsequent chapters; only a brief overview of relevant studies is presented here.

1.1.1 The flow past bluff bodies in freestream

Flows past bodies in freestream have been a subject of investigation for over a century, where the wake of a circular cylinder was first investigated by Bénard (1908) and von Kármán (1911). The variable parameter in this case is the velocity of the oncoming flow or its non-dimensional counterpart, the Reynolds number (Re), given by the ratio of the inertial to the viscous forces on the body. The flow transitions that occur

in the low Reynolds number regime have been extensively investigated both experimentally (Williamson 1988a,b, 1996a), and numerically (Karniadakis & Triantafyllou 1992; Thompson *et al.* 1996; Barkley & Henderson 1996). The flow remains steady for $Re \lesssim 46$, and on increasing the Reynolds number, the transitions to periodic flow occurs via a Hopf bifurcation (Norberg 2003), where vortices are alternately shed periodically from either side of the cylinder. At a Reynolds number of $Re \simeq 190$, spanwise waviness develops in the wake, leading to three-dimensional flow. At onset, the spanwise wavelength was found to be approximately $4D$, and was termed the *mode A* instability (Williamson 1988b). At slightly higher Reynolds numbers, $Re \simeq 230$, the three-dimensional wake becomes unstable to a second instability, having a characteristic wavelength of $\simeq 1D$, and this is termed *mode B*. These transitions were confirmed by the numerical analysis of Barkley & Henderson (1996), who employed linear stability analysis to obtain the critical Reynolds numbers for the onset of these three-dimensional modes. The critical Reynolds number for the onset of Mode A instability was determined to be $\simeq 188.5$ for a spanwise wavelength of $3.96D$, while mode B became unstable at $Re \simeq 260$ for a spanwise wavelength of $0.8D$. In reality, of course, mode B develops on the saturated three-dimensional wake state of mode A. These three-dimensional modes were visualised by the Direct Numerical Simulations (DNS) of Thompson *et al.* (1996) amongst others. According to stability analysis, Mode A was found to still be the dominant mode at $Re = 280$ (Barkley & Henderson 1996), while mode B becomes the fastest growing mode for $Re > 300$ (Blackburn *et al.* 2005). However, in practice, mode B becomes dominant at lower Reynolds numbers ($Re \gtrsim 230$). At higher Reynolds numbers ($Re \simeq 400$), the flow quickly becomes chaotic (Henderson 1997).

The three-dimensional modes described above have analogues in the wakes of other geometries. Modes A and B are known to develop in the wakes of square cylinders (Robichaux *et al.* 1999) and rings Sheard *et al.* (2003), and are commensurate with the periodicity of the base flows. Modes which are non-synchronous with the base flow are also known to exist in bluff body wakes, and these modes are quasi-periodic. A mode with this characteristic for a circular cylinder was termed mode QP (Blackburn & Lopez 2003). When the symmetry of the Kármán street is broken for a less symmetric body, a different three-dimensional mode develops. Subharmonic modes are periodic over twice the period of the base flow. Modes of such nature are observed when a control wire is placed in the wake of a circular cylinder (Zhang *et al.* 1995), or in the case of flow over

rings (Sheard *et al.* 2003, 2005a,b) and inclined square cylinders (Sheard *et al.* 2009; Sheard 2011).

The studies described here detail the important transitions that occur in the low Reynolds number range for a flow past a circular cylinder. These studies will form the basis for further studies described here. Although the circular cylinder is the simplest configuration investigated, the flow dynamics can be significantly altered by placing an identical body in its vicinity, by induced rotation, or by bringing it near a plane boundary. The effect of these changes on the flow dynamics is described in the following sections.

1.1.2 The flow past multiple circular cylinders in freestream

The studies on multiple bodies were investigated in light of flow stabilisation that occurs by placing an identical cylinder downstream of the original cylinder at various longitudinal spacings. At very close and very large spacings, the associated flow dynamics are effectively identical to a single body in freestream. Based on the separation distance, S/D , various researchers (Igarashi 1981; Zdravkovich 1987; Didier 2007) have identified different regimes of flow. The broad classifications based on this parameter are:

- $0.1 \leq S/D \leq 0.2 - 0.8$, a region of close spacing, where the shear layers shed from the upstream cylinder do not reattach on the downstream cylinder. The two cylinders behave as a single extended body and vortices formed are from the detached shear layers of the downstream cylinder.
- $0.2 - 0.8 \leq S/D \leq 2.4 - 2.8$, an intermediate regime where the shear layers shed from the upstream cylinder reattach onto the downstream cylinder, and shedding takes place behind the downstream cylinder. Also observed in this regime was the intermittent vortex formation behind the upstream cylinder and reattachment of the shear layers.
- $S/D \geq 2.8$, vortices are shed from both cylinders.

Another important observation was that the drag force coefficient on the downstream cylinder was negative until the critical spacing of $S/D \simeq 2.5$, and this distance was labelled the “drag inversion distance”. Mizushima & Suehiro (2005) reported the delay in transition to periodic flow to higher Reynolds numbers at close spacings. For

$S/D = 1$ and 3, the critical values for the transition were $Re = 68$ and 78.5, respectively, which are much higher than that observed for an isolated cylinder. Furthermore, by placing a downstream cylinder in this critical region, the onset of three-dimensional flow can be controlled. The three-dimensional investigations by Deng *et al.* (2006) show that the flow remains two-dimensional largely due to the limiting space for the shed vortices to roll up when the separation distances are small. They further observed that the flow became increasingly three-dimensional as the critical spacing distance is reached.

Recent numerical investigations of the flow around isolated tandem cylinders by Carmo *et al.* (2010) on the onset of three-dimensionality showed the growth of three new modes at various separation distances for $Re \geq 200$. For low separation distances, the onset of three-dimensionality occurs via *mode T1*, whose spatio-temporal symmetry resembles that of the mode B instability observed in the wake of an isolated circular cylinder at higher Reynolds numbers. This mode had a spanwise wavelength of $\simeq 2D$. Two other modes were observed when the cylinders were spaced between $0.8 \leq S/D \leq 1.5$. The physical mechanism of the *mode T2* instability was believed to be centrifugal, while *mode T3* had similar characteristics to mode A. Mode T2 had a spanwise wavelength of $\simeq 3D$, while mode T3 had a spanwise wavelength of $\simeq 4.6D$ at onset. At large separations, the mode A instability was followed by the mode B instability, akin to that observed for an isolated cylinder in freestream.

1.1.3 The flow past a spinning circular cylinder in freestream

The rotation of a circular cylinder has previously been used to control the flow dynamics and achieve flow stabilisation. Due to the imposed rotation, the flow on one side of the cylinder remains attached while on the other side, flow separation occurs, leading to a net lift force in the direction away from the side where the flow is attached. This is known as the ‘‘Magnus effect’’ and one of its earliest applications was in the propulsion of ships (Prandtl 1925).

Several researchers have investigated the flow at different rotation rates both experimentally and numerically. Although early numerical work was carried out at very low Reynolds numbers $Re \leq 40$ (Ingham 1983; Badr *et al.* 1989, 1990), recent studies (Chen *et al.* 1993; Chew *et al.* 1995; Kang *et al.* 1999; Stojković *et al.* 2002; Pralits *et al.* 2010) have extended the Reynolds number range to higher values. Vortex shedding occurred

for $\alpha \lesssim 1.9$, beyond which vortex shedding was suppressed. The rotation rate at which vortex shedding ceased was found to vary with Reynolds number.

Mittal & Kumar (2003) performed numerical experiments at $Re = 200$ for $\alpha \leq 5$. At this Reynolds number, vortex suppression was observed around $\alpha = 2$, and the flow remained steady until higher rotation rates, where vortex shedding reappeared over a small range of rotation rates ($4.34 \leq \alpha \leq 4.75$). The vortex shedding in this regime was single-sided and the shedding frequency was much lower compared to that at lower rotation rates. A similar study performed by Stojković *et al.* (2003) showed that the range of α at which the two shedding regimes (two- and one-sided) existed varied with Reynolds number. The upper limit at which primary shedding ceased, increased monotonically with Reynolds number. The range at which secondary shedding was observed shifted to lower rotation rates at high Reynolds numbers. Also, the range was narrower at lower Reynolds numbers. The Strouhal number was found to be dependent more on the rotation rate than the Reynolds number.

Recent experimental investigations were performed by Kumar *et al.* (2011) $\alpha \leq 5$ using the hydrogen bubble technique to obtain flow field visualisations for $Re \leq 400$. At $Re = 200$, they report that the vortex street behind the body was deflected for $\alpha \leq 1.9$, beyond which the vortex shedding becomes less pronounced and being suppressed for $\alpha \simeq 2$. At higher rotation rates, the single-sided vortex shedding observed numerically by Mittal & Kumar (2003) and others was confirmed by the use of Particle Image Velocimetry (PIV). In addition, they visualised the flow for $Re = 300$ and 400 and computed the variation of Strouhal number at different rotation rates. In the primary shedding mode, the shedding frequency was independent of the rotation rate, while in the secondary shedding regime, the shedding frequency decreased on increasing the rotation rate. The experimentally obtained values of Strouhal number in the secondary shedding regime were consistent with the numerical studies of Akoury *et al.* (2008) and Mittal & Kumar (2003). At higher Reynolds numbers, the wake was reported to be highly three-dimensional.

The onset of three-dimensionality for rotation rates of $\alpha > 0$ had not been investigated until recently, although it has been generally stated that the flow is three-dimensional beyond $Re = 200$. Akoury *et al.* (2008) performed direct numerical simulations in two and three dimensions for a rotating cylinder. From their two-dimensional studies, they mapped the variation of St at increasing rotation rates at

different Reynolds numbers for $\alpha \leq 6$. The secondary shedding regime, where a single-sided vortex is shed from the cylinder, broadened at higher Reynolds number, with the regime shifting towards lower rotation rates. This was attributed to the decreasing influence of the viscous component at higher Reynolds numbers (Stojković *et al.* 2003). This secondary shedding regime occurred between $\alpha = 4.75$ and $\alpha = 5.25$ at $Re = 100$, while at $Re = 500$, secondary shedding occurred in the range $3.6 \leq \alpha \leq 5$. The Strouhal number was $\simeq 0.05$, much lower than that observed for the spinning cylinder at low rotation rates, consistent with the findings of Mittal & Kumar (2003). The Strouhal number decreased as rotation rate was increased in this regime. Three-dimensional simulations were performed for the cylinder rotating at $\alpha \leq 1.5$. At $Re = 300$, the growth of the spanwise component of velocity grew steadily, indicating the onset of three-dimensional flow. This transition was found to occur through a supercritical bifurcation. Using Landau modelling, they determined the critical Reynolds number for the transition to three-dimensional flow for $\alpha = 0.5$ to occur at $Re_c = 219.8$. Further investigations at $\alpha = 1.5$ and $Re = 200$ showed damping of the spanwise component of flow, indicating two-dimensional flow. Using proper orthogonal decomposition, they reconstructed the three-dimensional modes for $\alpha = 0.5$. The reconstructed mode was found to have a similar spanwise wavelength to the mode A instability ($\simeq 4D$) observed for a non-rotating cylinder at the onset of three-dimensionality (Williamson (1988b), Thompson *et al.* (1996)). Furthermore, at $Re = 300$, the wake retained its mode A structure, possibly due to enhanced stability of the vortex pairs attributed to the vorticity induced by cylinder rotation in the spanwise direction. The critical values of transition to three-dimensional flow for rotation rates other than $\alpha = 0.5$ were not reported.

The effect of three-dimensional instabilities at higher rotation rates has been investigated by Mittal (2004) for $\alpha = 5$ at $Re = 200$. The two-dimensional flow field is steady while the three-dimensional simulations show the growth of centrifugal instabilities. They also tested the effect of various boundary conditions for cylinders of different aspect ratios (the ratio of the cylinder diameter to its length). For aspect ratios of 5, 10 and 15 with slip walls, the time-history of the drag coefficient showed oscillatory behaviour. The cylinder with lower aspect ratio and slip walls resembled two-dimensional flow (which was steady). However, longer aspect ratio cylinders with no-slip walls showed fluctuations, primarily because of the interaction of the boundary

layer of the wall and the rotating cylinder. The three-dimensional flow was associated with centrifugal instabilities of around $1D$ spanwise wavelength. This instability was predicted to cause a reduction in lift and an increase in drag.

Recent linear stability investigations by Meena *et al.* (2011), at $Re = 200$ for $3 \leq \alpha \leq 5$, indicate the presence of modes with purely real growth rates (indicating they are synchronised with the two-dimensional flow) for $\alpha \leq 4.3$. Their three-dimensional investigations show what appear to be centrifugal instabilities near the cylinder and the time histories of the force coefficients indicate the onset of aperiodic flow.

Although modes A and B are known to occur for a non-rotating cylinder, the critical values at the onset of these modes for higher rotation rates is not known. Furthermore, at higher rotation rates of $\alpha \gtrsim 3$, centrifugal instability is said to dominate in the near wake. Nonetheless, the parameter map of $Re - \alpha$ remains to be explored for the onset of three-dimensional flow.

1.1.4 The flow past bluff bodies near a wall

1.1.4.1 The flow past a cylinder near a wall

Several studies (Bearman & Zdravkovich (1978); Price *et al.* (2002); Lei *et al.* (2000) and others) have considered the changes in flow features brought about by placing a bluff body near a planar surface, where the lower wall remains stationary, leading to the formation of a boundary layer upstream of the cylinder. Compared to a cylinder in freestream, several changes, including that of flow structures, are evident. For a circular cylinder near a wall, vortex shedding occurs by the pairing of the shear layer rolled up behind the cylinder and the oppositely signed boundary layer on the wall, where the induced vorticity lifts away from the wall to form a compact vortical structure which convects downstream. The changes in the shedding frequency and the force coefficients have been documented. Very few studies (Huang & Sung 2007; Yoon *et al.* 2010) have considered a circular cylinder translating near a stationary wall, where a wall boundary layer does not exist.

Huang & Sung (2007) performed two-dimensional simulations for a circular cylinder moving near a wall for $0.1 \leq G/D \leq \infty$ and $Re \leq 600$. The gap height, G , at which alternate vortex shedding disappeared decreased from $0.28D$ to $0.25D$ as the Reynolds number was increased from 300 to 600. The non-dimensionalised shedding frequency (St) at different Reynolds numbers increased as the cylinder was brought closer to the

wall ($\simeq 0.5D$), followed by a rapid decrease as the gap height was decreased. They further quantified the lift and drag coefficients, with the lift coefficient showing a linear increase as the cylinder was brought closer to the wall. They however, did not rule out the possibility that three-dimensional effects would be important for such flows.

Using an immersed boundary technique, Yoon *et al.* (2010) performed numerical investigations at various gap heights for a circular cylinder moving parallel to a wall at $Re \leq 200$. The time-averaged lift and drag coefficients decreased exponentially as the gap height was increased. They observed steady flow at higher Reynolds numbers as the gap height was decreased. Vortex shedding persisted at $Re = 120$ for the cylinder with $G/D = 0.1$.

Mahir (2009) investigated the onset of three-dimensional flow for a square cylinder near a fixed wall for $Re \leq 250$ as the gap height was increased from 0.1 to 4. At $Re = 185$, mode A type vortex structures of spanwise wavelength $3D$ were observed for gap heights greater than $G/D = 1.2$, whilst at $G/D = 0.8$, mode B type vortex structures with $1D$ spanwise wavelength were observed. Below $G/D = 0.5$, neither mode A nor B type vortex structures were observed. At $Re = 250$, mode B type vortex structures were observed at larger gap heights, whilst at lower gap heights the vortex structure was strongly distorted in the vicinity of the cylinder. In the frequency spectra of the streamwise and spanwise velocities for $G/D = 0.8$ and $Re = 185$, period-doubling was observed.

Stewart *et al.* (2006, 2010b) performed numerical and experimental investigations for a circular cylinder rolling along a wall at a very small gap height ($G/D = 0.005$) and $Re \leq 500$ for $1 \leq \alpha \leq -1$. For the non-rotating cylinder, they reported that the flow was steady up to $Re \simeq 160$, beyond which periodic flow was observed, where oppositely signed vortex structures combined and self-propelled away from the wall. This value is much higher than that observed for an identical cylinder in freestream. The effect of rotation on the flow dynamics and force coefficients was reported. Forward rolling lowered the transitional Reynolds number to periodic flow, while reverse rolling delayed the onset of periodic flow to higher Reynolds numbers. From their linear stability analysis, the transition to three-dimensional flow occurred in the steady regime for all rotation rates, which is in contrast to that observed for a cylinder in isolation. A decrease in the spanwise wavelength of the three-dimensional instability was observed as the rotation rate was decreased to lower values. Furthermore, their experimental wake

visualisations for the cylinder near a wall in a water tunnel were in good agreement with the numerical simulations.

The two-dimensional studies have detailed the two-dimensional structures for bodies in freestream and near a wall; very little is known about the onset of three-dimensional flow for intermediate gap heights. To reiterate, for cylinders in freestream, the flow first transitions to a periodic state prior to becoming three-dimensional, while for bodies near a wall, the flow becomes three-dimensional in the steady regime prior to the onset of periodic flow. Furthermore, for bodies near a wall, the effect on the flow structures on increasing the rotation rate to higher values is unknown. The influence of the spanwise flow on the two-dimensional structures is yet to be determined.

1.1.4.2 The flow past multiple cylinders near a wall

Numerous studies have been conducted investigating the flow dynamics of multiple cylinders in freestream and for bodies near a wall; very few studies have considered the two effects in tandem. Bhattacharyya & Dhinakaran (2008) conducted numerical simulations for a pair of tandem square cylinders in a linear shear flow at $G/D = 0.5$ for $Re \leq 200$. Below $Re = 125$, the shear layers, which separate from the two sides, are unable to interact and cause vortex shedding. At a spacing of $S/D \leq 2$, the two cylinders effectively behave as one body at $Re \leq 200$. However, for a spacing of $S/D = 2 - 3$, vortices were shed from the downstream cylinder only. Beyond this range, vortices were shed from both cylinders; at even larger separation distances, the St recorded on the cylinders matched that of a single cylinder under a similar flow condition. The height above the wall and the spacing distance were critical for the shear layers to interact leading to the formation of vortices.

Harichandan & Roy (2012) performed numerical investigations for circular cylinders in tandem when close to a wall at Reynolds numbers $Re = 100$ and 200 for separation distances of $S/D = 1$ and 4 . The bodies were placed at $0.5D$ and $1D$ above the stationary wall. They observed that the dependence on the separation distance is greater for the flow stability compared to the gap to the wall. Vortex shedding occurred when the gap heights and the separation distance were both large.

For multiple bodies near a wall, the stabilising effect of the flow structures is unknown. Furthermore, the transition to three-dimensionality for cylinders at various spacings near a wall is yet to be determined.

1.1.4.3 The flow past a sphere near a wall

We here extend the studies examined to consider flows past spheres near a wall. For a sphere in freestream, the flow transitions from a steady axisymmetric state to a steady asymmetric state at $Re = 212$ (Johnson & Patel 1999) with the formation of a “double threaded wake” with a planar symmetry. A second transition occurs at $Re = 272$, where this double threaded kinks to form hairpin vortices. The two transitions were found to be supercritical in nature (Ghidersa & Dušek 2000; Thompson *et al.* 2001). Numerical simulations indicate that the planar symmetry is broken at $Re \simeq 345$ (Mittal 1999), which is in line with experimental investigations of Sakamoto & Haniu (1990) who suggested that a transitional regime exists for $420 \leq Re \leq 480$, wherein the hairpin vortices are intermittently displaced to either side of the wake centreline. At higher Reynolds numbers ($Re \gtrsim 650$), chaotic flow was observed (Mittal & Najjar 1993).

Direct numerical simulations were performed by Zeng *et al.* (2005) for a sphere moving parallel to a wall. Their study showed that as the sphere was moved closer to the wall, the transition to the unsteady state occurred at Reynolds numbers lower than for the freestream case ($Re < 272$), with a sudden increase observed for the closest tested distance of $0.25D$. The effect of free rotation was also studied. In their investigations, a symmetry plane was used, curtailing the development of a lateral wake. Zeng *et al.* (2009) also performed direct numerical simulations for a stationary spherical particle close to a plane wall in a linear shear flow. They present results for gap ratios between $0.005 \leq G/D \leq 3.5$, using a symmetry plane. The double-threaded wake is observed at $Re = 200$ for larger gap ratios, while a toroidal structure engulfing the particle is observed for lower Reynolds numbers. These findings are similar to the results of Stewart *et al.* (2010a), where the transition to an unsteady state for the non-rotating sphere was in excess of $Re = 300$. Furthermore, they propose empirical relationships for the lift and drag coefficient variation with distance from the wall.

Stewart *et al.* (2010a) also performed experimental and numerical simulations for a rolling sphere at other rotation rates. For a forward rolling sphere at $\alpha = +1$, unsteady flow was first observed at $Re = 150$, where vortex shedding occurred by the formation of hairpin vortices, which convected away from the wall and diffusing in the far wake. The same was observed in their experimental and numerical visualisations at $Re = 200$. For a reverse rolling sphere at $\alpha = -1$ and $Re = 300$, the unsteady wake developed lateral oscillations on addition of white noise in their numerical simulations. Recent

experimental findings of Bolnot *et al.* (2011) showed the development of a sinuous mode in the wake of a forward rolling sphere. Their dye visualisations at $Re = 190$ showed that the wake maintained planar symmetry, while at $Re = 230$, the hairpin vortices were displaced across the wake centreline.

From the above studies, the non-planar symmetric wake modes in the wake of a rolling sphere have not been observed numerically, possibly due to the prohibitive computational expense for such studies. Furthermore, the instabilities grow from small amplitudes ($O(10^{-5})$) before attaining a saturated state, requiring time integration over several hundred time units, unless external noise is added to achieve a speed up effect. Furthermore, the nature of these transitions has not been investigated.

1.2 Aims of this study

This study aims to compute the flow past bluff bodies, such as circular cylinders and spheres, to determine the flow structures by varying the spatial location of the body with respect to a fixed boundary and/or by imposing a rotation. The study also extends to the investigation of flow past multiple bluff bodies and the resulting influence on the flow state. A two-dimensional spectral element numerical solver is employed to obtain the base flow solutions, following which the stability of these flows to three-dimensional perturbations is investigated for the above scenarios. The transitional values of Reynolds number are ascertained in each case, mapping regions of stability.

For the spinning cylinder in freestream, the major focus is to determine regions of stability (or instability) on the $\alpha-Re$ plane, apart from determining the spatio-temporal symmetries of unstable modes. The stability is investigated not only with respect to the periodicity of the base flow, but also with respect to the three-dimensionality of the base flow. The following study on the translating cylinders at varied gap heights bridges the existing knowledge gap between the bodies in isolation and those near a wall. In this case, the two parameters varied are the gap height and the Reynolds number, while the rotation rate is fixed at zero. The other studies extend the parameter space by investigating the flow features at a wide range of rotation rate and by introducing an identical body at close distances to the original. The final study investigates the route to chaotic flow for a sphere rolling along a wall at a fixed rotation rate as the Reynolds number is varied.

The overall study aims to explore and extend the parameter ranges with respect

to bluff bodies over a multi-dimensional parameter space. The study further aims to investigate the new three-dimensional modes which are observed in the wake of a spinning cylinder.

These studies are generally motivated by a desire to extend and improve our understanding of fluid-particle and fluid-structure systems, between the limits of creeping flow and high Reynolds number turbulent regimes. It is clear that the wake instability modes persist, albeit in a less distinct state, for wakes after the flow has become fully turbulent, and contribute to the persistent larger scale structures in the flow. These larger scale structures have a strong part to play in cross stream energy and momentum transport. In addition, the mean and time-dependent forces on particles and structures are also imminently tied to the wake flow characteristics.

1.3 Problem overview

The effect on the flow dynamics of a bluff body is investigated by a numerical study involving a set of control parameters, which are selectively varied. A schematic diagram of the studies undertaken is shown in figure 1.1. The governing parameters which are used to describe the problem are the non-dimensionalised rotation rate, α , defined by the ratio of the angular velocity of the body to the freestream velocity, U . It is mathematically given by $\alpha = \omega D/2U$. Here, ω is the rotation rate of a circular cylinder of diameter D . For the circular cylinder rotating forward, where the cylinder rotation at the top is in the opposite direction of the oncoming flow is assigned positive values of α , while for reverse rotation, α takes negative values. In order to represent bodies in freestream, we define a second parameter, G/D , known as the gap height. This parameter represents the distance of a body away from a plane wall. For cylinders at large distances to a wall, $G/D = \infty$, while for bodies in close proximity to the wall, $G/D \simeq 0$. The third parameter widely used in this study is the Reynolds number, defined as the ratio of the inertial forces to the viscous forces and is given by, $Re = \rho U D/\mu$, where ρ and μ are the density and viscosity of the fluid. For ease of computation, the frame of reference is attached to the centre of the bluff body under investigation, and in this frame the velocity of the lower wall is set to that of the oncoming flow velocity.

The first study involves the investigation of a circular cylinder in freestream, where the gap height is maintained constant at $G/D = \infty$, while α and Re are varied. This is shown in the top left of the image. The second study involves the variation of gap

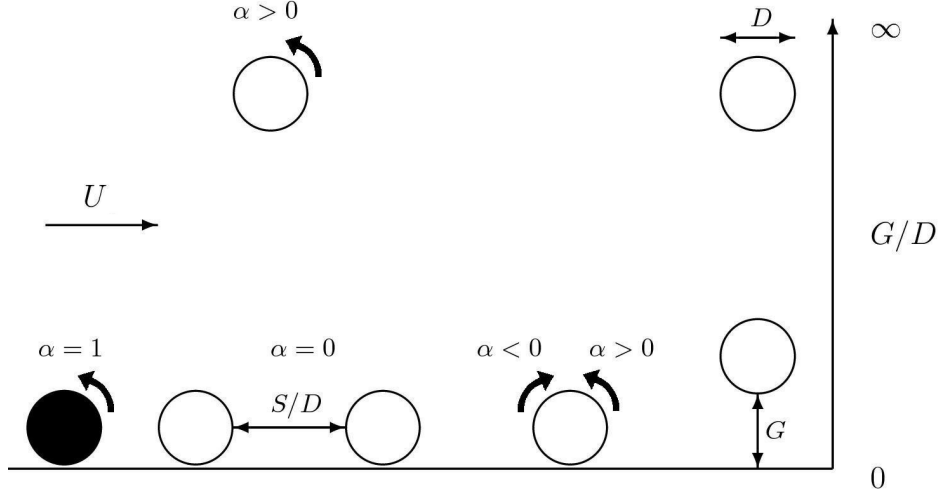


FIGURE 1.1: Schematic showing the relationship between the problems investigated. The open circles represent cylinders, while the filled circle represents a sphere. The frame of reference is attached to the centre of the bluff body and the lower wall translates with a velocity equal to the oncoming fluid velocity.

height for bodies away from the wall to that on the wall. In this case, the rotation rate is fixed at zero, while the Reynolds number and gap height are varied. For bodies on the wall, the flow features are investigated by varying the rotation rate. The study is further extended to multiple bodies, where a second cylinder, having the same diameter is placed downstream. The separation distance between the two cylinders is non-dimensionalised by the cylinder diameter and is represented by S/D , where S is the distance between the two cylinders. The final study involves the simplest three-dimensional bluff body, a sphere of diameter D , shown by the fully filled circle. In this case, the rotation rate and gap height are held constant, while the Reynolds number is varied. The limits of the parameter space are mentioned in each study.

Several constraints are imposed in this study. The fluid around the bluff body is assumed to be homogeneous, incompressible, and invariant to thermal effects. The oncoming flow is assumed to be laminar, uniform and having zero turbulence intensity upstream of the body. The fluid is further assumed to be Newtonian, where the shear stress of the fluid varies directly with the rate of strain. The simulations are performed using an unsteady solver generally starting from a quiescent initial state, and the fluid flow equations are marched forward in time, for several hundred time units. The non-dimensional time is represented by τ , where $\tau = tU/D$, with t being the time. The forces

on the bluff bodies are monitored after the initial transience has died out and the flow is steady or periodic. The body forces are computed by the summation of the pressure and viscous forces acting on the body in a particular direction. The body force components are non-dimensionalised by the upstream dynamic pressure and frontal area of the body, to obtain the force coefficients. For the circular cylinder, the force coefficients (per unit width) take the form $C_{x,y} = F_{x,y}/(0.5\rho U^2 D)$, while for the spherical bluff body, the force coefficients take the form, $C_{x,y,z} = 8F_{x,y,z}/(0.5\rho U^2 \pi D^2)$. For cases where the flow is periodic, the shedding frequency is measured by the Strouhal number, St , and is given by $St = fD/U$, where f is the frequency of shedding.

1.4 Structure of the thesis

The remainder of this thesis is organised as follows. The following chapters contain results from the studies of bluff bodies. Each chapter consists of a brief overview followed by the submitted/accepted/published journal article. Chapter 2 details the wake of a rotating circular cylinder in freestream, where a number of new three-dimensional modes are observed. The following chapter, chapter 3, deals with the onset of three-dimensional flow as the circular cylinder is brought closer to a plane wall. Chapter 4 deals with bodies rolling along a wall at different rotation rates, while chapter 5 investigates the flow features for multiple bodies near a wall. The final chapter, chapter 6, deals with the new wake mode observed behind a rolling sphere at higher Reynolds numbers and rapid transition to chaotic flow as the Reynolds number is increased. Finally, broad conclusions and future directions are presented.

Chapter 2

Flow past a spinning cylinder in freestream: Three-dimensional effects

2.1 Overview

This chapter presents the findings of the linear stability analysis in the wake of a spinning cylinder in the low Reynolds number range. For a non-rotating cylinder ($\alpha = 0$), the linear stability analysis of Barkley & Henderson (1996) showed that the two-dimensional wake becomes unstable to a long wavelength instability ($\simeq 4D$) around $Re = 190$, followed by a short wavelength instability ($\simeq 4D$) at higher Reynolds numbers. The analysis confirmed the previous experimental investigations by (Williamson 1988b, 1996b) and was further supported by the DNS of Thompson *et al.* (1996). The numerical studies for a spinning cylinder have mainly focussed on the flow features from a two-dimensional perspective, while generalising that a three-dimensional flow state exists for $Re \gtrsim 200$. Nonetheless, the spinning cylinder studies have gained interest from a flow stability perspective, due to the cessation of the vortex street for rotation rates $\gtrsim 1.9$ (Mittal & Kumar 2003; Akoury *et al.* 2008; Kang *et al.* 1999; Stojković *et al.* 2003). Vortex shedding was found to resume at higher rotation rates, with a single-sided vortex being shed with a low shedding frequency. This regime occurred over a small range of Reynolds numbers and rotation rate.

The recent DNS of Akoury *et al.* (2008) for a spinning cylinder for $\alpha \leq 1.5$, showed that the critical Reynolds number for the onset of three-dimensional flow was delayed to $Re = 220$ for $\alpha = 0.5$, with mode A type instability at the onset, which persisted in the wake even at $Re = 300$. They further report that the flow was two-dimensional at $\alpha = 1.5$, $Re = 200$. The occurrence of three-dimensionality for other rotation rates is

yet to be determined. Further questions arise regarding the three-dimensional nature of the wake. How does the onset of three-dimensional flow vary on increasing rotation rate and Reynolds number? Does the breaking of the flow symmetry by induced body rotation give rise to other three-dimensional modes? What three-dimensional modes occur in the steady regime of flow when vortex shedding ceases?

To answer these questions, two-dimensional numerical simulations are performed for $\alpha \leq 2.5$ and $Re \leq 400$, followed by linear stability analysis. Curves of marginal stability of the three-dimensional modes are presented on the α, Re plane. The characteristics of each of the three-dimensional modes is described and the physical mechanisms of instability for the modes are proposed. Furthermore, the regions of steady-unsteady flow are also obtained using a steady solver.

2.2 Three-dimensional flow features of a spinning cylinder in freestream

The following article was submitted in 2012 to *Journal of Fluid Mechanics*. This work was co-authored by J. S. Leontini, M. C. Thompson and K. Hourigan, and is entitled, “*On the three-dimensionality of a spinning cylinder in freestream*”. The paper is reproduced in this thesis directly from the version submitted to the editor for review.

Declaration for manuscript included in PhD Thesis

Monash University

Declaration for Thesis Chapter 2

Declaration by candidate

In the case of Chapter 2, the nature and extent of my contribution to the work was the following:

Nature of contribution	Extent of contribution (%)
Conceived ideas, initiated the paper, performed numerical simulations, analysed the data, wrote the manuscript	70

The following co-authors contributed to the work. Co-authors who are students at Monash University must also indicate the extent of their contribution in percentage terms:

Name	Nature of contribution	Extent of contribution (%) for student co-authors only
Dr. J. Leontini	Analysed data, co-wrote the manuscript	N. A.
Prof. M.C. Thompson	Co-wrote the manuscript	N. A.
Prof. K. Hourigan	Co-wrote the manuscript	N. A.

Candidate's Signature *A. Aravath* Date 18 JUNE 2012

Declaration by co-authors

The undersigned hereby certify that:

- 1) the above declaration correctly reflects the nature and extent of the candidate's contribution to this work, and the nature of the contribution of each of the co-authors.
- 2) they meet the criteria for authorship in that they have participated in the conception, execution, or interpretation, of at least that part of the publication in their field of expertise;
- 3) they take public responsibility for their part of the publication, except for the responsible author who accepts overall responsibility for the publication;
- 4) there are no other authors of the publication according to these criteria;
- 5) potential conflicts of interest have been disclosed to (a) granting bodies, (b) the editor or publisher of journals or other publications, and (c) the head of the responsible academic unit; and
- 6) the original data are stored at the following location(s) and will be held for at least five years from the date indicated below:

Location(s) Dept. Of Mechanical and Aerospace Engineering, Monash University, Clayton

Signature 1	<u><i>M. Thompson</i></u> (M. THOMPSON)	Date	<u>19/6/2012</u>
Signature 2	<u><i>J. Leontini</i></u> (J. LEONTINI)		<u>19/6/2012</u>
Signature 3	<u><i>K. Hourigan</i></u> (K. HOURIGAN)		<u>19/6/2012</u>

On the three-dimensionality of a spinning cylinder in freestream

By A. RAO¹, J. LEONTINI¹, M.C. THOMPSON¹,
AND K. HOURIGAN^{1,2}

¹Fluids Laboratory for Aeronautical and Industrial Research (FLAIR), Department of Mechanical and
Aerospace Engineering, Monash University, Melbourne, Victoria 3800, Australia

²Division of Biological Engineering, Monash University, Melbourne, Victoria 3800, Australia

(Received 22 June 2012)

The wake of a rotating circular cylinder in a freestream is investigated for Reynolds numbers $Re \leq 400$ and non-dimensional rotation rates of $\alpha \leq 2.5$. Two aspects are considered. The first is the transition from a steady flow to unsteady flow characterised by periodic vortex shedding. The two-dimensional computations show the onset of unsteady flow is delayed to higher Reynolds numbers as the rotation rate is increased, and vortex shedding is suppressed for $\alpha \geq 2.1$ for all Reynolds numbers in the parameter space investigated. The second aspect investigated is the transition from two-dimensional to three-dimensional flow using linear stability analysis. It is shown that at low rotation rates of $\alpha \leq 1$, the three-dimensional transition scenario is similar to that of the non-rotating cylinder. However, at higher rotation rates, the three-dimensional scenario becomes increasingly complex, with three new modes identified that bifurcate from the unsteady flow, and two modes that bifurcate from the steady flow. Curves of marginal stability for all of the modes are presented in a parameter space map, the defining characteristics for each mode presented, and physical mechanisms of instability discussed.

Key Words: Wakes, vortex shedding, vortex streets, parametric instability

1. Introduction

The flow past a rotating cylinder is a function of two non-dimensional parameters. These are the Reynolds number, $Re = UD/\nu$, where U is the freestream velocity, D is the cylinder diameter, and ν is the kinematic viscosity, and $\alpha = \omega D/2U$, where ω is the rotational speed of the cylinder. This latter parameter is therefore the ratio of the surface velocity of the cylinder to the freestream velocity.

Flow past a non-rotating circular cylinder in the low Reynolds number range and the bifurcations from one state to another have been extensively studied, and several regimes of flow have been identified. Experimental work on the transition between the steady and unsteady regime have been discussed by Williamson (1996b) and others. Numerical investigations have also contributed to the understanding of the flow. Several research groups, e.g., Barkley & Henderson (1996), Karniadakis & Triantafyllou (1992), Thompson *et al.* (1996) have investigated the transition from two-dimensional vortex shedding to three-dimensional flow at $Re \simeq 190$, where the wake vortices develop a waviness in the spanwise direction at a wavelength of around $4D$, where D is the diameter of the cylinder. This wake flow is known as mode A (Williamson 1988), and has also been shown to be the saturated form of a linear mode growing on the two-dimensional base flow (Barkley & Henderson 1996). Further increasing Re sees a second type of three-dimensional flow develop, with fine-scale (a wavelength of around $0.8D$ in the spanwise

direction) streamwise vortices developing in the braid shear layers between wake vortices. This flow is known as mode B (Williamson 1988). Even though in reality this flow develops from the already three-dimensional mode A wake, it is also well described by a linear mode growing on the two-dimensional base flow (Barkley & Henderson 1996).

Both of the linear modes corresponding to mode A and B are commensurate with the base flow, introducing no new frequencies. However, a mode which is incommensurate has also been observed in the wakes of cylinders. Due to the introduction of a second frequency, this mode is expected to be quasi-periodic, and so is designated mode QP (Blackburn & Lopez 2003).

When the spatio-temporal symmetry of the vortex street is broken (as occurs when the cylinder is rotating), further modes become possible. In particular, subharmonic modes which repeat over two cycles of the two-dimensional base flow can occur. Such a mode was detected by Zhang *et al.* (1995) in the wake of a circular cylinder with a control wire, by Sheard (2011); Sheard *et al.* (2009) in the wake of an inclined square cylinder, by Leontini *et al.* (2007) in oscillating cylinder wakes, and in a series of papers (Sheard *et al.* 2003, 2005*a,b*), a subharmonic mode has been described in the wakes of rings. It is expected that similar modes should occur for rotating cylinders.

The effect of rotation is to cause opposing viscous effects on either side of the cylinder centreline. Depending on the rotation rate, the flow may remain attached on one side of the cylinder while separating off the other, causing a net lift force directed away from the side where the flow remains attached. This is known as the Magnus effect (Prandtl 1925).

One of the earliest numerical studies was performed by Ingham (1983), where steady state solutions were obtained for $Re \leq 40$ and for rotation rates of $\alpha \leq 0.5$. At $Re = 5$, the drag force increases with rotation rate while at a slightly higher Reynolds number of $Re = 20$, the drag force increases after a slight decrease. Further investigations by Badr *et al.* (1989) were performed in the steady and unsteady regimes of flow. The major focus of their work dealt with the flow behaviour of an impulsively started rotating and translating cylinder. They observed periodic flow at Reynolds numbers greater than 60 for $0 \leq \alpha \leq 1$. Badr *et al.* (1990) expanded the parameter range by performing two-dimensional simulations and experiments for Reynolds numbers between 10^3 and 10^4 for rotation rates of $0.5 \leq \alpha \leq 3$. The flow patterns obtained from the numerical simulations at $Re = 1000$ compared well with those from their experiments. They further showed that vortex shedding is suppressed for $\alpha > 2$. The numerical simulations of Chen *et al.* (1993) showed a single vortex being shed at $\alpha = 3.25$ at $Re = 200$.

Chew *et al.* (1995) investigated the flow dynamics of cylinder rotation at $Re = 1000$ for $\alpha \leq 6$ numerically by using a hybrid vortex method. Vortex shedding of the Kármán type ceased for $\alpha \geq 2$, where a closed streamline formed around the cylinder. The authors suggested that three-dimensional instabilities may occur in real flows in this regime. They further quantified the lift and drag coefficients. The shedding frequency was reported to increase as the rotation rate increased.

Two-dimensional numerical simulations were performed for $Re < 160$ and $\alpha < 2.5$ by Kang *et al.* (1999), following which the lift and drag coefficients were quantified. The critical Reynolds number for the transition to periodic flow increased as rotation rate was increased, with the dependence being logarithmic. They further reported that the Strouhal number was independent of the rotation rate, while being strongly dependent on the Reynolds number. The mean lift force was found to increase and the mean drag force decreased as the rotation rate was increased. The pressure force on the rotating cylinder contributed to over 90% of the lift force at low Reynolds numbers. Further, the amplitude of the lift coefficient remained constant with rotation rate, while the amplitude of the drag coefficient increased linearly with rotation rate.

Stojković *et al.* (2002) performed two-dimensional finite-volume numerical simulations for $Re \leq 100$, and rotation rates of $\alpha < 12$. For $Re = 100$, vortex shedding was suppressed at $\alpha = 1.8$ and reappeared for a narrow range of $4.8 \leq \alpha \leq 5.15$. They performed three-dimensional

simulations with periodic boundary conditions to confirm that the shedding occurs irrespective of the flow having a spanwise component. Various relations between the force coefficients with rotation rates were obtained at low Reynolds numbers. In a subsequent investigation, Stojković *et al.* (2003) obtained the stability diagrams for $Re \leq 200$. The shedding frequency was found to be much lower than that in the initial shedding regime. Furthermore, they quantified the drag force coefficient at various rotation rates. On increasing the rotation rate, the averaged drag force was initially found to decrease until the onset of the secondary shedding, where the drag force coefficient increased marginally before becoming negative and then increased for rotation rates past the secondary instability.

Numerical simulations have been performed by Mittal & Kumar (2003) at $Re = 200$ for a wide range of rotation rates ($0 \leq \alpha \leq 5$). Two shedding regimes were reported. For $0 \leq \alpha \leq 1.91$, double sided vortex shedding was observed. In this first shedding regime, the reduction in the lateral width of the wake and the decrease in the shedding frequency was reported. The wake was displaced away from the centreline as the rotation rate was increased. For $\alpha \gtrsim 2$, the disappearance of vortex shedding was reported until higher values of α . Vortex shedding reappeared between $4.35 \leq \alpha \leq 4.76$, where one sided shedding occurred. The frequency of shedding in second regime was found to be quite low.

A similar study performed by Stojković *et al.* (2003) showed that the range of α at which the two shedding regimes (two- and one-sided) existed varied with Reynolds number. The upper limit at which primary shedding ceased increased monotonically with Reynolds number. The range at which secondary shedding was observed shifted to the lower rotation rates at high Reynolds numbers. Also, the range was narrower at lower Reynolds numbers. The Strouhal number in the secondary vortex shedding regime was found to be much lower than that in the primary shedding regime. The Strouhal number was found to be dependent more on the rotation rate than the Reynolds number.

The effect of three-dimensional instabilities at higher rotation rates has been investigated by Mittal (2004) for $\alpha = 5$ at $Re = 200$. The two-dimensional flow field is steady while the three-dimensional simulations show the growth of centrifugal instabilities. They also tested the effect of various boundary conditions for cylinders of different aspect ratios (the ratio of the cylinder diameter to its length). For aspect ratios of 5, 10 and 15 with slip walls, the time-history of the drag coefficient showed oscillatory behaviour. The cylinder with lower aspect ratio and slip walls resembled two-dimensional flow (which was steady). However, longer aspect ratio cylinders with no-slip walls showed fluctuations, primarily because of the interaction of the boundary layer of the wall and the rotating cylinder. The three-dimensional flow was associated with centrifugal instabilities of around $1D$ spanwise wavelength. This instability was predicted to cause a reduction in lift and increase in drag.

The onset of three-dimensionality for rotation rates of $\alpha > 0$ had not been investigated until recently, although it has been generally stated that the flow is three-dimensional beyond $Re = 200$. Akoury *et al.* (2008) performed direct numerical simulations in two- and three-dimensions for a rotating cylinder. From their two-dimensional studies, they mapped the variation of St at increasing rotation rates at different Reynolds numbers for $\alpha \leq 6$. The secondary shedding regime, where a single-sided vortex is shed from the cylinder, broadened at higher Reynolds number, with the regime shifting towards lower rotation rates. This was attributed to the decreasing influence of the viscous component at higher Reynolds numbers (Stojković *et al.* 2003). This secondary regime occurred between $\alpha = 4.75$ and $\alpha = 5.25$ at $Re = 100$, while at $Re = 500$, secondary shedding occurred in the range $3.6 \leq \alpha \leq 5$. The Strouhal number was $\simeq 0.05$, much lower than that observed for the spinning cylinder at low rotation rates, consistent with the findings of Mittal & Kumar (2003). The Strouhal number decreased as rotation rate was increased in this regime. Three-dimensional simulations were performed for the cylinder rotating at $\alpha \leq 1.5$. At $Re = 300$, the growth of the spanwise component of velocity grew steadily, indicating the onset

of three-dimensional flow. This transition was found to occur through a supercritical bifurcation. Using Landau modelling, they determined the critical flow speed for the transition to three-dimensional flow for $\alpha = 0.5$ to occur at $Re_c = 219.8$. Further investigations at $\alpha = 1.5$ and $Re = 200$ showed the damping of the spanwise component of flow, indicating two-dimensional flow. Using proper orthogonal decomposition, they reconstructed the three-dimensional modes for $\alpha = 0.5$, which have the spanwise wavelength of the mode A instability ($\simeq 4D$), similar to that of a non-rotating cylinder at the onset of three-dimensionality (Williamson (1988), Thompson *et al.* (1996)). Furthermore, at $Re = 300$, the wake retained its mode A structure, possibly due to enhanced stability of the vortex pairs attributed to the vorticity induced by cylinder rotation in the spanwise direction. The critical values at the onset of three-dimensional flow at higher rotation rates was not stated.

Recent experimental investigations were performed by Kumar *et al.* (2011) for $Re \leq 400$ and $\alpha \leq 5$ using the hydrogen bubble technique to obtain flow field visualisations to replicate the secondary shedding regime. At $Re = 200$, they report that the vortex street behind the body is deflected for $\alpha \leq 1.9$, beyond which the vortex shedding became less pronounced with the wake forming a sinuous pattern until $\alpha \simeq 2$, where steady flow is observed. Furthermore, the single-sided vortex shedding found numerically by Mittal & Kumar (2003) was confirmed by the use of Particle Image Velocimetry (PIV). In addition, they visualised the flow field for $Re = 300$ and 400 and computed the Strouhal number. In the primary shedding mode, the shedding frequency was found to be independent of the rotation rate. The experimentally obtained Strouhal numbers in the secondary regime were consistent with those obtained by the numerical investigations of Akoury *et al.* (2008) and Mittal & Kumar (2003). The development of the spanwise structures in the wake has not been discussed.

Recent linear stability investigations by Meena *et al.* (2011), at $Re = 200$ for $3 \leq \alpha \leq 5$, indicate the presence of modes with purely real growth rates (indicating they are synchronised with the two-dimensional flow) for $\alpha \leq 4.3$. Their three-dimensional investigations show what appear to be centrifugal instabilities near the cylinder and the time histories of the force coefficients indicate the onset of aperiodic flow.

All of these previous studies indicate that the flow is a function of both Re and α , with a wide variety of vortex shedding regimes and three-dimensional modes occurring. This paper is therefore a systematic study of the wakes of rotating cylinders as a function of both these variables. The remainder of this article is organised as follows. The numerical method employed in our investigations is detailed in §3, supplemented by validation studies. This is followed by the presentation of results. In that section, first the two-dimensional flow structures observed as a function of Re and α are described in §4. Particular attention is paid to the transition from steady to unsteady flow. This is followed by the results of linear stability analysis in §5, investigating the transition to three-dimensional flow from the established two-dimensional flows. Curves of marginal stability of each of these three-dimensional modes are presented in the Re, α plane, and the characteristics of each of these modes are described. Physical mechanisms of instability are proposed for a number of these modes. This is followed by some concluding remarks.

2. Problem definition

A schematic diagram of the problem under consideration is shown in figure 1. The cylinder of diameter D spins in an anticlockwise sense at a constant angular velocity, ω . The oncoming uniform flow velocity is represented by U . Results for $0 \leq Re \leq 400$ and $0 \leq \alpha \leq 2.5$ are presented.

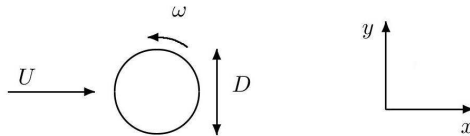


Figure 1: Schematic representation of the spinning cylinder in freestream.

3. Numerical formulation

3.1. Fluid flow equations

For the base flow, the incompressible Navier-Stokes equations are solved in two dimensions using a spectral-element approach. The computational domain consists of quadrilateral elements which are concentrated in the regions of high velocity gradients to accurately capture the flow dynamics. The boundaries of these quadrilateral elements are straight except in the vicinity of the cylinder, where curved edges are used to accurately represent the circular cylinder. These elements are further subdivided with internal node points distributed according to the Gauss-Legendre-Lobatto quadrature points, with the velocity and pressure fields represented by tensor products of Lagrangian polynomial interpolants. Despite being only formally C_0 continuous across element boundaries, these methods are known to provide spectral convergence as the polynomial order is increased (Karniadakis & Sherwin 2005). The number of node points ($N \times N$) can be specified at runtime with the interpolant polynomial order in each direction being $N - 1$. A second-order fractional time-stepping technique is used to sequentially integrate the advection, pressure and diffusion terms of the Navier-Stokes equations forward in time. The unsteady solver is used to investigate the parameter range covering both the steady and unsteady regimes of flow.

More details of the solver can be found in Thompson *et al.* (2006a); and the solver has been previously used in the studies of bluff body flows (Thompson *et al.* 1996; Leontini *et al.* 2007; Thompson *et al.* 2006b) and in the studies of flows over rolling cylinders near a wall (Stewart *et al.* 2006, 2010; Rao *et al.* 2011).

It may be recalled that the critical parameters for transition are sensitive to the placement of boundaries and the resolution of the wake. In order to reduce blockage effects to acceptable levels, the boundaries of the domain have been placed at $100D$ from the cylinder in all directions.

3.2. Linear stability analysis

The focus of this investigation is to determine the three-dimensional stability of the two-dimensional base flows to perturbations with an imposed spanwise wavelength. Equations for the evolution of perturbations are formed by first decomposing the velocity and pressure fields into base and perturbation components. This decomposition is then substituted into the governing Navier-Stokes equations, and the terms for the base flow subtracted out. The resulting equations are then linearised by removing the quadratic perturbation term. Because the coefficients do not depend on z , the perturbation fields can be decomposed into a set of Fourier modes in the spanwise direction, and the perturbation equations then reduce to a set of decoupled equations describing the different spanwise modes. The process of forming these equations is well described in Barkley & Henderson (1996). The result is that perturbation fields for an imposed spanwise wavelength can be solved for.

The eventual perturbation equations can be viewed as a linear operator that takes the perturbation solution from one time to another. If the base flow is periodic, this results in an operator

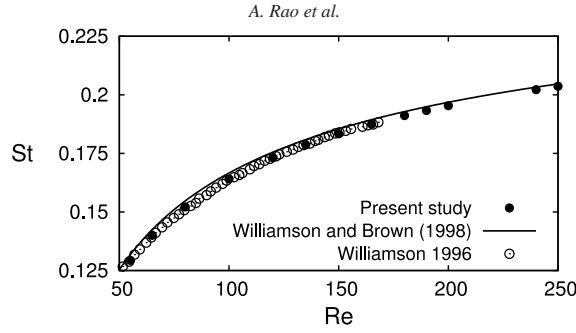


Figure 2: Verification of the spectral-element code and the domain used. Comparisons with previous results of the vortex shedding frequency for a fixed cylinder in two-dimensional flow. The solid line is the three-term fit for $St - Re$ variation below $Re < 1000$ from Williamson & Brown (1998).

that takes the perturbation from one period to the next. This operator is never explicitly formed; application of the operator is obtained by simply integrating the perturbation equations forward in time. Eigenvalues μ of this operator indicate whether the base flow is steady to perturbations of a prescribed wavelength; $|\mu| < 1$ indicates that the flow is stable as perturbations decrease in size from one period to the next; $|\mu| > 1$ indicates that the base flow is unstable as perturbations grow from one period to the next. For periodic problems, μ is referred to as the Floquet multiplier. Marginal stability occurs when $|\mu| = 1$.

Of interest are the eigenmodes (Floquet modes or linear instability modes) with the largest eigenvalues, as these are the modes which grow the fastest (or decay the slowest). As the linear operator is never explicitly formed, these leading eigenmodes and eigenvalues are found through indirect iterative methods. Here, an Arnoldi method is employed (e.g., Mamun & Tuckerman 1995) that can resolve the leading eigenmodes and the complex component of the eigenvalues of μ . When μ is purely real and positive, the periodicity of the three-dimensional mode is synchronous with the base flow; e.g., modes A and B, which are observed in the wake of a non-rotating cylinder, are purely real modes (Barkley & Henderson 1996). When μ is complex, the eigenmode introduces a new frequency. If the base flow is steady, this predicts that the three-dimensional flow will be periodic; if the base flow is periodic, the introduction of this second frequency predicts that the three-dimensional flow will be quasi-periodic. Finally, if the Floquet multiplier is purely real but negative, subharmonic modes are predicted. Further details of this method and its implementation can be found in Stewart *et al.* (2010).

3.3. Comparisons with previous studies

Shown in figure 2 is a comparison of the St with Re for the non-rotating cylinder in freestream, with the values of Strouhal number, St , from the current study and those from Williamson (1996a). Here, $St = fD/U$, where f is the frequency of vortex shedding. The comparison is excellent. The solid line in the figure is from the three-term fit by Williamson & Brown (1998), where the St is given by

$$St = (0.2731 - \frac{1.1129}{\sqrt{Re}} + \frac{0.4821}{Re}). \quad (3.1)$$

Spatial resolutions studies were carried out for the rotating cylinder at $\alpha = 2$ and $Re = 400$ to investigate the accuracy of the predictions. This study was performed at the highest rotation rate for which the unsteady flow was observed. The solutions at $N \times N = 49$ converge to within

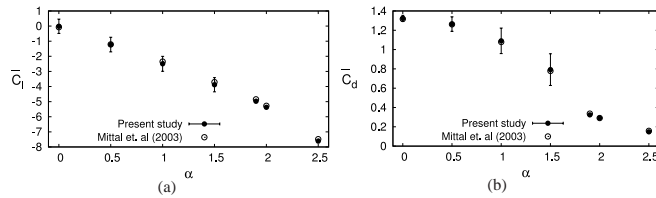


Figure 3: Comparison of the time-averaged force coefficients with the results from Mittal & Kumar (2003). Variation of the (a), time-averaged lift coefficient, \bar{C}_l , (b) and drag coefficient, \bar{C}_d . The vertical error bars represent one standard deviation of the instantaneous force coefficients.

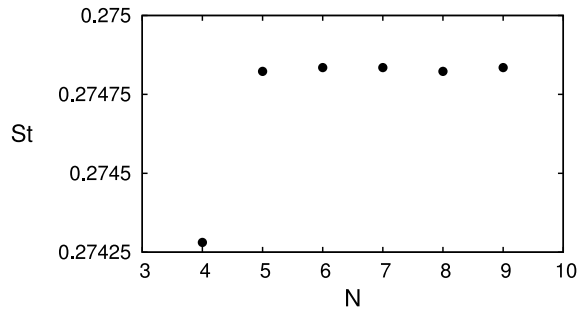


Figure 4: Spatial resolution study at $\alpha = 2$ and $Re = 400$. Variation of the shedding frequency with increasing internal node points is shown.

0.2% of the maximum tested resolution at $N \times N = 81$. Furthermore, the values of the time-averaged force coefficients for a resolution of $N \times N = 36$ are well within 1% of the maximum tested values. A resolution of $N \times N = 49$ was therefore determined to be sufficient to capture the forces accurately up to $\alpha \leq 2.5$, however a resolution of $N \times N = 64$ was used to accurately capture the forces for all rotation rates beyond $\alpha > 2$. Shown in figure 3 is the comparison of the time-averaged lift and drag coefficients with rotation rate. Shown in figure 4 is the variation of St on increasing internal node points. The figures show that the selected resolution is adequate to resolve the flow accurately.

A linear stability analysis validation study was also performed for the non-rotating cylinder at $Re = 280$, and the growth rates obtained were compared with the results of Barkley & Henderson (1996). The growth rates of the two primary modes (modes A and B) from Barkley & Henderson (1996) match closely with the results of the present study. The very slight differences can be attributed to difference between the domain sizes in the computational domains used.

4. Flow structures

Over the range of the parameters tested, three two-dimensional flow regimes have been identified. Instantaneous snapshots of vorticity providing examples of each of these regimes are presented in figure 6, all at $\alpha = 1.9$. The regimes shown are the steady regime (figure 6(a), 6(b), and 6(d)), the low frequency regime (figure 6(c), 6(g), and 6(h)) and the high frequency regime

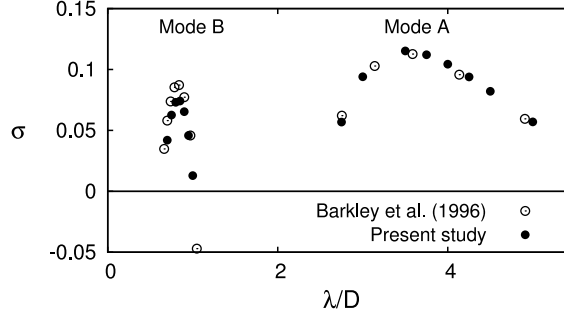


Figure 5: Validation of the stability analysis at higher Reynolds numbers for a non-rotating cylinder: comparison of the growth rate at different spanwise wavenumbers at $Re = 280$. Open circles (\circ) represent the values of Barkley & Henderson (1996), while closed circles (\bullet) represent the values from the present study. The neutral stability line at $\sigma = 0$ is marked by a solid line.

(figure 6(e) and 6(f)). As for the limiting case of a stationary cylinder, at low Reynolds numbers the flow is steady. For $\alpha \lesssim 1.95$, periodic vortex shedding is found to occur above a critical Reynolds number, which is a function of α . For $\alpha \gtrsim 1.95$, the two-dimensional flow was found to remain steady up to at least $Re = 400$.

However, as the sequence of images of figure 6 show, increases in Re restabilise the two-dimensional flow, for a narrow band of α centred around $\alpha = 1.9$. This indicates that the value of Re at the steady-unsteady transition is not a monotonic function of α . This finding is further expanded upon in § 5.

The periodic vortex shedding can be further divided into two regimes, based upon the frequency of the oscillation. The variation of the shedding frequency as a function of Re , for $1.8 \leq \alpha \leq 2.0$, is shown in figure 7. Clearly discernible is the development of two “branches”, with a “high” frequency and “low” frequency branch appearing for $Re \geq 260$. At $\alpha = 1.8$, the $St-Re$ curve is continuous. For $\alpha \geq 1.9$, the behaviour is much more complex. Taking $\alpha = 1.9$ as an example, for $Re < 190$, the frequency of oscillation remains on the low frequency branch. For $190 < Re < 260$, the flow is stabilised, and no vortex shedding occurs (figure 6(d)). Then for $260 \lesssim Re \lesssim 340$, the vortex shedding moves to the high frequency branch (figure 6(e)), before dropping back again to the low frequency branch for $Re > 340$ (figure 6(h)).

Shown in figure 8 are force coefficient phase diagrams for $\alpha = 1.9$ at the specified Reynolds numbers. The variation of the drag coefficient with lift coefficient is shown over one complete period of shedding. The flow states in the steady regimes are represented by singular points, while those in the periodic states are characterised by closed orbits. These phase diagrams also provide an indication of the amplitude of shedding. The amplitude of force (and wake) oscillations is small at low Reynolds numbers, and remains so on the “high” frequency branch. In comparison, larger amplitudes observed at high Reynolds numbers, when the flow returns to the “low” frequency branch.

5. Stability analysis

The results presented in § 4 show that, over the parameter space investigated, all of the two-dimensional flows are either steady or periodic. This means that all are amenable to either linear stability analysis (for the steady flows) or Floquet stability analysis (for the periodic flows). In

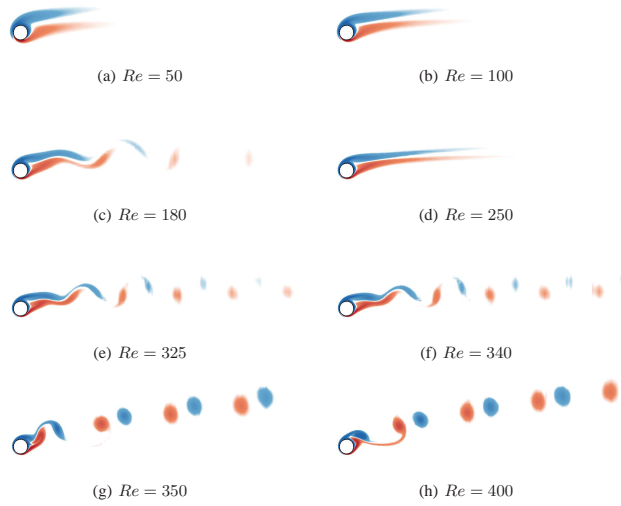


Figure 6: Flow structures at $\alpha = 1.9$ at the specified Reynolds numbers. Contour levels between $\pm 5 D/U$. The flow is from left to right.

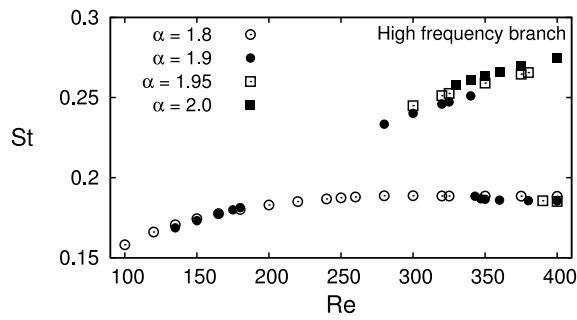


Figure 7: Variation of the shedding frequency with Reynolds numbers for the specified rotation rates. For $\alpha \geq 1.9$, two branches or regimes of shedding occur.

fact, the two techniques are effectively identical in practice, if the steady flow is treated as a flow with arbitrary period. Stability analysis was performed on the flows over the parameter space ($Re \leq 350, 0 \leq \alpha \leq 2.5$) to determine the critical transitional values for the onset of a number of three-dimensional modes, that govern the transition to three-dimensional flow.

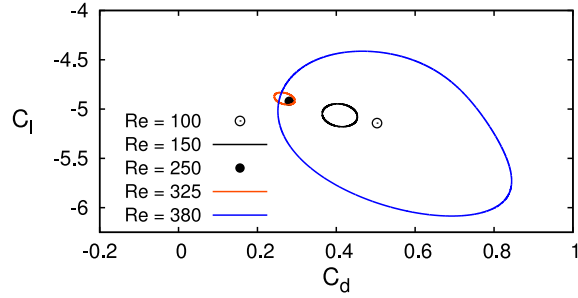


Figure 8: Phase diagrams of the force coefficients at the specified Reynolds numbers for $\alpha = 1.9$.

For the limiting case of a non-rotating cylinder ($\alpha = 0$), the transition to three-dimensionality has been well documented by various numerical studies (Barkley & Henderson 1996; Thompson *et al.* 1996) and is found to occur at $Re = 188.5 \pm 1$ for a spanwise wavelength of $\lambda/D = 3.96$. For a cylinder rotating at $\alpha = 0.5$, a recent study by Akoury *et al.* (2008) found the critical value of transition to three-dimensionality to occur at $Re = 220$. They report that the wake structure was similar to the mode A structure obtained for the flow past a non-rotating cylinder, and it remained unchanged at $Re = 300$. At much higher rotation rates of $\alpha = 5$, $Re = 200$, the primary cause of three-dimensionality has been attributed to centrifugal instabilities (Mittal 2004). The variation of the critical Reynolds number at other rotation rates has not been investigated. Therefore, a systematic study of the three-dimensional modes present in the (Re, α) plane is presented in § 5.1.

5.1. Transition diagram

Figure 9(a) shows curves of marginal stability for seven separate three-dimensional modes growing on the two-dimensional base flows outlined in § 4. Also shown is the boundary for the steady-unsteady transition. The results compare well with the predictions of Pralits *et al.* (2010) for $\alpha \leq 2$. The points on each of the curves denotes a point at which the marginal stability of the mode in question has been established; the curves have then been fitted to these points. As the majority of the modes' marginal stability curves occur in the top-right corner of the figure, this region is presented "zoomed in" in figure 9(b). These curves have been found by first resolving the two-dimensional flows over a grid of points in the (Re, α) plane, then performing the stability analysis over a spectrum of wavelengths at each of these points, and then refining this grid in the region of marginal stability for each mode. This process was very computationally intensive; the data for the current study consumed the order of 10^5 CPU hours.

There are a number of features of figure 9 that are examined in some detail in the following sections. First, the variation of the steady-unsteady transition is described. Following this, descriptions of each of the three-dimensional modes are presented, including the mode structure, critical wavelengths, spatio-temporal symmetries, and some further analysis and interpretation of the physical mechanisms of instability.

5.2. The steady-unsteady transition

For lower rotation rates ($\alpha \leq 1$), the transition to the unsteady regime occurs at a value of Re close to that of the non-rotating cylinder. However, for $\alpha \gtrsim 1.3$, small changes in the rotation

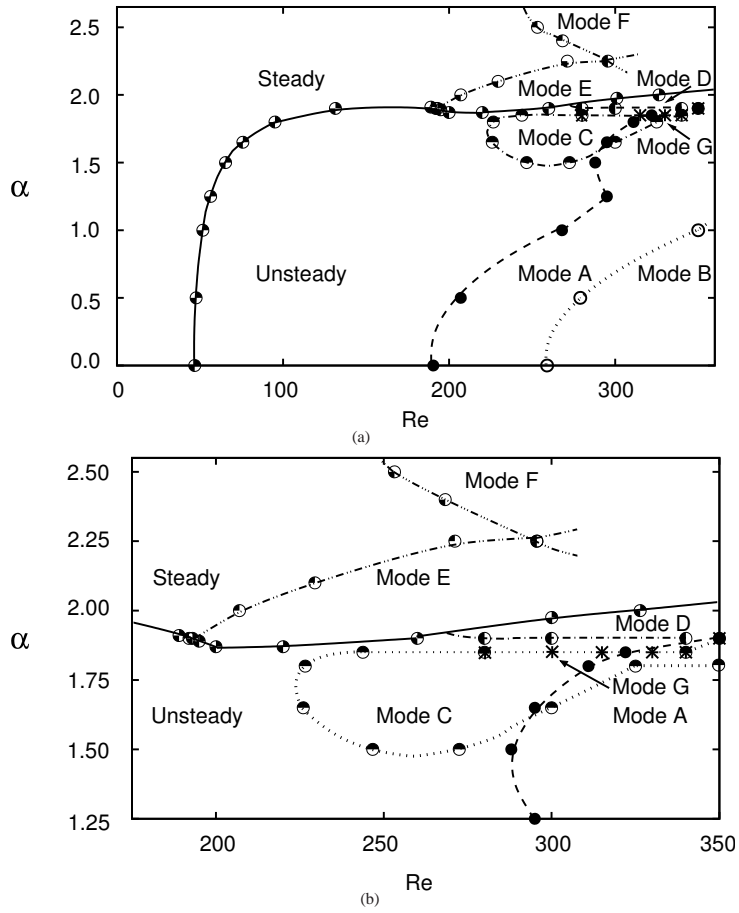


Figure 9: (a) Diagram showing the lines of marginal stability in the parameter space investigated. Modes are typically unstable to the right of each line. (b) Enlarged view of (a) between $1.25 \leq \alpha \leq 2.5$, $175 \leq Re \leq 350$. For both images, the steady-unsteady transition is marked by a continuous line, while the boundaries of the stability of the three-dimensional modes are shown by the broken lines.

rate rapidly shift the transition to higher Reynolds numbers. For $\alpha \geq 2.1$, the two-dimensional base flow is seen to remain steady up to at least $Re = 400$.

As shown in figure 6, for a small band of α centred around $\alpha = 1.9$, further increases in Re can restabilise the flow. This is shown particularly clearly in figure 9(b), where the solid line marking this transition is shown to descend over the range $180 < Re \lesssim 220$, and then ascend for $Re \gtrsim 220$. The cause of this complicated behaviour is not clear. The onset of the high-frequency regime shown in figure 7 roughly coincides with the point at which the curve again begins to ascend; it is therefore possible that this high-frequency regime is due to an instability of the stabilised flow, however further work is required to fully understand this phenomenon.

5.3. Properties of the three-dimensional modes

5.3.1. The mode A instability

For a non-rotating cylinder in freestream, the onset of three-dimensional flow is observed around $Re = 180$ in experiments, with a spanwise wavelength of approximately $4D$ (Williamson 1996b). This same mode has been observed numerically by the three-dimensional simulations of Thompson *et al.* (1996), and the linear stability analysis (Barkley & Henderson 1996) explained the basis of the transition. This mode is referred to as mode A and for a non-rotating cylinder has been shown to be the fastest-growing linear mode up to $Re = 280$ (also see figure 5). The physical mechanism of this mode has been associated with an elliptic instability of the forming vortex cores (Thompson *et al.* 2001; Leweke & Williamson 1998).

From the stability analysis of this paper, mode A is found to persist for $\alpha \leq 1.9$, over the entire range where the two-dimensional base flow is unsteady. As shown in figure 9, the critical Reynolds number with respect to the marginal stability of mode A is a strong function of α . For $\alpha \leq 1.25$, the critical Reynolds number increases on increasing the rotation rate. Over this range, mode A is also the first mode that occurs with increasing Re , and so will lead the transition to three-dimensionality. The Floquet multiplier obtained is positive and real.

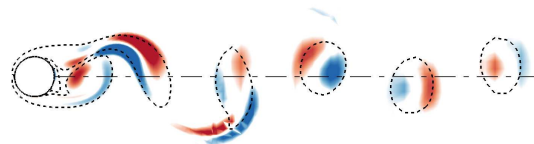
Previous studies using fully three-dimensional DNS (Akoury *et al.* 2008) have found that, for $\alpha = 0.5$, the critical Reynolds number for the transition to three-dimensional flow occurred at $Re \simeq 220$. This result matches well with the curve of marginal stability for mode A in figure 9(a).

The critical wavelength at the onset of this instability was approximately $4D$. At a higher rotation rate of $\alpha = 1.5$, the transition occurs at $Re_c \simeq 288$, and occurs at higher Reynolds numbers as the rotation rate is increased (figure 9).

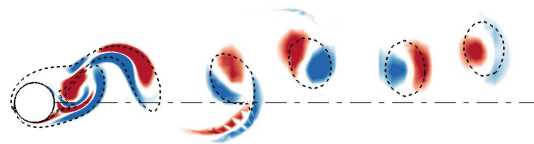
Shown in figure 10 are the perturbation vorticity contours at Reynolds numbers just beyond the critical Re , for a series of increasing α . The images are all shown at a similar phase in the vortex shedding process of the base flow. The images show that the spatial structure of this mode is essentially retained at higher rotation rates, regardless of the fact that the vortex shedding becomes increasingly asymmetric about the centreline with increasing α .

5.3.2. The mode B instability

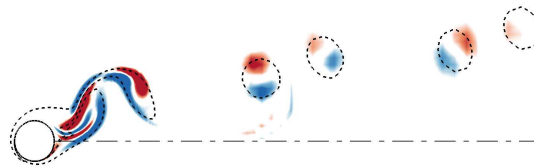
For a non-rotating cylinder, mode B is observed to become unstable at Reynolds numbers higher than that observed for mode A. In the experimental visualisations of Williamson (1988), this mode was observed intermittently alongside mode A for $Re \simeq 230$ with a spanwise wavelength of approximately $1D$. The numerical simulations of Barkley & Henderson (1996) predicted the onset of this linear mode from the two-dimensional base flow at $Re = 259$ with a spanwise wavelength of $\lambda \simeq 0.8D$. The contrast to the experimental findings is due to the fact, in experiments, the flow is already three-dimensional due to the presence of mode A. Barkley *et al.* (2000) showed the presence of mode A is destabilising on the mode B instability, leading to mode B occurring at lower Reynolds numbers in experiments. The linear mode associated with



(a) $\alpha = 0$, $Re = 200$, $\lambda/D = 4$



(b) $\alpha = 1$, $Re = 280$, $\lambda/D = 4$



(c) $\alpha = 1.9$, $Re = 350$, $\lambda/D = 4$

Figure 10: Spanwise perturbation vorticity contours in the wake of the rotating cylinder between levels ± 0.1 at the specified rotation rates and Reynolds number at an arbitrary time in the shedding cycle. Base flow vorticity contours at levels $\pm 1 U/D$ are overlaid as dashed lines. A centreline line is drawn in the streamwise direction behind the cylinder.

mode B is the fastest growing mode for $Re > 300$ (Blackburn *et al.* 2005; Barkley & Henderson 1996) for the non-rotating cylinder.

The simulations of this paper recover mode B, and show that it continues to exist up to at least $\alpha = 1$. Similar to the non-rotating cylinder, the Floquet multiplier for this mode remains purely real and positive. As shown on figure 9(a), the value of Re at marginal stability is a strong function of α , increasing as α is increased. However, the characteristic wavelength is relatively unaffected by α , remaining close to $\lambda = 0.8D$. Over the range of the parameter space tested,

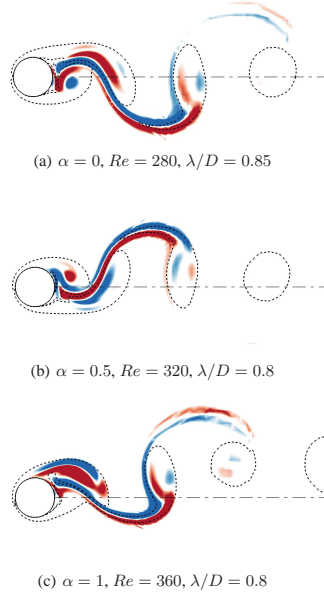


Figure 11: Spanwise perturbation vorticity contours showing the mode B type structures observed at higher Reynolds numbers for the specified rotation rates. The contour shading is as per figure 10.

mode B is always found to become unstable at Re higher than that at which mode A becomes unstable.

Figure 11 shows the perturbation vorticity contours of mode B at rotation rates of $\alpha = 0, 0.5$ and 1 . Note that for the case at $\alpha = 0.5$ (figure 11(b)), the base flow is approximately half a period out of phase with respect to the other images, however the similarity in the structure of the mode is evident. For all α , the perturbations grow strongly in the braid regions between the shed vortices, similar to that observed for a non-rotating cylinder (shown as $\alpha = 0$ in figure 11(a)).

5.3.3. The mode C instability

The previous modes described, A and B, are basically extensions of the modes found in the wake of a non-rotating cylinder. However, there are a number of modes presented on figure 9 that occur only for the rotating cylinder. The first of these is mode C.

The mode C instability occurs in an apparently closed region of the (Re, α) plane, centred around $Re = 260, \alpha = 1.7$. The Floquet multiplier for mode C is purely real but negative, indicating that this mode is subharmonic, repeating over two cycles of the base flow. The critical spanwise wavelength for this mode is marginally higher than mode B, but lower than mode A, and encompasses the range $0.8 < \lambda_c/D < 1.2$ (Sheard *et al.* 2005a).

The group theory analysis of the symmetries of bluff body wakes of Blackburn *et al.* (2005)

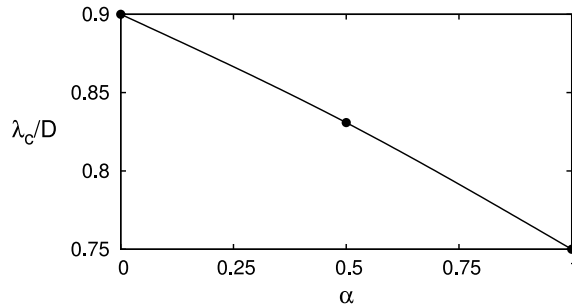


Figure 12: Variation of the spanwise wavelength of the mode B instability at marginal stability as a function of rotation rate, α .

shows that for flows with the spatio-temporal symmetry of the wake of a non-rotating cylinder (reflection about the wake centreline plus evolution in time of half a period), subharmonic instabilities are not generic, and are therefore not likely to be discovered. However, once this spatio-temporal symmetry is broken, subharmonic modes become possible. Here, the spatio-temporal symmetry is broken by the rotation of the cylinder, hence the presence of the subharmonic mode C. In structure, mode C appears very similar to the subharmonic mode C found in the wakes behind rings (Sheard *et al.* 2003, 2005*a,b*). In both of these flows, the symmetry is broken by a local acceleration of the flow on one side of the body; here the acceleration is due to the rotation of the cylinder, in ring wakes it is caused by the acceleration of the flow through the constriction of the centre of the ring. Similar subharmonic modes have been found in other wake flows, such as cylinders with trip wires (Zhang *et al.* 1995), and in the wakes of transversely oscillating cylinders after undergoing spontaneous transition to a $P + S$ base state (Leontini *et al.* 2007), and more recently in the wakes of inclined square cylinders (Sheard 2011; Sheard *et al.* 2009).

Shown in figure 13 are the instantaneous perturbation vorticity contours of mode C at half-period intervals at $\alpha = 1.5$, $Re = 250$. Clearly, the perturbation field reverses in sign every period, indicating that this mode is periodic over $2T$, where T is the period of the two-dimensional periodic base flow.

The growth rates of mode C are highest in the centre of the region over which it is unstable. Unlike mode A or mode B, the magnitude of the Floquet multiplier does not show a monotonic increase with rotation rate. Shown in figure 14 are the variation of growth rate at constant rotation rate (figure 14(a)), and at a constant Reynolds number (figure 14(b)). These values have been chosen to traverse the region where mode C is unstable. The figures show conclusively the closed boundary region of the mode C instability, and the variation of the growth rate σ with both Re and α .

5.3.4. The mode D instability

The mode D instability develops on the unsteady base flow, becoming unstable in a narrow region of the parameter space, for values of α just below those at which the base flow is stabilised, as shown on figure 9. The Floquet multiplier for this mode is real and positive. The mode grows with a characteristic spanwise wavelength of approximately $2D$.

Of particular interest is the region of occurrence of this instability; it occurs in essentially the same region of the parameter space as the high frequency shedding regime (figure 7 and figure

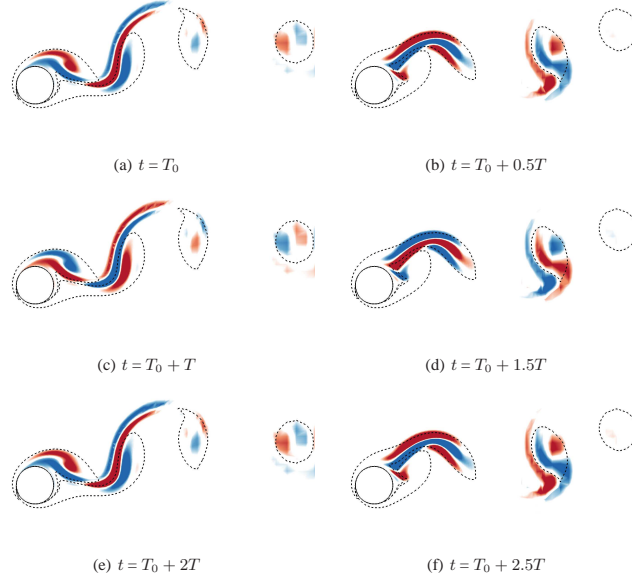


Figure 13: Spanwise perturbation vorticity contours of mode C at $\alpha = 1.5$, $Re = 250$, $\lambda/D = 1.2$, shown over a period of $2.5T$. Contour shading is as per figure 10. The perturbation vorticity contours are identical after two periods of the base flow.

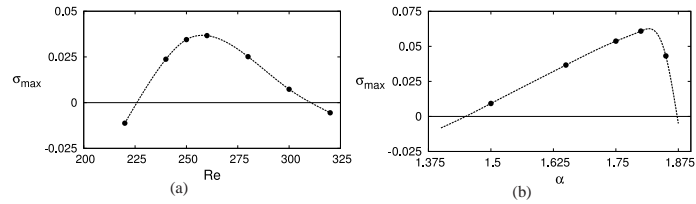


Figure 14: Variation of the maximum growth rate (σ_{max}) with respect to wavenumber (λ/D), for the mode C instability: (a) at constant rotation rate of $\alpha = 1.65$; and (b) constant Reynolds number $Re = 260$. These indicate the closed region of instability for mode C.

9). This high frequency shedding regime consists of two highly strained vortices trailing the cylinder, and small vortices are emitted from the end of these (see, for example, figure 6).

This instability grows in the region between these two strained vortices. Shown in figure 15 are the spanwise and streamwise perturbation vorticity contours at $\alpha = 1.9$ and $Re = 300$. This structure is very similar to mode E, described next, which grows on the steady base flow.

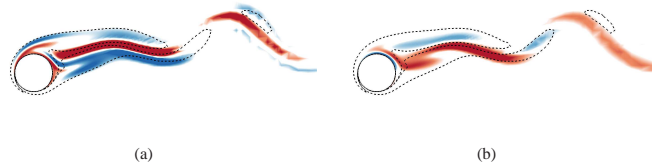


Figure 15: Perturbation vorticity contours in the wake of the rotating cylinder at $\alpha = 1.9$, $Re = 300$, $\lambda/D = 1.9$, highlighting the perturbation field structure for Mode D. (a) Spanwise vorticity. (b) Streamwise vorticity. Contour shading is as per figure 10.

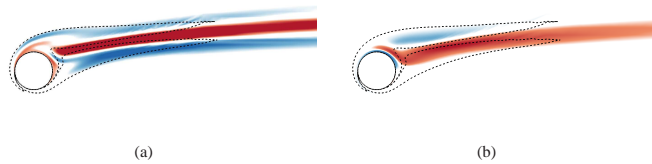


Figure 16: Perturbation vorticity contours in the wake of the rotating cylinder for mode E at $\alpha = 2$, $Re = 220$, $\lambda/D = 2.0$. (a) Spanwise vorticity. (b) Streamwise vorticity. Contour shading is as per figure 10.

In particular, disregarding the steady or unsteady nature of the base flow, the perturbation field structures appear similar. It is therefore hypothesised that modes D and E occur due to the same physical instability mechanism.

5.3.5. The mode E instability

The first three-dimensional mode to become unstable as α is increased on the steady base flow is mode E. The multipliers, or growth rates, for this mode are purely real, indicating that when this mode becomes unstable, it triggers a transition from a two-dimensional steady state to a three-dimensional steady state. The characteristic wavelength for this mode is approximately $2D$, again consistent with mode D. The spanwise wavelength at which the maximum growth rate occurs decreases as the Reynolds number is increased.

Shown in figure 16 are the perturbation vorticity contours for $\alpha = 2$ and $Re = 220$, showing an example of mode E. As already discussed above, this mode has similar characteristics to those of the mode D instability. The regions of high perturbation amplitude are similar to those of mode D in the near wake, while the instability extends in the flattened wake far downstream of the cylinder.

5.3.6. Physical nature of the mode D and E instability

Figure 17 shows the spanwise and streamwise perturbation vorticity as colour contours, overlaid with the streamlines of the base flow, for $\alpha = 2$, $Re = 220$. The base flow vorticity contours of figure 16 for the same case show regions of positive and negative vorticity in the wake. However, the streamlines of figure 17 show that only a single recirculation region exists.

Figure 17 shows that the perturbation vorticity is mostly focussed in a thin region emanating

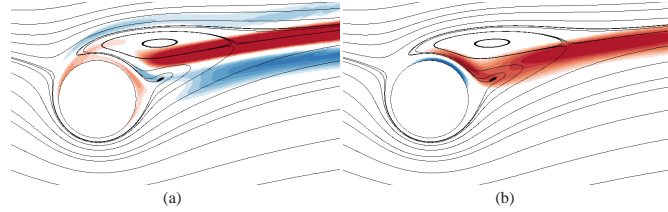


Figure 17: Perturbation vorticity contours, overlaid with streamlines, in the wake of the rotating cylinder for mode E at $\alpha = 2$, $Re = 220$, $\lambda/D = 2.0$. (a) Spanwise vorticity. (b) Streamwise vorticity. Contours range between ± 0.6 for spanwise vorticity, ± 0.4 for streamwise vorticity. The figure shows that the mode is focused in the extensional regions emanating from the hyperbolic point at the rear of the recirculation region.

both upstream and downstream of the hyperbolic stagnation point at the rear of this recirculation region. This region of the base flow is characterised by a stretching in the flow direction (along the streamlines); fluid particles increase in speed as they leave the hyperbolic point in this direction. Lagnado *et al.* (1983) showed, in an inviscid setting, that simple extensional flows lead to an amplification of perturbation vorticity. Leblanc & Godefert (1999) showed that in Taylor-Green cells (a square geometry containing four rotating cells of fluid, creating a hyperbolic point at the centre), the perturbation vorticity was most amplified along the streamlines leaving the hyperbolic point, forming rib vortices in between the rotating cells. A similar amplification mechanism has been proposed by Lewke & Williamson (1998) as the cause of the mode B instability.

Due to the clear amplification of perturbation vorticity along the streamlines leaving the hyperbolic point in figure 17, it is therefore proposed that this is the amplification mechanism that leads to mode E becoming unstable. The similarity in structure of the perturbation vorticity for modes D and E (albeit that mode D is periodic, with vortex shedding occurring downstream of the recirculation region as shown in figure 15) suggests that it is this same stretching mechanism that leads to the instability of mode D.

5.3.7. The mode F instability

A second three-dimensional mode is found to grow on the steady base flow, designated as mode F. This mode typically occurs at higher rotation rates ($\alpha \geq 2.25$) than mode E. The characteristic wavelength of this mode is approximately $0.45D$, much shorter than mode E which grows in region between the highly strained standing vortices in the wake.

Shown in figure 18 are the vorticity contours at $\alpha = 2.5$, $Re = 280$. The figure shows that mode F grows primarily in the boundary layer of the spinning cylinder, and in the near wake.

The Floquet multipliers for this mode occur in complex conjugate pairs. This indicates that while the two-dimensional base flow is steady, transition to this mode marks a transition to three-dimensional flow and the onset of time dependence.

The frequency of this time dependence can be ascertained from the complex component of the Floquet multiplier. This was done for values of $2.25 \leq \alpha \leq 2.5$. The frequencies calculated from these multipliers are presented in figure 19. The three-dimensional shedding frequency at the onset of the instability is computed as follows: $St_{3D} = \tan^{-1}(\text{Im}(\mu)/\text{Re}(\mu))/2\pi T$, where St_{3D} is the three-dimensional shedding frequency and T is the period of sampling. This frequency was also determined independently by directly measuring the perturbation field period to ensure that the choice of T had not caused aliasing to a different frequency. For all rotation rates at which this mode is unstable, the three-dimensional frequencies are low, considerably lower than

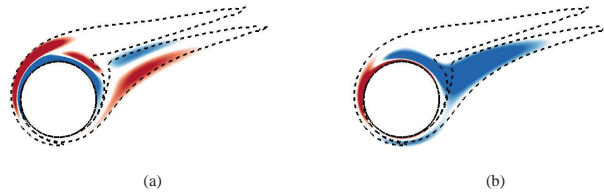


Figure 18: Perturbation vorticity contours in the wake of the rotating cylinder for mode F at $\alpha = 2.5$, $Re = 280$, $\lambda/D = 0.45$. (a) Spanwise vorticity. (b) Streamwise vorticity. Contour shading is as per figure 10.

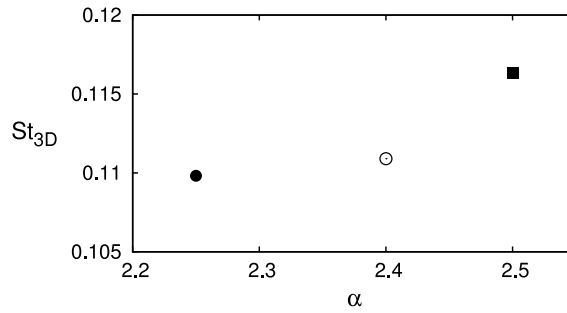


Figure 19: Variation of St_{3D} for the three rotation rates ($\alpha = 2.25$ (•), 2.4 (◊) and 2.5 (■)) at Reynolds number just beyond the onset of instability for mode F.

those of the unsteady two-dimensional base flows at lower values of α . Fully three-dimensional DNS, or experiments, are required to see if this predicted frequency corresponds to that found in the fully saturated three-dimensional flow, and what saturated spatial wake structure this three-dimensional flow will take.

5.3.8. Physical nature of the mode F instability

As discussed in the introduction, it has already been speculated that the higher rotation rate flows are subject to a centrifugal instability (e.g., Mittal 2004; Meena *et al.* 2011). The generalised centrifugal theory of Bayly (1988) has therefore been applied to investigate the nature of this instability mode. That work extends the classical analysis of Rayleigh (1917) to non-axisymmetric inviscid flows with closed streamlines. More recently it has been applied to analyse the recirculating flow downstream of a bump (Gallaire *et al.* 2007) and a semicircular hill (Griffith *et al.* 2007). In addition, there have been extensions of the theory to other cases such as to nonzero azimuthal wavenumbers (Billant & Gallaire 2005), and to rotating systems (Sipp & Jacquin 2000).

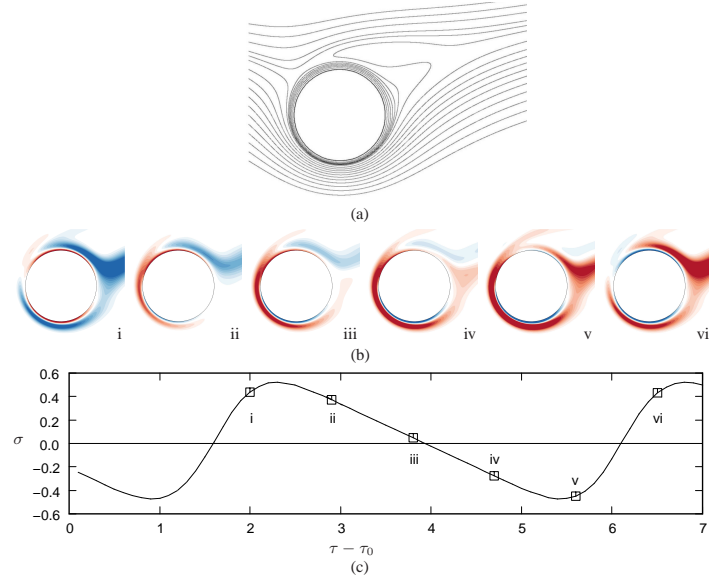


Figure 20: Physical evidence of centrifugal instability leading to mode F at $Re = 280$, $\alpha = 2.4$, for a wavelength $\lambda/D = 0.45$. (a) Streamlines of the base flow in the neighbourhood of the cylinder showing that the streamlines are closed in the vicinity of the cylinder. (b) Evolution of the perturbation streamwise vorticity field over half a period: (i) $t = 0T/10$; (ii) $T/10$; (iii) $2T/10$; (iv) $3T/10$; (v) $4T/10$; (vi) $5T/10$; where T is the period of the global instability. This progression shows that the period of the instability corresponds to the time taken for the perturbation to orbit the cylinder twice. (c) Instantaneous growth rate of the instability as a function of time. The times/growth rates corresponding to the set of images in (b) are marked.

Physical evidence of centrifugal instability

Figure 20a displays streamlines for the mode F base flow for $Re = 280$ and $\alpha = 2.4$. The closed streamlines in the neighbourhood of the surface of the cylinder are clearly apparent. Figure 20b also shows the evolution of the perturbation streamwise vorticity field over one half of a period (the period being $1/St_{3D}$ defined in figure 19). After a half period the perturbation field is identical but of opposite sign. The period therefore corresponds to the time it takes for a fluid element at the mean radial position of the instability to travel twice around the cylinder, hence in some sense the instability can be considered a subharmonic.

The development and evolution of the instability involves the development of streamwise perturbation vorticity at the north-west position on the cylinder, approximately at the point where the incoming fluid separates to move either over the top or the bottom of the cylinder. This is shown in figure 20b(i) at $t = 0T/10$. Subsequently, the instability grows as it is advected anticlockwise, following close to the cylinder surface, as shown in the next two images. Figure 20b(iv) shows some vorticity moves into the wake but some continues along the surface towards the dividing

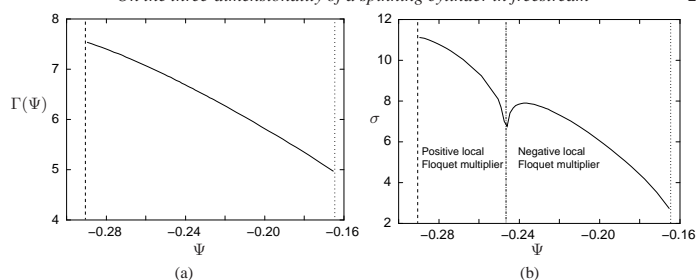


Figure 21: (a) Circulation ($\Gamma(\Psi)$) as a function of streamfunction (Ψ) moving from the cylinder surface (dashed line at $\Psi \simeq -0.29$) to the last closed streamline (dotted line). This clearly shows the circulation decreasing outwards as required for centrifugal instability. (b) Magnitude of the growth rate as a function of the streamfunction. The local Floquet multiplier is positive close to the cylinder, but becomes negative further away.

streamline, as shown in figures 20b(v) and 20b(vi). This last image shows the process starts again, but this time the development begins from vorticity of opposite sign. This image sequence confirms that the perturbation field remains strong predominantly near the cylinder surface, where the streamlines are closed, as would be expected for a centrifugal instability.

Figure 20c shows the instantaneous temporal growth rate as the instability evolves. This is obtained directly from integrating the perturbation field over a period and determining the amplitude of the instability field as a function of time. For figures 20b(i-iii), growth is positive as the instability advects anticlockwise around the cylinder. For figures 20b(iv) and 20b(v), growth is negative as it traverses across the wake region, before becoming positive again for figure 20b(vi). The Floquet multiplier for a single orbital period of $T = 4.513$ is 1.240, hence the growth rate is $\sigma = \log(1.240)/4.513 = 0.021$.

Application of inviscid centrifugal instability theory

The analysis of Bayly (1988) requires the existence of closed streamlines and the circulation to decrease outwards. Figure 20a shows the condition of closed streamlines is satisfied. Figure 21(a) shows the circulation ($\Gamma(\Psi)$) as a function of the streamfunction (Ψ), moving outwards from the cylinder surface. Clearly, the variation with increasing streamfunction, which also corresponds to increasing radius, is monotonically decreasing. The inviscid analysis of Bayly (1988) is used to determine the eigenvalues of the *local Floquet matrix* on integrating around an entire orbit for each closed streamline. The eigenvalues correspond to local Floquet multipliers, which can be reduced to Floquet exponents, i.e., growth rates, by taking the natural logarithm of the modulus and dividing by the orbital period. Thus the inviscid growth rate (σ_∞) can be determined as a function of streamfunction. Figure 21(b) shows this variation. The local Floquet multiplier is real and positive close to the cylinder, before it becomes real and negative out to the last closed streamline.

Bayly (1988) assumes that the actual instability mode is centred about the quadratic maximum of the growth rate curve, and uses an asymptotic expansion to determine an expression for the growth rate as a function of the wavenumber. In terms of the findings here, there is no quadratic maximum where the Floquet multiplier is positive real, although there is one in the streamfunction range where it is negative real. A negative real Floquet multiplier corresponds to the instability changing sign after each orbit, which figure 20b shows is the case here. The

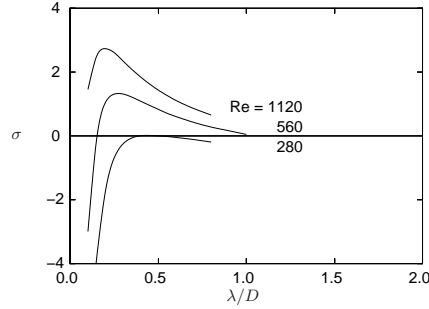


Figure 22: Computed growth rate curves as a function of wavelength from global stability analysis. The viscosity (Reynolds number) was varied only for the stability analysis of the base flow at $Re = 280$.

actual instability shown in the images of figure 20 is not centred at the streamline position of the streamfunction maximum of figure 21(b), but rather it appears to be centred near the streamline which has an orbital period equal to the measured period of the global instability mode, as would be expected for a centrifugal instability. The value of the streamfunction on this streamline is $\Psi \simeq -0.173$, i.e., close to the outer edge on the recirculation region (see figure 21(b)). The inviscid growth rate is close to $\sigma_\infty \simeq 3.5$ for that trajectory, which represents substantial positive growth.

Expanding about the quadratic maximum indicates that the growth rate should fall off linearly with wavelength (λ) (or inversely with wavenumber (k)) from the inviscid prediction corresponding to the $k \rightarrow \infty$ case. Also assuming that the effect of viscosity is mainly to damp the instability rather than change its character, the viscous correction to the growth rate should be proportional to the reciprocal of the square of the wavelength. That is,

$$\sigma(\lambda, Re) \simeq \sigma_\infty - A(\lambda/D) - \frac{4\pi^2 B}{Re(\lambda/D)^2}, \quad (5.1)$$

with B a constant of order one. As indicated above, it appears that the instability is not centred about either the absolute maximum or the local quadratic maximum of the inviscid growth curve, but rather about the streamline with the orbital period equal to the global mode period. This is perhaps not surprising given the strong forcing on the fluid from the rapidly spinning cylinder and subsequently stronger viscous effects towards the surface.

To investigate further, the variation of the global mode growth rate with wavelength is plotted in figure 22. The different curves correspond to different Reynolds numbers. The Reynolds number for the steady flow was fixed at 280; it was only varied for the linear stability equations, using the same steady frozen base flow. A similar procedure was used by Gallaire *et al.* (2007) to explore the centrifugal nature of the instability for flow over a bump. According to the proposed variation given by equation 5.1, the curves should fall inside an envelope curve, with the curves for increasing Reynolds number peaking at progressively smaller wavelengths. The y intercept of the envelope curve should correspond to the predicted inviscid growth rate σ_∞ . In practice the situation is a little more complex. Increasing the Reynolds number causes the global instability mode to be centred closer to the cylinder and the period to reduce. Table 1 shows this behaviour. Here, λ_{pref} is the wavelength with the maximum growth rate in figure 22, $T_{\lambda_{pref}}$ is half the measured global instability mode period from the global analysis (recall the mode repeats every

Re	λ_{pref}	$T_{\lambda_{pref}}$	$\Psi_{\lambda_{pref}}$	$\sigma_{inviscid}$
280	0.44	4.4	-0.172	3.5
560	0.30	3.0	-0.188	5.1
1120	0.22	2.5	-0.201	6.2

Table 1: Parameters for global stability analysis based on varying the Reynolds number for the stability equations only.

two orbits), $\Psi_{\lambda_{pref}}$ is the value of the streamfunction with this orbital period and $\sigma_{inviscid}$ is the predicted growth rate from the inviscid theory of Bayly (1988) shown in figure 21(b). In particular, this shows that as the effect of viscosity is reduced, the instability mode moves inwards, centred on streamlines that have smaller orbital periods and higher growth rates, as shown in figure 21(b). Thus, it is consistent that the computed growth rate curves shown in figure 22 move upwards, rather than asymptoting to an envelope curve.

Summary of the success of the inviscid theory

In summary, the mode F instability appears to be associated with a centrifugal instability, in terms of primary localisation to the region with both closed streamlines and circulation decreasing outwards. The preferred wavelength of the instability also appears to be related to, i.e., a small multiple of, the radial extent of the region with closed streamlines. In addition, the evolution of the periodic instability mode as it advects around the cylinder is consistent with the formation and growth of streamwise rollers, transferring faster moving fluid to larger radii and vice versa, as expected for a centrifugal instability. This growth happens as the perturbation moves from the dividing streamline at the north-west position of the cylinder until it reaches the wake region at the north-east position on the cylinder, perhaps reminiscent of Görtler vortices (Görtler 1955) for flow on curved streamlines. Analysis using the inviscid instability theory of Bayly (1988) to find the eigenvalues of the *local Floquet matrix* associated with an orbital period on a streamline predicts substantial amplification during the orbit. There is an inner region where the eigenvalues are positive, and an outer region where they are negative. Negative eigenvalues indicate that the instability changes sign each orbital period. This is precisely what happens with the global mode, i.e., it repeats every two orbits. However, the global mode is not centred close to the streamline at which there is a local maximum of the inviscid growth rate, but rather close to the streamline with the same orbital period. For that streamline, the inviscid growth rate is still strongly positive. Decreasing viscosity for the global mode calculation only, leads to a reduction in the global mode period, corresponding to the instability being centred closer to the cylinder surface, where the inviscid growth rate is higher. Thus, it does not seem that the generalised inviscid instability theory, even adjusted for the first-order effects of viscosity, can supply quantitative estimates of the growth rate or the preferred wavelength, although it certainly is qualitatively consistent with many features of the inviscid predictions.

Mode	λ/D	Nature of μ	Base flow	Symmetry
A	$\simeq 4$	Real and positive	Unsteady	$u(x, y, z, t) = u(x, y, z + n\lambda, t + T)$
B	$\simeq 0.8$	Real and positive	Unsteady	$u(x, y, z, t) = u(x, y, z + n\lambda, t + T)$
C	$\simeq 1$	Real and negative	Unsteady	$u(x, y, z, t) = u(x, y, z + n\lambda, t + 2T)$
D	$\simeq 1.9$	Real and positive	Unsteady	$u(x, y, z, t) = u(x, y, z + n\lambda, t + T)$
E	$\simeq 1.8$	Real and positive	Steady	$u(x, y, z, t) = u(x, y, z + n\lambda)$
F	$\simeq 0.4$	Complex	Steady	$u(x, y, z, t) = u(x, y, z + n\lambda, t + T_{3D})$
G	$\simeq 18$	Real and positive	Unsteady	$u(x, y, z, t) = u(x, y, z + n\lambda, t + T)$

Table 2: Summary of the modes showing the characteristic wavelength, nature of the Floquet multiplier (μ), the periodicity of the two-dimensional base flow and the spatial symmetries of these modes with respect to the streamwise velocity, u .

5.3.9. The mode G instability

The last three-dimensional mode discovered for this parameter space is mode G. This mode grows on the unsteady base flow, for α near the upper limit for the existence of the unsteady flow, and for $Re \geq 280$. This is a long wavelength mode, with a characteristic wavelength around $\lambda/D \simeq 18$. This mode has a purely real Floquet multiplier.

Shown in figure 23 are the perturbation vorticity contours of this long wavelength mode. The spatial structure of this instability is similar to that of the mode A instability, except for a small apparent phase shift of the perturbation relative to the base flow in the downstream vortices.

6. Discussion of the modes spanning the parameter space

A summary of the modes is shown in table 2. For the cylinder spinning at low rotation rates, the onset of the three-dimensional modes is similar to that observed for the non-rotating cylinder; that is, mode A occurs first with increasing Re , prior to the onset of mode B instability. This is essentially due to the similarities in base flow; the structure of the Bernard von Kármán vortex street is only changed slightly by the body rotation at these values of α . However, for $\alpha \gtrsim 1.3$, the wake structure becomes strongly asymmetric. Consistent with previous studies where the loss of wake symmetry leads to a different three-dimensional mode being observed, a subharmonic mode (mode C) is the first three-dimensional mode to become unstable to spanwise perturbations at these higher α . A mode with these symmetries and characteristics has been observed in earlier studies on flow past rings (Sheard *et al.* 2005a). At $\alpha = 1.5$, this mode is unstable for a small range of Reynolds numbers before decaying at higher Reynolds numbers, following which the onset of mode A instability is observed. However, at $\alpha > 1.75$, mode C is found to persist over a larger range of Reynolds numbers; for certain values of Re , multiple three-dimensional modes are predicted to be unstable. An instance of this is shown in figure 24, where modes C, A and G are observed at $\alpha = 1.85$, $Re = 330$. The mode C instability is the fastest growing mode followed by mode G and mode A.

The mode D instability occurs in the high frequency shedding region at rotation rates in excess of 1.9. Figure 9 shows that mode D exists in a region of the parameter space very close to the steady - unsteady transition of the two-dimensional base flow; in some senses, mode D can be

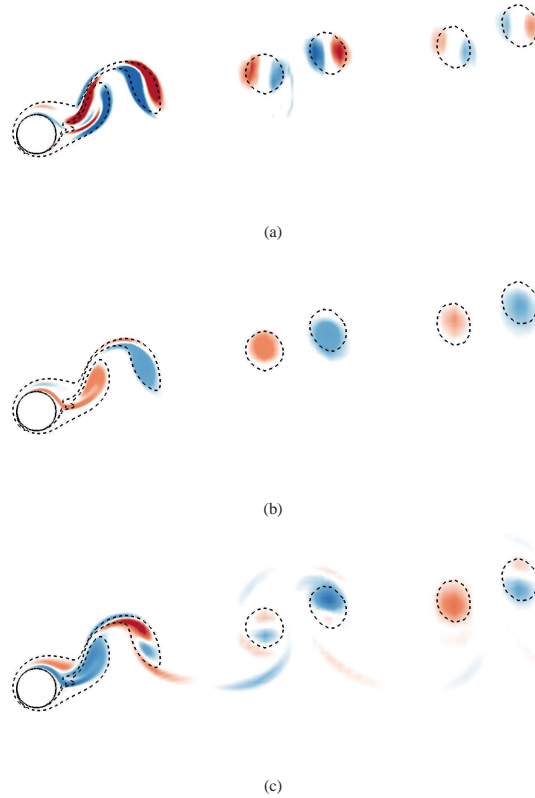


Figure 23: Perturbation vorticity contours for mode G at $\alpha = 1.85$, $Re = 330$, $\lambda/D = 20$. (a) Spanwise vorticity. (b) Streamwise vorticity. (c) The streamwise vorticity contours for $\lambda/D = 3.75$ (mode A) are plotted for comparison. Contour shading is as per figure 10.

viewed as the “periodic” state of mode E. Figures 15 and 16 clearly show the similarities in the structure of these two modes.

For a given rotation rate, the spanwise wavelength at which the maximum growth rate of the mode D and E instabilities occur, decreases as Reynolds number is increased. For instance, the mode E instability at $\alpha = 2$, $Re = 220$ (a case just past the onset of three-dimensionality) has a peak wavelength of $1.96D$, while at $Re = 340$ the peak wavelength decreases to $1.8D$. Further, as rotation rate is increased from $\alpha = 2$ to $\alpha = 2.25$, the peak wavelength at $Re = 300$ decreases from $1.9D$ to $1.65D$.

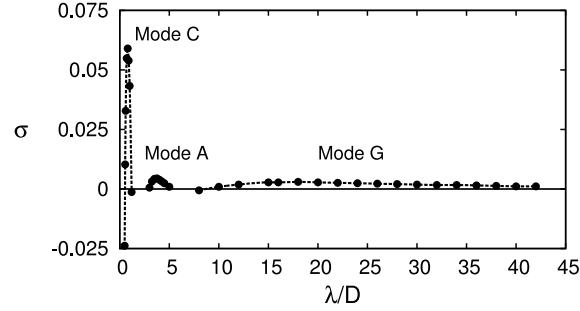


Figure 24: Growth rate curves showing the three modes which are unstable to perturbations at $\alpha = 1.85$, $Re = 330$.

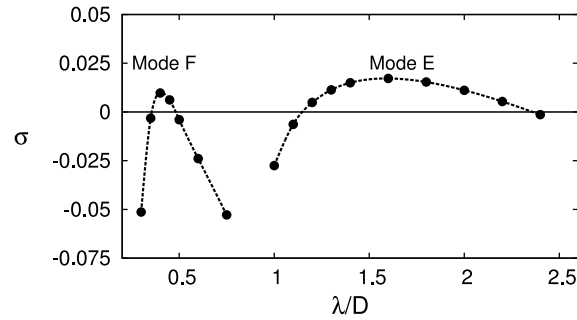


Figure 25: Growth rate curves showing the mode E and mode F instabilities at $\alpha = 2.25$, $Re = 320$.

At $\alpha = 2.25$, the mode E instability exists alongside the mode F instability (see figure 25). The short wavelength instability of mode F has a complex Floquet multiplier, indicating it is periodic as it occurs in the steady regime of flow. The spanwise wavelength is much smaller than that predicted by the DNS of Meena *et al.* (2011) at slightly higher rotation rates. Further analysis of the nature of the instability using the inviscid instability theory of Bayly (1988) is consistent with it being primarily centrifugal in nature, although the influence of viscosity appears too strong for the theory to provide realistic estimates for wavelengths or growth rates.

7. Conclusions

The results of the linear stability analysis for a spinning cylinder in a freestream have been presented. These results build upon the existing knowledge of the three-dimensional wake modes that were first observed in the wake of a non-rotating cylinder by Williamson (1988). The non-dimensionalised rotation rate, α , and Reynolds number, Re , were varied over a wide parameter space to first obtain the base flow over which stability analysis was performed to determine

the growth (or decay) of perturbations. Furthermore, stability analysis was used to predict the characteristic wavelength of each instability, and the spatio-temporal symmetries.

At low rotation rates, the change in the structure of the Kármán shedding is minimal, and the onset of the three-dimensional modes resembles that of the non-rotating cylinder, although the critical values for the onset of the mode A and mode B instabilities are delayed to higher Reynolds numbers. At higher rotation rates, a subharmonic mode, mode C, is unstable to the perturbations and is unstable in a closed region of the parameter space. This mode is the first three-dimensional mode which becomes unstable with increasing Re , followed by the onset of the mode A type instability. At higher rotation rates of $\alpha = 1.85$, a long wavelength instability is observed alongside mode C and mode A instabilities.

For high rotation rates ($\alpha > 2$), the rotation stabilises the vortex shedding, resulting in a steady two-dimensional base flow. This class of steady base flows has been shown to be unstable to at least two modes: mode E, which appears to be due to amplification of perturbations in the high-strain regions of the near wake; and mode F, which is a centrifugal instability of the closed region of flow near the cylinder surface for high rotation rates.

The authors acknowledge computing-time support from the Victorian Life Sciences Computation Initiative (VLSCI), the National Computational Infrastructure (NCI) and Monash Sungrid, Clayton. The authors acknowledge financial support from Australian Research Council grants DP0877327 and DP110102141.

REFERENCES

- AKOURY, R. EL, BRAZA, M., PERRIN, R., HARRAN, G. & HOARAU, Y. 2008 The three-dimensional transition in the flow around a rotating cylinder. *Journal of Fluid Mechanics* **607**, 1–11.
- BADR, H.M., DENNIS, S.C.R. & YOUNG, P.J.S. 1989 Steady and unsteady flow past a rotating circular cylinder at low Reynolds numbers. *Computers and Fluids* **17** (4), 579–609.
- BADR, H. M., COUTANCEAU, M., DENNIS, S. C. R. & MENARD, C. 1990 Unsteady flow past a rotating circular cylinder at Reynolds numbers 10^3 and 10^4 . *Journal of Fluid Mechanics* **220**, 459–484.
- BARKLEY, D. & HENDERSON, R. D. 1996 Three-dimensional Floquet stability analysis of the wake of a circular cylinder. *Journal of Fluid Mechanics* **322**, 215–241.
- BARKLEY, D., TUCKERMAN, L. S. & GOLUBITSKY, M. 2000 Bifurcation theory for three-dimensional flow in the wake of a circular cylinder. *Phys. Rev. E* **61**, 5247–5252.
- BAYLY, B. J. 1988 Three-dimensional centrifugal-type instabilities in inviscid two-dimensional flows. *Physics of Fluids* **31**, 56–64.
- BILLANT, P. & GALLAIRE, F. 2005 Generalised Rayleigh criterion for non-axisymmetric centrifugal instabilities. *Journal of Fluid Mechanics* **542**, 365–379.
- BLACKBURN, H. M. & LOPEZ, J. M. 2003 On three-dimensional quasiperiodic Floquet instabilities of two-dimensional bluff body wakes. *Physics of Fluids* **15**, L57–L60.
- BLACKBURN, H. M., MARQUES, F. & LOPEZ, J. M. 2005 Symmetry breaking of two-dimensional time-periodic wakes. *Journal of Fluid Mechanics* **552**, 395–411.
- CHEN, YEN-MING, OU, YUH-ROUNG & PEARLSTEIN, ARNE J. 1993 Development of the wake behind a circular cylinder impulsively started into rotatory and rectilinear motion. *Journal of Fluid Mechanics* **253**, 449–484.
- CHEW, Y. T., CHENG, M. & LUO, S. C. 1995 A numerical study of flow past a rotating circular cylinder using a hybrid vortex scheme. *Journal of Fluid Mechanics* **299**, 35–71.
- GALLAIRE, F., MARQUILLE, M. & EHRENSTEIN, U. 2007 Three-dimensional transverse instabilities in detached boundary layers. *Journal of Fluid Mechanics* **571**, 221–233.
- GÖRTLER, H. 1955 Dreidimensionales zur stabilitätstheorie laminarer grenzschichten. *Journal of Applied Mathematics and Mechanics* **35** (9–10), 362–363.
- GRIFFITH, M. D., THOMPSON, M. C., LEWEKE, T., HOURIGAN, K. & ANDERSON, W. P. 2007 Wake behaviour and instability of flow through a partially blocked channel. *Journal of Fluid Mechanics* **582**, 319–340.
- INGHAM, D.B. 1983 Steady flow past a rotating cylinder. *Computers and Fluids* **11** (4), 351–366.

- KANG, S. M., CHOI, H. C. & LEE, S. 1999 Laminar flow past a rotating circular cylinder. *Physics of Fluids* **11** (11).
- KARNIADAKIS, G. E. & SHERWIN, S. J. 2005 *Spectral/hp Methods for Computational Fluid Dynamics*. Oxford: Oxford University Press.
- KARNIADAKIS, G. E. & TRIANTAFYLLOU, G.S. 1992 Three-dimensional dynamics and transition to turbulence in the wake of bluff objects. *Journal of Fluid Mechanics* **238**, 1–30.
- KUMAR, S., CANTU, C. & GONZALEZ, B. 2011 Flow past a rotating cylinder at low and high rotation rates. *Journal of Fluids Engineering* **133** (4), 041201.
- LAGNADO, R.R., PHAN-THIEN, N. & LEAL, L.G. 1983 The stability of two-dimensional linear flow. In *Proceedings of the eighth Australasian Fluid Mechanics Conference*, pp. 7A5–7A7. University of Newcastle, New South Wales, Australia.
- LEBLANC, S. & GODEFERD, F.S. 1999 An illustration of the link between ribs and hyperbolic instability. *Physics of Fluids* **11** (2), 497–499.
- LEONTINI, J. S., THOMPSON, M. C. & HOURIGAN, K. 2007 Three-dimensional transition in the wake of a transversely oscillating cylinder. *Journal of Fluid Mechanics* **577**, 79–104.
- LEWEKE, T. & WILLIAMSON, C. H. K. 1998 Cooperative elliptic instability of a vortex pair. *Journal of Fluid Mechanics* **360**, 85–119.
- MAMUN, C. K. & TUCKERMAN, L. S. 1995 Asymmetry and Hopf-bifurcation in spherical Couette flow. *Physics of Fluids* **7** (1), 80–91.
- MEENA, J., SIDHARTH, G. S., KHAN, M. H. & MITTAL, S. 2011 Three dimensional instabilities in flow past a spinning and translating cylinder. In *IUTAM Symposium on Bluff Body Flows*.
- MITTAL, S. 2004 Three-dimensional instabilities in flow past a rotating cylinder. *Journal of Applied Mechanics* **71** (1), 89–95.
- MITTAL, S. & KUMAR, B. 2003 Flow past a rotating cylinder. *Journal of Fluid Mechanics* **476**, 303–334.
- PRALITS, JAN O., BRANDT, LUCA & GIANNETTI, FLAVIO 2010 Instability and sensitivity of the flow around a rotating circular cylinder. *Journal of Fluid Mechanics* **650**, 513–536.
- PRANDTL, L. 1925 Application of the “Magnus effect” to the wind propulsion of ships.
- RAO, A., STEWART, B.E., THOMPSON, M.C., LEWEKE, T. & HOURIGAN, K. 2011 Flows past rotating cylinders next to a wall. *Journal of Fluids and Structures* **27** (5-6), 668 – 679.
- RAYLEIGH, J. W. S. 1917 On the dynamics of revolving fluids. *Proc. R. Soc. Lond. Series A* **93**, 148–154.
- SHEARD, G. J. 2011 Wake stability features behind a square cylinder: Focus on small incidence angles. *Journal of Fluids and Structures* **27** (5-6), 734 – 742.
- SHEARD, G. J., FITZGERALD, M. J. & RYAN, K. 2009 Cylinders with square cross-section: wake instabilities with incidence angle variation. *Journal of Fluid Mechanics* **630**, 43–69.
- SHEARD, G. J., THOMPSON, M. C. & HOURIGAN, K. 2003 From spheres to circular cylinders: the stability and flow structures of bluff ring wakes. *Journal of Fluid Mechanics* **492**, 147–180.
- SHEARD, G. J., THOMPSON, M. C. & HOURIGAN, K. 2005a Subharmonic mechanism of the mode C instability. *Physics of Fluids* **17** (11), 1–4.
- SHEARD, G. J., THOMPSON, M. C., HOURIGAN, K. & LEWEKE, T. 2005b The evolution of a subharmonic mode in a vortex street. *Journal of Fluid Mechanics* **534**, 23–38.
- SIPP, D. & JACQUIN, L. 2000 Three-dimensional centrifugal-type instabilities of two-dimensional flows in rotating systems. *Physics of Fluids* **12**, 1740–1748.
- STEWART, B. E., HOURIGAN, K., THOMPSON, M. C. & LEWEKE, T. 2006 Flow dynamics and forces associated with a cylinder rolling along a wall. *Physics of Fluids* **18** (11), 111701–111701–4.
- STEWART, B. E., THOMPSON, M. C., LEWEKE, T. & HOURIGAN, K. 2010 The wake behind a cylinder rolling on a wall at varying rotation rates. *Journal of Fluid Mechanics* **648**, 225–256.
- STOKKOVIĆ, D., BREUER, M. & DURST, F. 2002 Effect of high rotation rates on the laminar flow around a circular cylinder. *Physics of Fluids* **1** (9).
- STOKKOVIĆ, D., SCHÖN, P., BREUER, M. & DURST, F. 2003 On the new vortex shedding mode past a rotating circular cylinder. *Physics of Fluids* **15** (5), 1257–1260.
- THOMPSON, M. C., HOURIGAN, K., CHEUNG, A. & LEWEKE, T. 2006a Hydrodynamics of a particle impact on a wall. *Appl. Math. Model.* **30**, 190–196.
- THOMPSON, M. C., HOURIGAN, K., RYAN, K. & SHEARD, G. J. 2006b Wake transition of two-dimensional cylinders and axisymmetric bluff bodies. *Journal of Fluids and Structures* **22**, 793–806.
- THOMPSON, M. C., HOURIGAN, K. & SHERIDAN, J. 1996 Three-dimensional instabilities in the wake of a circular cylinder. *Exp. Therm. Fluid Sci.* **12**, 190–196.

- THOMPSON, M. C., LEWEKE, T. & WILLIAMSON, C. H. K. 2001 The physical mechanism of transition in bluff body wakes. *Journal of Fluids and Structures* **15**, 607–616.
- WILLIAMSON, C & BROWN, G. L. 1998 A series in $1/\sqrt{Re}$ to represent the Strouhal-Reynolds number relationship of the cylinder wake. *Journal of Fluids and Structures* **12**, 1073–1085.
- WILLIAMSON, C. H. K. 1988 The existence of two stages in the transition to three-dimensionality of a cylinder wake. *Physics of Fluids* **31**, 3165–3168.
- WILLIAMSON, C. H. K. 1996a Three-dimensional vortex dynamics in bluff body wakes. *Experimental Thermal and Fluid Science* **12**, 150–168.
- WILLIAMSON, C. H. K. 1996b Three-dimensional wake transition. *Journal of Fluid Mechanics* **328**, 345–407.
- ZHANG, H-Q, FEY, U., NOACK, B. R., KONIG, M. & ECKELEMANN, H. 1995 On the transition of the cylinder wake. *Physics of Fluids* **7** (4), 779–794.

Chapter 3

Flow past a circular cylinder translating at different gap heights to a wall

3.1 Overview

The previous chapter explored the effects of rotation for a body in freestream, where new three-dimensional modes were observed as the rotation rate was increased. Here, we explore the flow characteristics as the cylinder is brought closer to a plane wall from large gap heights. For this case, the rotation rate is set to zero, while the gap height is varied. Recent two-dimensional simulations (Yoon *et al.* 2010, 2007; Huang & Sung 2007) show that the alternate vortex shedding ceases for $G/D \lesssim 0.25$ over a range of Reynolds numbers. For a circular cylinder in freestream, previous studies (Williamson 1988b, 1996a; Thompson *et al.* 1996) have shown the onset of three-dimensional flow to occur in the unsteady regime of flow at $Re \simeq 190$, while for cylinders sliding along a wall, Stewart *et al.* (2006, 2010b) showed the three-dimensional transition occurred in the steady regime of flow at $Re \simeq 71$ prior to the onset of unsteady flow at $Re \simeq 160$. However, the onset of three-dimensional flow between the two extremities of gap height has received very little attention. Mahir (2009) observed mode A type structures at gap heights $G/D \gtrsim 1.2$ and mode B type structures at $G/D = 0.8$ in the wake of a square cylinder near a fixed wall. At very low gap heights, neither mode A nor mode B type structures were observed.

We here investigate the variation of the onset of three-dimensionality for a circular cylinder as the gap height is varied from $G/D = \infty$ to $G/D \simeq 0$ by linear stability analysis. For the circular cylinder near a wall, the dominant three-dimensional modes at $Re = 200$ are investigated followed by three-dimensional simulations to visualise the

flow structures.

3.2 Flow dynamics of a cylinder translating parallel to a wall

The following article was submitted in 2012 to *Journal of Fluids and Structures*. This work was co-authored by M. C. Thompson, T. Leweke and K. Hourigan, and is entitled, “*The flow past a circular cylinder translating at different heights above a wall*”. The paper is reproduced in this thesis directly from the version submitted to the editor for review.

Declaration for manuscript included in PhD Thesis

Monash University

Declaration for Thesis Chapter 3

Declaration by candidate

In the case of Chapter 3, the nature and extent of my contribution to the work was the following:

Nature of contribution	Extent of contribution (%)
Conceived ideas, initiated the paper, performed numerical simulations, analysed the data, wrote the manuscript	80

The following co-authors contributed to the work. Co-authors who are students at Monash University must also indicate the extent of their contribution in percentage terms:

Name	Nature of contribution	Extent of contribution (%) for student co-authors only
Prof. M.C. Thompson	Co-wrote the manuscript	N. A.
Prof. T. Leweke	Co-wrote the manuscript	N. A.
Prof. K. Hourigan	Co-wrote the manuscript	N. A.

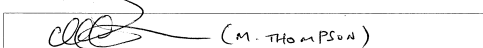
Candidate's Signature  Date 18 JUNE 2012

Declaration by co-authors

The undersigned hereby certify that:

- ^L 1) the above declaration correctly reflects the nature and extent of the candidate's contribution to this work, and the nature of the contribution of each of the co-authors.
- ^L 2) they meet the criteria for authorship in that they have participated in the conception, execution, or interpretation, of at least that part of the publication in their field of expertise;
- ^L 3) they take public responsibility for their part of the publication, except for the responsible author who accepts overall responsibility for the publication;
- ^L 4) there are no other authors of the publication according to these criteria;
- ^L 5) potential conflicts of interest have been disclosed to (a) granting bodies, (b) the editor or publisher of journals or other publications, and (c) the head of the responsible academic unit; and
- ^L 6) the original data are stored at the following location(s) and will be held for at least five years from the date indicated below.

Location(s)

Signature 1	 (M. THOMPSON)	Date 19/6/2012
Signature 2	 (T. LEWEKE)	19/6/2012
Signature 3	 (K. HOURIGAN)	19/6/2012

The flow past a circular cylinder translating at different heights above a wall

A. Rao^a, M.C. Thompson^a, T. Leweke^b, K. Hourigan^{a,c}

^aFluids Laboratory for Aeronautical and Industrial Research (FLAIR),
Department of Mechanical and Aerospace Engineering, Monash University, Clayton 3800, Australia

^bInstitut de Recherche sur les Phénomènes Hors Équilibre (IRPHE),

UMR 7342 CNRS, Aix-Marseille Université, F-13384 Marseille CEDEX 13, France

^cDivision of Biological Engineering, Monash University, Clayton 3800, Australia

Abstract

The flow past a circular cylinder moving through a fluid at different heights above a plane no-slip boundary is investigated numerically for Reynolds numbers ≤ 200 . The gap height is varied from large values, effectively corresponding to the freestream case ($G/D = \infty$), down to a small value where the cylinder is just above the wall ($G/D = 0.005$). The initial transition from steady two-dimensional flow can occur through either a Hopf bifurcation to unsteady flow or through a regular bifurcation to steady three-dimensional flow. The critical Reynolds numbers for each case are determined as a function of gap height. It is found that steady two- to three-dimensional transition occurs first at gap ratios $G/D \lesssim 0.25$, beyond which the initial transition is to unsteady flow. At $G/D = 0.3$, a sharp increase in the critical Reynolds number is observed at which three-dimensionality occurs. On increasing gap height, the critical Reynolds number initially decreases before again increasing towards the value observed for an isolated cylinder. The force coefficients and Strouhal numbers are quantified. Finally, three-dimensional simulations are performed at $Re = 200$ for the smallest gap ratio, effectively corresponding to a cylinder sliding along a wall, to examine how the wake evolves as it saturates.

Keywords: Wakes, Stability analysis, Body forces, Flow transition

1. Introduction

The flow past a circular cylinder has represented a generic fluid flow problem for more than a century, and the experimental and mathematical details of the transition to three-dimensional flow have been revealed over the last twenty five years. The flow undergoes an initial transition from two-dimensional periodic flow to three-dimensional flow via a sub-critical transition at $Re \approx 190$ (Barkley and Henderson, 1996; Williamson, 1996a,b), where the Reynolds number (Re) is based on the free-stream velocity (U) and the cylinder diameter (D). The spanwise modulation of this three-dimensional flow at onset was found to be approximately four cylinder diameters and the corresponding wake instability is commonly known as the *Mode A* instability. Another three-dimensional instability mode, *Mode B*, becomes unstable at a higher Reynolds number and the remnants of that mode seem to persist to much higher Reynolds numbers as the wake undergoes a transition to a chaotic state (Henderson, 1997; Williamson, 1996a,b). The equivalent modes have also been recognised in the wakes of other two-dimensional cylindrical bodies, such as square cylinders (Robichaux et al., 1999) and elongated cylinders (Ryan et al., 2005). Until recently, very few studies have investigated the related problem of flow past a circular cylinder moving parallel to a wall and the associated wake transitions.

Bearman and Zdravkovich (1978) performed experimental investigations for a cylinder near a fixed wall at $Re = 4.5 \times 10^4$ for $0 \leq G/D \leq 3.5$. The cylinder was located $36D$ from the start of a turbulent boundary layer which developed along the wall. They observed the suppression of regular vortex shedding for $G/D < 0.3$, with the Strouhal number remaining almost constant until this gap height was approached.

Price et al. (2002) visualised the flow for a circular cylinder at different gap heights from a fixed wall for Reynolds number in the range $1200 \leq Re \leq 4960$ and identified four different regimes of flow. For the case where the cylinder was close to the wall ($G/D < 0.125$), vortex shedding was suppressed and the wall boundary layer separation occurred both upstream and downstream of the cylinder. For $0.25 \leq G/D \leq 0.375$, the flow was qualitatively similar to that for the small gap ratios, while pairing occurred between the inner shear layer from the cylinder and the wall boundary

layer. Vortex shedding was detected for $G/D > 0.5$, and at higher gap heights, the flow resembled that of an isolated cylinder.

Experimental investigations undertaken by Bailey et al. (2002) for a square cylinder near a stationary wall at $Re = 1.89 \times 10^4$ showed the presence of dislocations (which are commonly associated with mode A type instability) for gap heights greater than $G/D = 0.7$. For $0.53 \leq G/D \leq 0.7$, the spanwise perturbations were suppressed as a result of higher flow velocities in the gap region, thereby leading to the flow being mainly two-dimensional and a reduction in the occurrence of dislocations. Below $G/D \leq 0.53$, intermittent vortex shedding was observed. Experimental investigations at a slightly higher Reynolds number of 22,000 by Bosch et al. (1996) showed that the vortex shedding was completely suppressed at $G/D = 0.25$, while low intensity intermittent shedding occurred at higher gap ratios.

Using a finite-difference method, Lei et al. (2000) performed numerical simulations for a circular cylinder for G/D between 0.1 and 3 and for Reynolds numbers $80 \leq Re \leq 1000$. In their simulations, the lower wall and the cylinder were fixed and a boundary layer started $16D$ upstream of the cylinder. They observed that the gap height at which vortex shedding was suppressed decreased as the Reynolds number was increased up to $Re = 600$. Beyond this value, the critical gap height remained constant. A similar study was performed by Harichandan and Roy (2012) for a flow starting $10D$ upstream of the cylinder at $Re = 100$ and 200. Single sided vortex shedding was observed for $G/D = 0.2$ and $Re = 200$, and as the gap height was increased, Kármán type shedding was observed.

One of the earliest visualisations of the wake of a circular cylinder moving parallel to a wall was by Taneda (1965), who visualised the vortex streets for the cylinder moving at gap heights of $G/D = 0.6$ and 0.1 at $Re = 170$. For $G/D = 0.1$, a single row of vortices formed and these were unstable and dissipated quickly. Furthermore, the wavelength of vortex street increased as the gap ratio was decreased.

Nishino et al. (2007) performed experimental investigations for a circular cylinder near a moving wall for higher Reynolds numbers ($O(10^5)$). For a cylinder with endplates, they reported that the flow essentially remained two-dimensional, with Kármán type vortices being shed for gap heights $G/D > 0.5$, and an intermediate shedding regime being observed for $0.35 \leq G/D \leq 0.5$, followed by complete cessation of shedding below $G/D < 0.35$. They further reported that the drag coefficient was nearly constant when the body was below $G/D < 0.35$. However, for a cylinder without endplates, they reported that the Kármán type vortices were not being generated and the drag coefficient was nearly constant in this regime.

Zerihan and Zhang (2000) investigated the variation of lift and drag forces on a single element wing (of chord c) with a moving ground in a wind tunnel at high Reynolds numbers ($O(10^4)$). For the airfoil tested, the (negative) lift coefficient increased from its value at low gap heights to a maximum value at height $h = 0.08c$, beyond which a decrease in the lift coefficient was observed. The drag coefficient decreased on increasing gap height. They further varied the incidence angle of the airfoil and observed that the gap height at which the maximum (negative) lift was generated varied marginally.

Zhang et al. (2005) investigated the ground effect of a half-cylinder using a moving ground in a wind tunnel facility for Reynolds numbers in the range $6.8 \times 10^4 \leq Re \leq 1.7 \times 10^5$. The critical gap height range over which vortex shedding was suppressed was found to be $0.525 \leq G/D \leq 0.55$. The drag force was nearly constant below this height but a sharp increase to twice the value was observed around the critical gap height. The lift coefficient decreased as the gap height was increased. Furthermore, the Strouhal number was found to be insensitive to the gap height.

Bhattacharyya and Maiti (2005) investigated the flow for a square cylinder near a moving wall for a wide range of Reynolds numbers (below 1400) for $0.1 \leq G/D \leq 0.5$. They observed that the mean lift coefficient decreased gradually as Reynolds number was increased, while the drag coefficient increased with Reynolds number. The lift and drag coefficients were higher for lower gap heights. They further observed that the Strouhal number decreased as the gap height was decreased. They obtained the velocity profiles in the gap between the cylinder and the wall.

Huang and Sung (2007) performed two-dimensional simulations for a circular cylinder moving near a wall for $0.1 \leq G/D \leq \infty$ for $Re \leq 600$. The gap height at which alternate vortex shedding disappeared decreased from $0.28D$ to $0.25D$ as the Reynolds number was increased from 300 to 600. The non-dimensionalised shedding frequency (St) at different Reynolds numbers increased as the cylinder was brought closer to the wall ($\approx 0.5D$) followed by a rapid decrease as the gap height was decreased. They further quantified the lift and drag coefficients, with the lift coefficient showing a linear increase as the cylinder was brought closer to the wall. They however did not rule out the possibility that three-dimensional effects would be important for such flows.

Using an immersed boundary technique, Yoon et al. (2010) performed numerical investigations at various gap

heights for a circular cylinder moving parallel to a wall at $Re \leq 200$. The time-averaged lift and drag coefficients decreased exponentially as the gap height was increased. They observed steady flow at higher Reynolds numbers as the gap height was decreased. Vortex shedding persisted at $Re = 120$ for the cylinder with $G/D = 0.1$.

For a body moving along a wall, Arnal et al. (1991) observed that the presence of a wall had a stabilising effect on the flow dynamics, delaying the transition to unsteady flow to higher Reynolds numbers. For a square cylinder sliding along a wall, they observed that the onset of unsteady flow occurred around $Re = 100$, where the vortex pair moved away from the wall. Instabilities of this nature occurred when vortex cores convected at slower velocities than the mean flow, as shown by the experimental investigations of Lim et al. (2004) for a flat plate boundary layer. Dipankar and Sengupta (2005) further showed that the instability occurs in the convecting vortex core shed from the freestream side of the cylinder.

Mahir (2009) investigated the onset of three-dimensional flow for a square cylinder near a fixed wall for $Re \leq 250$ as the gap height was increased from 0.1 to 4. At $Re = 185$, mode A type vortex structures of spanwise wavelength $3D$ were observed for gap heights greater than $G/D = 1.2$, whilst at $G/D = 0.8$, mode B type vortex structures with $1D$ spanwise wavelength were observed. Below $G/D = 0.5$, neither mode A nor B type vortex structures were observed. At $Re = 250$, mode B type vortex structures were observed at larger gap heights, whilst at lower gap heights the vortex structure was strongly distorted in the vicinity of the cylinder. In the frequency spectra of the streamwise and spanwise velocities for $G/D = 0.8$ and $Re = 185$, period-doubling was observed.

Stewart et al. (2006, 2010b) performed numerical and experimental investigations for a circular cylinder moving near a plane wall at a very small gap height ($G/D = 0.005$) for $Re \leq 200$. They reported that the flow was steady up to $Re = 165$, beyond which periodic flow was observed, where oppositely signed vortex structures combined and self-propelled away from the wall. They further performed linear stability analysis and determined the onset of three-dimensional flow. The flow became three-dimensional directly from steady flow at $Re_c = 70.5$, unlike the case for an isolated cylinder, for which the transition to a three-dimensional state occurs from the unsteady flow. Experimental wake visualisations for the cylinder near a wall in a water tunnel were in good agreement with the numerical simulations.

In this study, we perform two-dimensional simulations for a circular cylinder moving parallel to a wall at different gap heights using a spectral-element method. This is coupled with linear stability analysis to investigate the wake transitions and wake behaviour at different gap heights. The dependence of the force coefficients and the shedding frequency on Reynolds number and gap height is quantified.

2. Problem definition and methodology

The schematic representation of the cylinder moving parallel to the wall is shown in figure 1. A cylinder of diameter D is moving at a gap height of G from the wall. In the numerical setup, it is convenient to use a uniformly translating frame of reference centred on the cylinder. Relative to this non-accelerating frame, the fluid and the lower wall move at a uniform speed and the cylinder remains stationary. There are two controlling non-dimensional parameters: the Reynolds number, $Re = UD/\nu$, where ν is the kinematic viscosity of the fluid, and the gap ratio, G/D . For this study, the Reynolds number lies in the range $25 \leq Re \leq 200$. Computational domains were constructed for different gap heights from freestream ($G/D = \infty$, i.e., no wall) to a minimal gap ($G/D = 0.005$). The small gap was maintained to prevent a singular mesh element between the bottom of the cylinder and the lower wall. Previous studies (Rao et al., 2011; Stewart et al., 2010b, 2006) have shown good agreement between the flow structures visualised in the experiments and those observed numerically, even though the force coefficients are sensitive to gap height for small gaps. As is usual, the lift force (F_l) and drag force (F_d) are normalised by the dynamic pressure and area ($0.5\rho U^2 D$) to obtain the lift (C_L) and drag (C_D) coefficients, respectively. In the unsteady regime of flow, vortex shedding occurs and the force coefficients vary periodically, so time-averaged quantities are reported. The simulations were performed for $\tau > 400$, where time, t , is non-dimensionalised by U/D ($\tau = tU/D$). The frequency of shedding, f , is normalised by the cylinder diameter and flow speed to obtain the non-dimensional Strouhal number, $St = fD/U$.

2.1. Numerical formulation

The incompressible Navier-Stokes equations are solved using a spectral-element method. The computational domain is constructed from quadrilateral elements, mainly rectangular, while some have curved boundaries to accurately

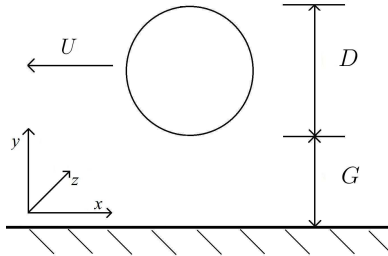


Figure 1: Schematic representation of the circular cylinder of diameter D at a distance G from the wall.

treat the curved surface of the cylinder. These elements are further subdivided into internal node points which are distributed according to the Gauss-Legendre-Lobatto quadrature points, with the velocity and pressure fields represented by tensor products of Lagrangian polynomial interpolants within the elements. Such methods are known to provide spectral convergence as the polynomial order of the interpolants is increased (Karniadakis and Sherwin, 2005). The number of node points ($N \times N$) is specified at runtime, with the interpolant polynomial order being $N - 1$. A fractional time-stepping technique is used to integrate the advection, pressure and diffusion terms of the Navier-Stokes equation forward in time. The unsteady solver is used to investigate the parameter range covering both the steady and unsteady regimes of flow. More details on this method can be found in Thompson et al. (2006a) and has previously been used in studies of bluff bodies in freestream (Thompson et al., 1996; Leontini et al., 2007; Thompson et al., 2006b) and for bodies near a wall (Stewart et al., 2006, 2010a,b; Rao et al., 2011; Thompson et al., 2007).

2.2. Linear stability analysis

For an isolated cylinder, three-dimensional flow occurs for $Re \gtrsim 190$ (Barkley and Henderson, 1996; Williamson, 1996a,b) in the unsteady regime, while for bodies close to a wall the flow becomes three-dimensional directly from a steady base flow (Stewart et al., 2010b; Rao et al., 2011). We here investigate the variation between these two extremes mapping the transition for different gap heights. The bifurcation to three-dimensional flow is determined using linear stability analysis. Numerically, the Navier-Stokes equations are linearised and the spanwise perturbations are constructed as a set of Fourier modes. The resulting equations are marched forward in time, and after several periods, the fastest growing or slowest decaying modes dominate the system. For unsteady (periodic) flows, the analysis is based on the growth over a base flow period (T) and is known as Floquet analysis. In that case, the ratio of the amplitudes of the perturbation field for consecutive periods is denoted by $\mu = e^{\sigma T}$, where μ is the Floquet multiplier or the amplification factor and σ is the growth rate. For exponentially growing modes, the Floquet multiplier returns a value of $|\mu| > 1$, or a positive growth rate ($\text{Re}(\sigma) > 0$). For a circular cylinder, the fastest growing modes at the onset of three-dimensionality have a purely real Floquet multiplier, i.e., the periodicity of the three-dimensional perturbations is the same as the base flow period. However, other unstable modes which are incommensurate with the base flow also occur, e.g., for a circular cylinder (Blackburn and Lopez, 2003), square cylinder (Robichaux et al., 1999) or flat plate (Thompson et al., 2006b). In addition, it is also possible for the perturbation modes to have twice the period of the base flow such as for the wake behind rings Sheard et al. (2003, 2004). These are termed sub-harmonic modes.

Details of the approach can be found in, e.g., Ryan et al. (2005) and Leontini et al. (2007).

2.3. Resolution studies

The domain used for the two-dimensional flow computations had boundaries positioned at large distances from the cylinder-wall system to minimise blockage. The inlet and outlet boundaries were placed $100D$ from the cylinder, while the transverse boundary was located $150D$ from the lower wall. Studies conducted by Rao et al. (2011) showed

negligible changes to the force coefficients and Strouhal number if larger domains were used. Furthermore, spatial resolution studies were conducted for $G/D = 0.01$ at $Re = 200$ by varying the number of internal nodes within each element ($N \times N$), between $N^2 = 4^2$ to 10^2 . For $N^2 = 7^2$, maximum variation in the force coefficients and Strouhal number from the most highly resolved case was less than 0.1%. However, because the macro-element mesh resolution is considerably lower away from the solid surfaces, to ensure adequate resolution of the flow structures in the far wake the internal resolution was set to $N^2 = 9^2$. Further, to ensure stability of the solver at these resolutions, which is governed by a Courant condition for the explicit non-linear sub-step, the time-step used was 0.001.

3. Results

3.1. Flow structures

The parameter investigation was carried out between $G/D = 0.005$ and $G/D \rightarrow \infty$ for Reynolds numbers $25 \leq Re \leq 200$. The flow for all cases investigated is steady at low Reynolds numbers and is characterised by the formation of recirculation zones behind the cylinder. For small gap heights, a single recirculation zone forms in the wake away from the wall, and as the gap height is increased, the formation of a secondary recirculation can be observed as the wake becomes more symmetrical. In line with the isolated cylinder case, the length of these recirculation zones increases as the Reynolds number is increased. At still higher Reynolds numbers, the flow undergoes transition to an unsteady state, with the wake state characterised by the periodic shedding of vortices. For bodies close to the wall ($G/D \leq 0.1$), the critical Reynolds number for transition to an unsteady state was higher than $Re = 165$, and as the gap height was increased, the unsteady transition occurred at lower Reynolds numbers. Recall that for bodies near a wall, three-dimensional flow occurs in the steady regime of flow (Stewart et al., 2010b). For bodies close to a wall, vortex shedding occurs when the negatively signed separating shear layer from the top of the cylinder combines with oppositely signed vorticity from the boundary layer at the wall to form vortex pairs, which self-propel away from the wall. However, for the cylinder moving at larger gap heights, the unsteady wake is characterised by the formation of the classical von Kármán vortex street. Shown in figure 2 are the coloured vorticity contour plots for the cylinder moving at different gap heights above the wall at $Re = 200$. The images shown are at instant of maximum lift coefficient in the shedding cycle.

The variation of the time-averaged drag and lift coefficients are shown in figure 3 in the steady regime of flow. Studies by Stewart et al. (2010b) show that the drag coefficient obeys a power law relationship with Reynolds number. Shown here on a log-log plot, the drag coefficient varies approximately linearly in the steady regime. There is a difference in the drag coefficient of approximately 2 between the smallest and largest gap cases. The mean lift coefficient varies substantially more since the mean lift approaches zero as $G/D \rightarrow \infty$.

The variation of the time-averaged drag and lift coefficients together with the standard deviations are shown in figure 4 for the unsteady regime of flow. Over this Reynolds number range the mean drag coefficient changes only by approximately 10% or less as the gap ratio or Reynolds number is varied.

Phase diagrams for various gap heights are provided in figure 5 at $Re = 200$. C_l is plotted against C_d at each gap height. The curves show the phase relationship between the force coefficients and the variation of the amplitude over one period of the lift coefficient. For $G/D = \infty$, the phase relationship is symmetric between two halves of the cycle, and an apparent loss in symmetry is observed for $G/D \leq 1$. For very small gaps ($G/D \leq 0.1$), the shedding becomes substantially one-sided, as shown in figure 2, where the lift and drag signals are out of phase by approximately 180° .

The variation of the shedding frequency (St) with gap height for various Reynolds numbers is shown in figure 6. The Strouhal number drops substantially as the cylinder is positioned closer to the wall, approaching a value of approximately 0.1 as the gap approaches zero. As the gap height is increased, the Strouhal number increases almost linearly initially before reaching a maximum for $0.5 \leq G/D \leq 0.75$, above which it decreases slightly as it asymptotes to the value for an isolated cylinder in freestream. Predictions from Huang and Sung (2007) and an independent immersed boundary code (J.S. Leontini, private communication) are in good agreement with the current Strouhal number predictions. It is also interesting that a similar decrease in Strouhal number is found when a cylinder approaches a free surface (Reichl et al., 2005).

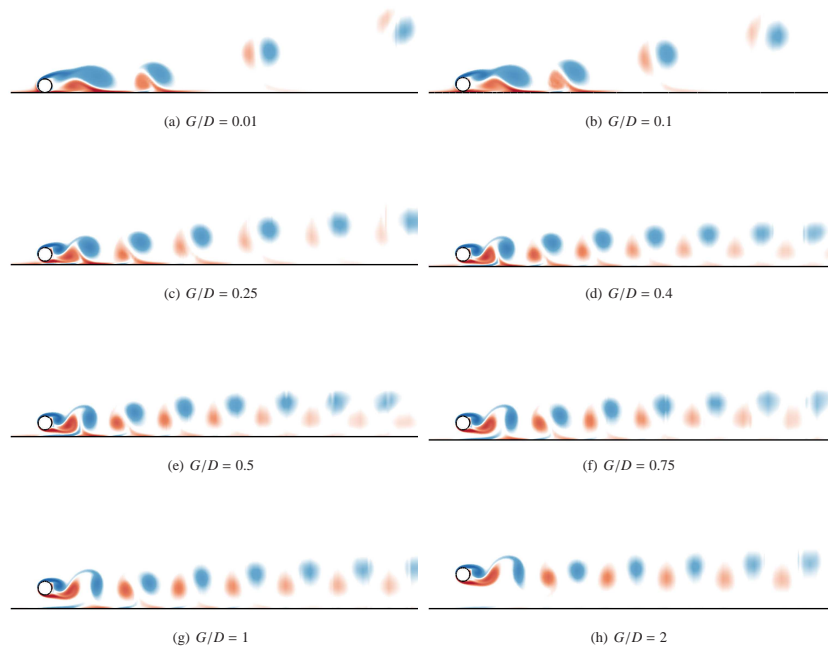


Figure 2: Flow structures at $Re = 200$ for the circular cylinder moving from right to left at the specified gap heights. Vorticity contours levels are between $\pm 5D/U$. The wake is visualised for a streamwise distance in excess of $25D$ downstream of the cylinder.

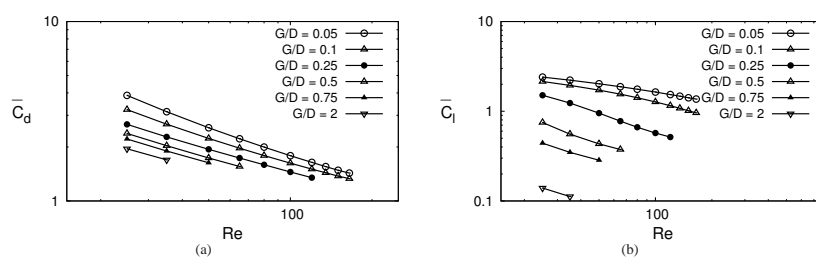


Figure 3: Variation of the drag (a) and lift (b) coefficients with Reynolds numbers for the gap heights shown. The flow is steady for these parameters.

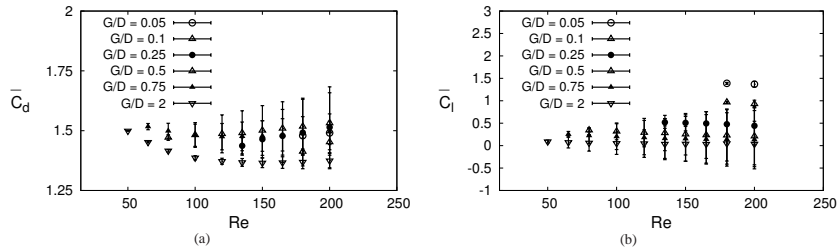


Figure 4: Variation of the force coefficients with Reynolds numbers in the unsteady regime for the gap heights shown. The error bars represent one standard deviation from the mean values.

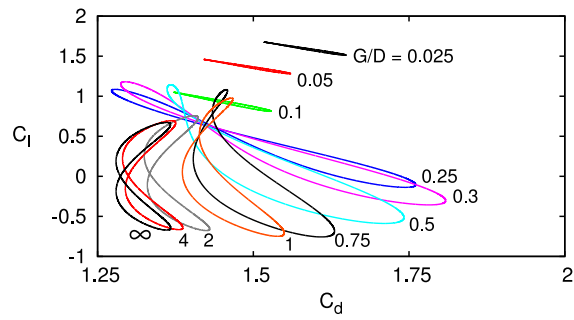


Figure 5: Force coefficient phase trajectories at different gap heights for periodic flow at $Re = 200$.

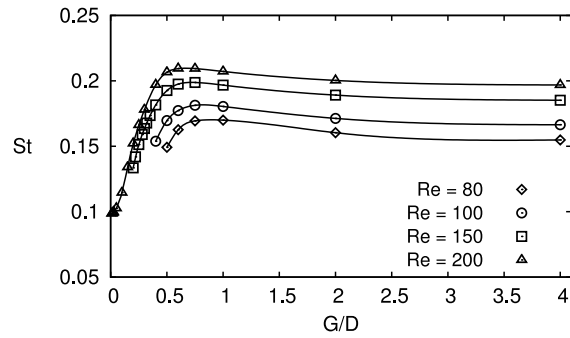


Figure 6: Variation of Strouhal number with gap height for different Reynolds numbers.

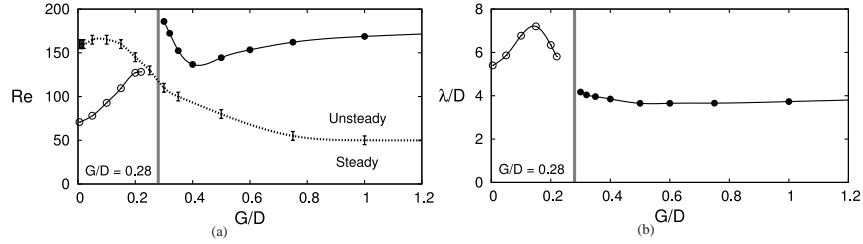


Figure 7: Variation of critical values for the onset of three-dimensional flow with gap height. Left: Variation of the critical Reynolds number with G/D . The boundary of the transition between the steady and unsteady regimes obtained using a two-dimensional base flow is shown by the dotted line. Right: Variation of the critical spanwise wavelength with G/D . The three-dimensional modes which grow on the steady base flow are marked by open circles (\circ) and those on the unsteady base flow by filled circles (\bullet). In each diagram, the gap height at which the flow is stable to three-dimensional perturbations for $Re \leq 200$ is shown by the vertical grey line.

3.2. Stability Analysis

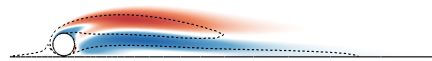
The stability of the flow to spanwise perturbations is investigated for cylinders moving at different gap heights above the wall. Two-dimensional steady or unsteady flow solutions are used to provide base flows to investigate the stability to three-dimensional perturbations.

For $G/D = \infty$, Barkley and Henderson (1996) showed that the flow became linearly unstable to three-dimensional perturbations at $Re_c = 188.5$ for $\lambda_c/D = 3.96$. Our stability analysis performed on the unsteady base flow showed that for this case the flow becomes unstable at $Re_c = 190.5$ for the same spanwise wavelength. The marginal variation in the critical Reynolds number between these two predictions ($O(1\%)$) can be attributed to the considerably larger domain size used here, which also leads to a slightly different Strouhal number to that found by Barkley and Henderson (1996). Stability analysis performed on the steady base flow at $G/D = 0.005$ (Rao et al., 2011) is in agreement with the previous studies of Stewart et al. (2010b). The current investigation was carried out to quantify the variation with gap height, mapping the boundary between the two- and three-dimensional regimes.

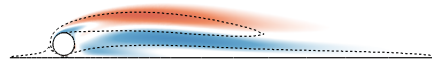
The variation of the critical spanwise wavelength and critical Reynolds number with gap height are shown in figure 7 for gap heights $G/D \leq 1.2$. In figure 7(a), the approximate demarcation between the steady and unsteady regimes is shown by the dotted line.

For $G/D \leq 0.22$, stability analysis was performed on a steady base flow, where the power method was used to resolve the dominant growing mode. However, for gap heights greater than $G/D = 0.22$, stability analysis was performed on an unsteady base flow using the Arnoldi method to resolve the dominant Floquet modes based on Krylov subspace iterates. This method can resolve both the real and imaginary components of the Floquet multiplier of the first few most-dominant modes. Domains used for the computations of the steady base flow were used for the stability analysis for the steady regime, while the computational domain had to be resized for the analysis in the unsteady regime. In that case, the perturbation fields were not adequately resolved in the far wake ($x/D > 30$), where the macro-elements are large. Since the modes are global modes (with the same growth rate everywhere), inadequate resolution, such as in the far wake, can lead to spurious growth rate predictions if unphysical large mode amplitudes occur there. To combat this problem, new computational domains were constructed with boundaries closer to the cylinder. The Strouhal numbers for the smaller domains were computed. The variation in the Strouhal number values between the larger and smaller sized domains were $\approx 15\%$. Although this will affect the accuracy of critical Reynolds numbers and growth rates by a similar percentage, it is unlikely to affect the underlying physics.

Figure 8 shows the computed spanwise perturbation vorticity contours for the most unstable wavelengths near the critical Reynolds numbers for onset of the instability. Spanwise vorticity contours of the base flow are overlaid to highlight the relative position of high mode amplitudes. This instability contours resemble those for a backward-facing step (Blackburn et al., 2008), flow downstream of a blockage or sudden expansion (Griffith et al., 2007, 2008; Marquet et al., 2008) or even the instability in the flow over a forward-facing blunt plate (Thompson, 2012). Those



(a) $G/D = 0.05$, $Re = 80$, $\lambda/D = 6$, $|\mu| = 1.027$



(b) $G/D = 0.1$, $Re = 100$, $\lambda/D = 7$, $|\mu| = 1.072$



(c) $G/D = 0.2$, $Re = 135$, $\lambda/D = 6$, $|\mu| = 1.037$

Figure 8: Spanwise perturbation vorticity colour contours (between levels $\pm 0.1D/U$) for the cylinder moving at different gap heights at the specified Reynolds number and spanwise wavelength. Base flow vorticity contours between levels $\pm 1D/U$ are overlaid. The cylinder is moving from right to left in each image.

Table 1: Variation of λ_c/D and Re_c with G/D . The values above the horizontal line are obtained from a steady base flow and those below from a periodic base flow.

G/D	λ_c/D	Re_c
0.005	5.48	70.91
0.05	5.86	78.07
0.1	6.77	92.85
0.15	7.27	109.55
0.2	6.34	127.20
0.22	5.81	128.23
0.25	5.24	128.11
0.3	4.17	185.90
0.32	4.04	172.30
0.35	3.96	152.45
0.4	3.85	136.68
0.5	3.65	144.39
0.6	3.65	153.45
0.75	3.66	162.16
1	3.73	168.75
2	3.98	177.48
4	4.03	181.22
∞	3.96	190.5

cases have in common an attached downstream recirculation zone, and lead to a large spanwise-wavelength steady three-dimensional instability, which generates recirculating flows in the horizontal (x - y) plane.

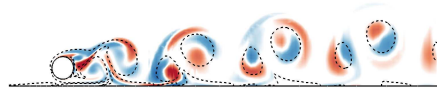
At $G/D = 0.28$, the flow remained two-dimensional for $Re \leq 200$. For larger gap ratios ($G/D \gtrsim 0.3$), the three-dimensional instability first manifests after the flow has already become unsteady. This case is analogous to Mode A for an isolated circular cylinder, with the critical Reynolds number and wavelength curves shown in figure 7 indicating a continuous transition towards the corresponding Mode A values. The mode structures for different gap heights are shown in figure 9, highlighting the broad similarities in the perturbation fields. In particular, the near wake shows high perturbation amplitude in the forming vortex cores as well as in the sheared region between the cores, and further downstream the perturbation is high in the vortex cores and drops to zero at the edge, reminiscent of the perturbation field structure for an elliptic instability as found for mode A, e.g., Thompson et al. (2001) and Leweke and Williamson (1998). Although for small gap heights there is some interaction with the no-slip wall contributing to the mode structure, this does not dominate the evolving perturbation field.

Table 1 provides the critical values of Reynolds number and spanwise wavelength for the three-dimensional transition as a function of the gap height.

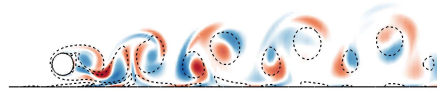
3.3. Stability analysis at higher Reynolds numbers for bodies near a wall

Previous studies by Rao et al. (2011) and Stewart et al. (2010b) reported three-dimensional flow in the steady regime at low Reynolds numbers prior to the onset of unsteady flow for a circular cylinder near a wall. Barkley and Henderson (1996) performed stability analysis at $Re = 280$ for an isolated cylinder and observed a short wavelength instability, commonly known as mode B. Here, we perform a similar analysis to predict all the amplified growing modes at a higher Reynolds numbers well past the transition value, and then we use three-dimensional direct numerical simulations to further investigate the nature of the saturated wake state.

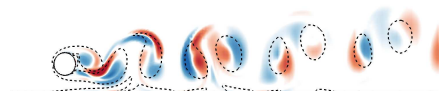
For a cylinder (effectively) sliding along a wall ($G/D = 0.005$), the two-dimensional flow undergoes transition to an unsteady wake state at $Re \approx 160$. Stability analysis was performed on the unsteady base flow at $Re = 200$ to obtain the fastest growing modes. The growth rates curves are shown in figure 10. Four distinct modes are observed for $\lambda/D \leq 25$, with the shortest wavelength mode at $\lambda/D = 2.4$ (termed Mode I) being the fastest growing. Three other modes whose maximum growth rate peaks are at $\lambda/D = 4.55, 5.35$ and 11 and are termed mode II, mode III and mode



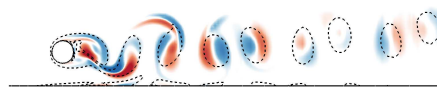
(a) $G/D = 0.3, Re = 200, \lambda/D = 4, |\mu| = 1.12$



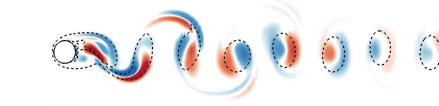
(b) $G/D = 0.5, Re = 150, \lambda/D = 3.75, |\mu| = 1.046$



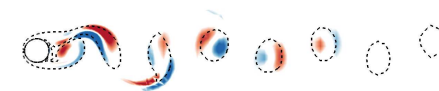
(c) $G/D = 0.75, Re = 165, \lambda/D = 3.75, |\mu| = 1.025$



(d) $G/D = 1, Re = 180, \lambda/D = 3.75, |\mu| = 1.086$



(e) $G/D = 2, Re = 180, \lambda/D = 4, |\mu| = 1.028$



(f) $G/D = \infty, Re = 200, \lambda/D = 4, |\mu| = 1.084$

Figure 9: Spanwise perturbation vorticity contours at the specified gap heights. The contour shading is as per figure 8.

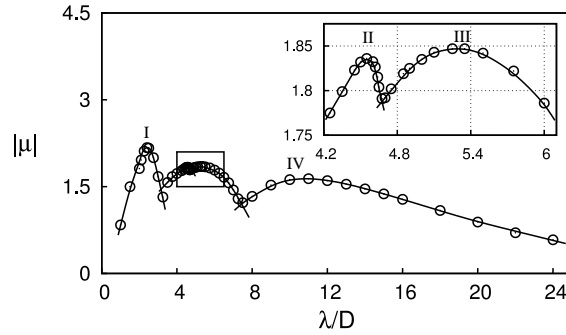


Figure 10: Growth of the linear wake modes for the circular cylinder sliding along a wall at $Re = 200$. The inset shows the two modes between $4 \leq \lambda/D \leq 6$.

IV, respectively. The corresponding spanwise perturbation vorticity fields at these preferred spanwise wavelengths are shown in figure 11.

To further investigate the nature of these modes, the real and imaginary components of the resulting Floquet multipliers are resolved. These are plotted in the complex plane for each of the four modes in figure 12. The horizontal and the vertical axis corresponds to the real and imaginary components of the Floquet multipliers, respectively. The unit circle ($|\mu| = 1$) is shown by the solid line. This separates the region where perturbations decay (inside the circle) from where perturbations grow (outside the circle). Modes I, III and IV were found to be quasi-periodic, i.e., the period of the mode is not commensurate with that of the base flow. Mode II, on the other hand, as a purely real and negative Floquet multiplier, which indicates that it is subharmonic.

To validate the results of the stability analysis and to investigate the evolution towards a saturated wake state, we performed a three-dimensional direct numerical simulation. This was initialised from the two-dimensional periodic flow for $Re = 200$, using a three-dimensional version of the computational code employing a Fourier expansion in the spanwise direction (Thompson et al., 1996; Karniadakis and Triantafyllou, 1992; Ryan et al., 2005; Leontini et al., 2007). Low intensity white noise ($O(10^{-4})$) was added to trigger the development of three-dimensional flow. The selection of the spanwise domain size restricts the number of wavelengths of each of the modes that can fit into the domain to discrete values. Here, this length was chosen as $12D$, sufficient to contain 5, 3, 2 and 1 mode I, II, III and IV wavelengths, respectively. In addition, 64 Fourier planes were used for this simulation. Whilst this is clearly a compromise, it is sufficient to verify the initial linear evolution of the fastest growing perturbation mode, and it likely to give an idea of the complex evolution towards the asymptotic wake state as the different modes grow towards saturation and interact non-linearly.

Figures 13(a) and 13(b) show time traces of the u and w velocity components at a point in the wake as the perturbed two-dimensional flow evolves towards a three-dimensional state. These plots show that the two-dimensional state is maintained for more than 100 non-dimensional time units. Beyond approximately 160 time units, the periodicity in the u trace effectively disappears as strong spanwise flow develops. Figure 13(c) is a depiction of mode I from the linear stability analysis using isosurfaces of positive and negative streamwise vorticity to indicate the wake structure. This should be compared with the DNS isosurfaces shown in figure 13(d), which correspond to $\tau = 95$, while Mode I is still undergoing exponential amplification. This relative time is shown by the first filled circles in figures 13(a) and (b). Figure 13(e) shows the complex nature of the wake at a later time ($\tau = 240$) after the wake has become highly non-linear. As indicated above, in this state even the remnants of periodicity in the u velocity component are lost. Also, there does not appear to be a clearly dominant spanwise wavelength. In any case, the two-dimensional base flow is clearly no longer an adequate model of the real flow in this regime.

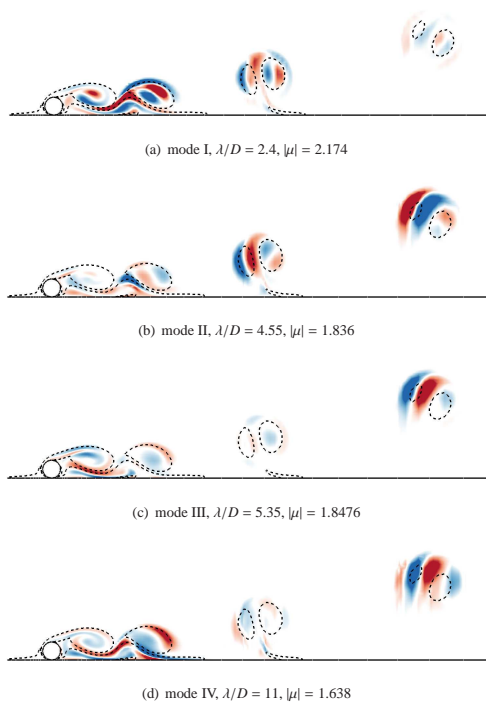


Figure 11: Spanwise perturbation vorticity contours for the cylinder sliding along a wall ($G/D = 0.005$) at $Re = 200$. The cylinder is travelling from right to left in each image. The contour shading is as per figure 8.

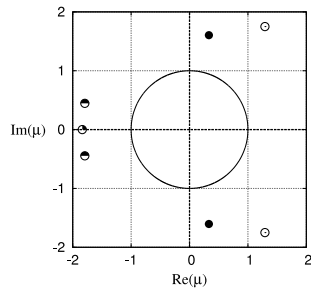


Figure 12: The Floquet multipliers for each of the four unstable modes at $Re = 200$. The modes and their conjugate pairs (if they exist) are shown along with the unit circle ($|\mu| = 1$). Mode I is shown by open circles ($\lambda/D = 2.4$), mode II is shown by quarter filled circles ($\lambda/D = 4.55$), mode III is shown by half filled circles ($\lambda/D = 5.35$) and mode IV is shown by fully filled circles ($\lambda/D = 11$).

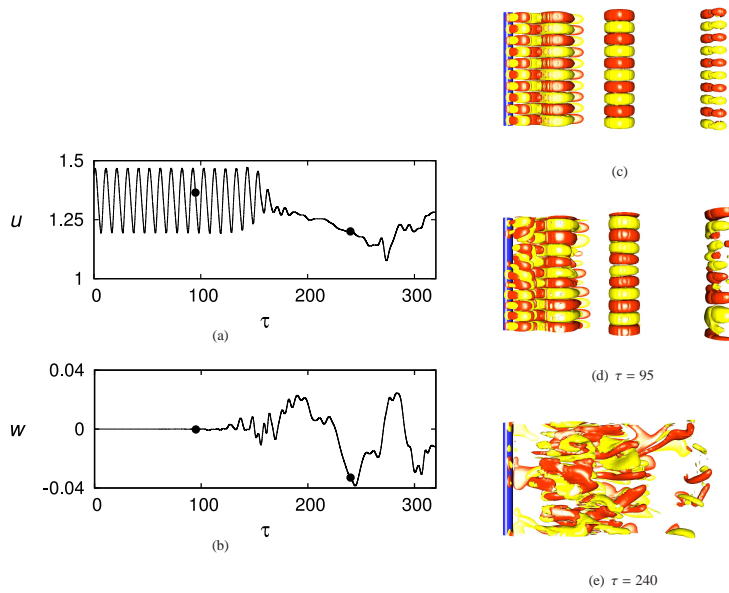


Figure 13: Direct numerical simulation (DNS) results for a circular cylinder sliding along a wall at $Re = 200$. Left: The time histories of the streamwise and spanwise velocity components for a location in the wake downstream of the cylinder. Right: Visualisations using streamwise vorticity isosurfaces viewed from above. Here (c) shows isosurfaces for $\lambda/D = 2.4$ from linear stability analysis, which can be compared with the perturbation field obtained from DNS at $\tau = 95$ in image (d). The final image (e) shows perturbation isosurfaces at $\tau = 240$ after the wake has become chaotic.

4. Conclusions

We have investigated the flow past a circular cylinder translating parallel to a no-slip wall at different gap heights. Two-dimensional simulations show the onset of unsteady flow is delayed to much higher Reynolds numbers relative to the isolated cylinder as the gap height is decreased. For a given gap height, the Strouhal number increased with Reynolds number. The force coefficients at various gap heights have been computed. The critical Reynolds numbers and spanwise wavelengths for the onset of three-dimensional flow are established as the gap height is varied. For $G/D \leq 0.22$, the onset of three-dimensional flow occurs in the steady flow regime. Beyond this, three-dimensional flow develops from unsteady two-dimensional flow at considerably higher Reynolds numbers (e.g., $Re_c = 185$ at $G/D = 0.3$; $Re_c \approx 137$ at $G/D = 0.4$), before moving towards values approaching those observed for an isolated cylinder ($Re_c = 190.5$ and $\lambda/D = 3.96$). The wake development for a Reynolds number well in excess of the initial critical value was also investigated for the lowest gap height case, $G/D = 0.005$, effectively a cylinder sliding along a wall. At $Re = 200$, Floquet analysis shows that the two-dimensional periodic wake is unstable to four different instability modes. The evolution of the wake was followed using DNS for this case as the initially two-dimensional weakly perturbed flow evolves towards its asymptotic state. This simulation shows that initial development of the fastest growing mode, in agreement with the stability analysis, and subsequent rapid transition to a chaotic wake state, for which even quasi-periodic shedding of two-dimensional rollers into the wake seems to be suppressed.

5. Acknowledgements

The support from Australian Research Council Discovery Grants DP0877327 and DP0877517 and computing time from the National Computational Infrastructure (NCI), Victorian Life Sciences Computation Initiative (VLSI) and Monash Sungrid are gratefully acknowledged. A. R. also acknowledges the support of a Monash University Departmental Postgraduate Scholarship. We also thank J. S. Leontini for his assistance in validating some of our results using an immersed boundary code.

References

- Arnal, M., Goering, D., Humphrey, J.A.C., 1991. Vortex shedding from a bluff body adjacent to a plane sliding wall 113, 384–398.
- Bailey, S., Martinuzzi, R., Kopp, G., 2002. The effects of wall proximity on vortex shedding from a square cylinder: Three-dimensional effects. *Physics of Fluids* 14, 4160–4177.
- Barkley, D., Henderson, R.D., 1996. Three-dimensional Floquet stability analysis of the wake of a circular cylinder. *J. Fluid Mech.* 322, 215–241.
- Bearman, P.W., Zdravkovich, M.M., 1978. Flow around a circular cylinder near a plane boundary. *Journal of Fluid Mechanics* 89, 33–47.
- Bhattacharyya, S., Maiti, D.K., 2005. Vortex shedding from a square cylinder in presence of a moving wall. *International Journal for Numerical Methods in Fluids* 48, 985–1000.
- Blackburn, H.M., Barkley, D., Sherwin, S.J., 2008. Convective instability and transient growth in flow over a backward-facing step. *Journal of Fluid Mechanics* 603, 271–304.
- Blackburn, H.M., Lopez, J.M., 2003. On three-dimensional quasiperiodic Floquet instabilities of two-dimensional bluff body wakes. *Physics of Fluids* 15, L57–L60.
- Bosch, G., Kappler, M., Rodi, W., 1996. Experiments on the flow past a square cylinder placed near a wall. *Experimental Thermal and Fluid Science* 13, 292–305.
- Dipankar, A., Sengupta, T.K., 2005. Flow past a circular cylinder in the vicinity of a plane wall. *Journal of Fluids and Structures* 20, 403–423.
- Griffith, M.D., Leweke, T., Thompson, M.C., Hourigan, K., 2008. Steady inlet flow in stenotic geometries: Convective and absolute instabilities. *Journal of Fluid Mechanics* 616, 111–133.
- Griffith, M.D., Thompson, M.C., Leweke, T., Hourigan, K., Anderson, W.P., 2007. Wake behaviour and instability of flow through a partially blocked channel. *Journal of Fluid Mechanics* 582, 319–340.
- Harichandan, A., Roy, A., 2012. Numerical investigation of flow past single and tandem cylindrical bodies in the vicinity of a plane wall. *Journal of Fluids and Structures* available online.
- Henderson, R., 1997. Nonlinear dynamics and pattern formation in turbulent wake transition. *Journal of Fluid Mechanics* 352, 65–112.
- Huang, W.X., Sung, H.J., 2007. Vortex shedding from a circular cylinder near a moving wall. *Journal of Fluids and Structures* 23, 1064–1076.
- Karniadakis, G.E., Sherwin, S.J., 2005. *Spectral/hp Methods for Computational Fluid Dynamics*. Oxford University Press, Oxford.
- Karniadakis, G.E., Triantafyllou, G.S., 1992. Three-dimensional dynamics and transition to turbulence in the wake of bluff objects. *Journal of Fluid Mechanics* 238, 1–30.
- Lei, C., Cheng, L., Armfield, S., Kavanagh, K., 2000. Vortex shedding suppression for flow over a circular cylinder near a plane boundary. *Ocean Engineering* 27, 1109–1127.
- Leontini, J.S., Thompson, M.C., Hourigan, K., 2007. Three-dimensional transition in the wake of a transversely oscillating cylinder. *Journal of Fluid Mechanics* 577, 79–104.
- Lewke, T., Williamson, C.H.K., 1998. Three-dimensional instabilities in wake transition. *European Journal of Mechanics B/Fluids* 17, 571–586.

- Lim, T.T., Sengupta, T.K., Chattopadhyay, M., 2004. A visual study of vortex-induced subcritical instability on a flat plate laminar boundary layer. *Experiments in Fluids* 37, 47–55.
- Mahir, N., 2009. Three-dimensional flow around a square cylinder near a wall. *Ocean Engineering* 36, 357 – 367.
- Marquet, O., Sipp, D., Chomaz, J.M., Jacquin, L., 2008. Amplifier and resonator dynamics of a low-Reynolds-number recirculation bubble in a global framework. *Journal of Fluid Mechanics* 605, 429.
- Nishino, T., Roberts, G., Zhang, X., 2007. Vortex shedding from a circular cylinder near a moving ground. *Physics of Fluids* 19, 025103–1–025103–12.
- Price, S.J., Sumner, D., Smith, J.G., Leong, K., Paidoussis, M.P., 2002. Flow visualization around a circular cylinder near to a plane wall. *Journal of Fluids and Structures* 16, 175–191.
- Rao, A., Stewart, B., Thompson, M., Leweke, T., Hourigan, K., 2011. Flows past rotating cylinders next to a wall. *Journal of Fluids and Structures* 27, 668 – 679.
- Reichl, P., Hourigan, K., Thompson, M.C., 2005. Flow past a circular cylinder close to a free surface. *Journal of Fluid Mechanics* 533, 269–296.
- Robichaux, J., Balachandrar, S., Vanka, S.P., 1999. Three-dimensional Floquet instability of the wake of a square cylinder. *Phys. Fluids* 11, 560–578.
- Ryan, K., Thompson, M.C., Hourigan, K., 2005. Three-dimensional transition in the wake of elongated bluff bodies. *Journal of Fluid Mechanics* 538, 1–29.
- Sheard, G.J., Thompson, M.C., Hourigan, K., 2003. From spheres to circular cylinders: the stability and flow structures of bluff ring wakes. *Journal of Fluid Mechanics* 492, 147–180.
- Sheard, G.J., Thompson, M.C., Hourigan, K., 2004. From spheres to circular cylinders: Non-axisymmetric transition in the flow past rings. *Journal of Fluid Mechanics* 506, 45–78.
- Stewart, B.E., Hourigan, K., Thompson, M.C., Leweke, T., 2006. Flow dynamics and forces associated with a cylinder rolling along a wall. *Physics of Fluids* 18, 111701–1–111701–4.
- Stewart, B.E., Thompson, M.C., Leweke, T., Hourigan, K., 2010a. Numerical and experimental studies of the rolling sphere wake. *Journal of Fluid Mechanics* 643, 137–162.
- Stewart, B.E., Thompson, M.C., Leweke, T., Hourigan, K., 2010b. The wake behind a cylinder rolling on a wall at varying rotation rates. *Journal of Fluid Mechanics* 648, 225–256.
- Taneda, S., 1965. Experimental investigation of vortex streets. *Journal of the Physical Society of Japan* 20, 1714–1721.
- Thompson, M.C., 2012. Effective transition of steady flow over a square leading-edge plate. *Journal of Fluid Mechanics* to appear.
- Thompson, M.C., Hourigan, K., Cheung, A., Leweke, T., 2006a. Hydrodynamics of a particle impact on a wall. *Appl. Math. Model.* 30, 190–196.
- Thompson, M.C., Hourigan, K., Ryan, K., Sheard, G.J., 2006b. Wake transition of two-dimensional cylinders and axisymmetric bluff bodies. *Journal of Fluids and Structures* 22, 793–806.
- Thompson, M.C., Hourigan, K., Sheridan, J., 1996. Three-dimensional instabilities in the wake of a circular cylinder. *Exp. Therm. Fluid Sci.* 12, 190–196.
- Thompson, M.C., Leweke, T., Hourigan, K., 2007. Sphere-wall collisions: vortex dynamics and stability. *Journal of Fluid Mechanics* 575, 121–148.
- Thompson, M.C., Leweke, T., Williamson, C.H.K., 2001. The physical mechanism of transition in bluff body wakes. *J. Fluids Struct.* 15, 607–616.
- Williamson, C.H.K., 1996a. Three-dimensional wake transition. *Journal of Fluid Mechanics* 328, 345–407.
- Williamson, C.H.K., 1996b. Vortex dynamics in the cylinder wake. *Annual Review of Fluid Mechanics* 28, 477–539.
- Yoon, H., Lee, J., Seo, J., Park, H., 2010. Characteristics for flow and heat transfer around a circular cylinder near a moving wall in wide range of low Reynolds number. *Int. J. Heat Mass Transfer* 53, 5111 – 5120.
- Zerihan, J., Zhang, X., 2000. Aerodynamics of a single element wing in ground effect. *Journal of Aircraft* 37, 1058–1064.
- Zhang, X., Mahon, S., Den-Berg, M.V., Williams, C., 2005. Aerodynamics of a half-cylinder in ground effect, in: *Engineering Turbulence Modelling and Experiments* 6. Elsevier Science B.V., pp. 461 – 470.

Chapter 4

Flow past a cylinder rolling along a wall

4.1 Overview

The previous chapters have investigated the effect of rotation on circular cylinders in freestream and the variation in flow structures observed when close to a plane wall. The combination of the two is investigated here. Flows past bluff bodies rolling near a wall are investigated here, extending the studies of Stewart *et al.* (2006, 2010b) to higher rotation rates. Of primary interest is the exploration of the flow structures as the rotation rate is extended for $-3 \leq \alpha \leq 3$. As the rotation rate is increased from $\alpha = 0$, the vortex pairs which are formed become larger in size, and a decrease in the critical Reynolds number for the onset of periodic flow is observed, while on decreasing the rotation rate to negative values ($\alpha < 0$), the onset of vortex shedding occurs at higher Reynolds numbers and for $\alpha \leq -1.5$, vortex shedding is suppressed. On increasing the rotation rate, three-dimensionality occurs at increasingly low Reynolds numbers, while on decreasing the rotation rate to negative values, the onset of three-dimensionality is delayed to higher Reynolds numbers and altogether suppressed for $\alpha \leq -2$.

The following section contains the journal article describing the above stated flow features, with a significant focus on the variation of the drag coefficient with rotation rate. Also, briefly introduced here is the topic of flow past multiple bodies near a wall, and the drag reduction on the trailing body as the separation distance and Reynolds numbers are varied.

4.2 Flow dynamics of a rolling cylinder near a wall

The following article was published in 2011 in *Journal of Fluids and Structures*. This work was co-authored by B.E. Stewart, M. C. Thompson, T. Leweke and K. Hourigan, and is entitled, “*Flows past rotating cylinders next to a wall*”. The paper is reproduced in this thesis directly from the version published online.

Declaration for manuscript included in PhD Thesis

Monash University

Declaration for Thesis Chapter 4

Declaration by candidate

In the case of Chapter 4, the nature and extent of my contribution to the work was the following:

Nature of contribution	Extent of contribution (%)
Conceived ideas, initiated the paper, performed numerical simulations, analysed the data, wrote the manuscript	70

The following co-authors contributed to the work. Co-authors who are students at Monash University must also indicate the extent of their contribution in percentage terms:

Name	Nature of contribution	Extent of contribution (%) for student co-authors only
Dr. B. E. Stewart	Performed experimental investigations	N. A.
Prof. M.C. Thompson	Co-wrote the manuscript	N. A.
Prof. T. Leweke	Co-wrote the manuscript	N. A.
Prof. K. Hourigan	Co-wrote the manuscript	N. A.

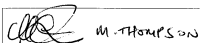
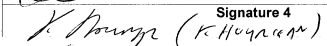
Candidate's Signature  Date 18 JUNE 2012

Declaration by co-authors

The undersigned hereby certify that:

- 1) the above declaration correctly reflects the nature and extent of the candidate's contribution to this work, and the nature of the contribution of each of the co-authors.
- 2) they meet the criteria for authorship in that they have participated in the conception, execution, or interpretation, of at least that part of the publication in their field of expertise;
- 3) they take public responsibility for their part of the publication, except for the responsible author who accepts overall responsibility for the publication;
- 4) there are no other authors of the publication according to these criteria;
- 5) potential conflicts of interest have been disclosed to (a) granting bodies, (b) the editor or publisher of journals or other publications, and (c) the head of the responsible academic unit; and
- 6) the original data are stored at the following location(s) and will be held for at least five years from the date indicated below:

Location(s)

Signature 1	 M. THOMPSON	Signature 3	Date
Signature 2	 (K. HOURIGAN)	Signature 4	19/6/2012
	 (FOR B.E. STEWART)		19/6/2012
	 (FOR T. LEWEKE)		19/6/2012



Contents lists available at ScienceDirect

Journal of Fluids and Structures

journal homepage: www.elsevier.com/locate/jfs



Flows past rotating cylinders next to a wall

A. Rao^a, B.E. Stewart^a, M.C. Thompson^a, T. Leweke^b, K. Hourigan^{a,c,*}

^a Fluids Laboratory for Aeronautical and Industrial Research (FLAIR), Department of Mechanical and Aerospace Engineering, Monash University, Clayton 3800, Australia

^b Institut de Recherche sur les Phénomènes Hors Équilibre (IRPHE), CNRS/Universités Aix-Marseille, 49 rue Frédéric Joliot-Curie, B.P. 146, F-13384 Marseille Cedex 13, France

^c Division of Biological Engineering, Monash University, Clayton 3800, Australia

ARTICLE INFO

Article history:

Received 19 October 2010

Received in revised form

21 March 2011

Accepted 25 March 2011

Available online 20 May 2011

Keywords:

Rotating bodies

Stability analysis

Wakes

Body forces

Flow transition

ABSTRACT

Two-dimensional simulations are used to investigate the flow past rotating circular cylinders near a wall in the low Reynolds number regime ($20 \leq Re \leq 750$). For the single cylinder case, rotation rates higher than previously studied are considered. For cylinders rolling forward, the wake flow structures observed are similar to those seen in previous studies; however, it is found that reverse rotation of the cylinder can completely suppress vortex shedding. The drag force on the cylinder is quantified. Linear stability analysis is used to determine the onset of three-dimensionality in the wake. Increased forward rotation triggers three-dimensionality at increasingly lower Reynolds numbers, while reverse rotation delays this transition to much higher values. For the highest reverse rotation rate, three-dimensionality was suppressed at the higher end of the Reynolds number range investigated. A study of two sliding cylinders is also performed, especially focusing on the interaction of the first wake with the second, the effect on the overall wake dynamics and quantification of the drag on each cylinder.

© 2011 Elsevier Ltd. All rights reserved.

1. Introduction

The separated flow over a circular cylinder is one of the classical fluid dynamics problems, studied in detail for over a century since the pioneering investigations of Bénard (1908) and von Kármán (1911). Since then, there have been many comprehensive review articles, including Williamson (1996a,b), Norberg (2003), and reviews of wake transition for other cylindrical or axisymmetric bluff bodies (e.g., Thompson et al., 2006b). The flow dynamics are dramatically altered when such bodies are placed close to a plane wall. A significant change in shedding frequency and forces experienced by these bodies is observed, compared with similar bodies in an unbounded flow. An added parameter to such investigations is the effect of body rotation. By use of a numerical solver, we examine the flow structures and wake dynamics, and compute the forces on a circular cylinder as a function of rotation rate and Reynolds number, and then extend this study to examine two sliding cylinders.

One motivation for this study is to improve our understanding of the flow dynamics of, and forces on, cells near blood vessel walls of which the current problem is a simplified two-dimensional analogue. Certain cell types such as platelets and leukocytes depend on rolling and sliding along a vessel wall as part of the activation process to initiate the clotting or

* Corresponding author at: Fluids Laboratory for Aeronautical and Industrial Research (FLAIR), Department of Mechanical and Aerospace Engineering, Monash University, Clayton 3800, Australia.

E-mail address: Kerry.Hourigan@monash.edu (K. Hourigan).

immune response (Lawrence and Springer, 1991; Wagner and Frenette, 2008). This study is a prelude to studies investigating flow behaviour at much lower Reynolds numbers, which may be directly applicable to the above mentioned examples. The current study is also applicable to many particle–particle and particle–wall interactions, (e.g., particles in a sedimentation tank), as it considers a wider parameter range.

2. Flows around a single cylinder close to a plane wall

The effect of placing a body in close proximity to a wall brings about a substantial change to the wake flow structure and consequently the forces experienced by the body, compared with an unbounded flow. Investigations in a wind tunnel by Bearman and Zdravkovich (1978) showed a strong suppression of vortex shedding for a gap to diameter ratio $G/D=0.3$, for a cylinder adjacent to a stationary wall. The lift force experienced by the cylinder was directed away from the wall for the cases investigated but the Strouhal number (St) remained approximately constant as the cylinder moved closer towards $G/D=0.3$.

A single row of vortices was observed by Taneda (1965) for a cylinder moving close to a wall at $Re=170$. The experiments were conducted using condensed milk and aluminium dust to visualise the vortex structures. It was noted that the time period for the vortex formation was longer than that in free stream.

Lei et al. (2000) investigated the effect of gap ratio (G/D) between 0.1 and 3 for a Reynolds number range of 80–1000. Using a finite-difference method, they describe the flow structure formation behind the cylinder for $G/D < 3$. The lower wall is stationary, leading to the formation of a boundary layer, which interacts with the shear layer shed from the lower side of the cylinder. At different gap ratios and Reynolds numbers, the opposite signed vorticity in the wall shear layer and the shear layer shed from the cylinder cancel each other out, leading to the suppression of vortex shedding. It was also found that the critical gap ratio at which the shedding ceases decreases with an increase in Reynolds number, asymptoting to 0.2 at higher values.

Nishino et al. (2007) conducted experiments in a wind tunnel for intermediate Reynolds numbers $O(10^5)$ with a moving wall to prevent the development of a boundary layer. Three regions of vortex shedding based on the gap height were identified. For $G/D > 0.5$, regular vortex shedding was observed; and as the cylinder was moved closer to the wall, the shedding became intermittent and ceased to exist for gap ratios ≤ 0.35 . The experiments showed a decrease in drag coefficient as the cylinder was moved progressively closer to a wall, becoming constant for $G/D \leq 0.35$.

Numerical simulations for a stationary cylinder close to a moving wall have been performed by Huang and Sung (2007). They obtained a critical vortex suppression value of $G/D=0.28$, which is close to that observed for simulations conducted with a stationary wall. Furthermore, they attributed the formation of the vortex from the lower side of the cylinder to the higher flow rate between the cylinder and the moving wall. For a constant gap ratio, the lift and drag values increased as the Reynolds number was increased from 200 to 500. Numerical simulations have also been carried out for rotating bodies close to a stationary wall. Using the lattice Boltzmann method, Cheng and Luo (2007) obtained flow structures and quantified the forces on a rotating cylinder near a stationary wall. The magnitude and sense of rotation affect the critical height at which vortex shedding is suppressed. For a given gap ratio, the lift coefficient increased as the rotation rate was changed from retrograde to prograde, while the drag coefficient showed the reverse trend.

Two- and three-dimensional studies for a square cylinder near a stationary wall have been conducted by Mahir (2009). The mean drag force decreased as the cylinder was brought close to a wall. It was also noted that the two-dimensional simulations overpredicted the mean lift and drag values. Their simulations considered a body adjacent to a stationary wall, while the present work focuses on a body in motion along a plane surface.

Stewart et al. (2010) conducted two- and three-dimensional numerical simulations for a single cylinder rolling along a wall. The gap ratio was maintained at 0.005 to prevent the grid singularity that occurs if the cylinder is touching the wall. Forward rolling of the cylinder destabilised the flow, reducing the Reynolds number at which shedding first occurred, while reverse rolling stabilised it. The lift and drag values were found to be highly dependent on the rotation rates. The steady and unsteady regimes of the flow for different rotation rates were mapped. In the unsteady regime, the shear layer shed from the top of the cylinder combined with the wall shear layer downstream, forming a vortex pair with a net rotation. Their stability analysis reported that the wake undergoes a transition to three-dimensionality and then becomes unsteady, as the Reynolds number is increased. The transition mechanism to three-dimensionality was not clearly understood. Experimental work carried out in a water channel confirmed the flow features visualised in the numerical simulations. The current work is an extension of that study: first to higher forward and reverse rotation rates and then to multiple circular cylinders.

3. Problem definition and methodology

This study is an extension to the generic flow problem of a single cylinder rolling, without slipping, along a wall in a quiescent fluid. That problem is governed by a single parameter, the Reynolds number $Re = UD/\nu$, where D is the cylinder diameter, U the velocity of its centre, and ν the kinematic viscosity of the fluid. In the general case, in which slip between the cylinder and the wall is allowed, another parameter is needed to fully describe the flow. A convenient choice is the rotation speed at the cylinder surface relative to the linear speed at its centre $\alpha = (\omega D/2)/U$, where ω is the angular velocity. Forward rolling (i.e., rotation against the flow at the top of the cylinder—anti-clockwise in this case) corresponds

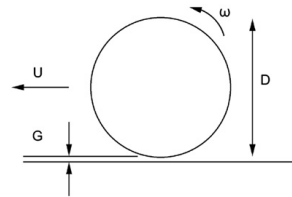


Fig. 1. Schematic representation of the cylinder.

to positive α values, and reverse rolling (i.e., aiding the flow or clockwise) corresponds to negative α values. The range of Reynolds numbers considered in this study is between 20 and 200 for $\alpha \geq 0$ and between 20 and 750 for $\alpha < 0$. In the current study, α is varied between -2 and $+2$. A schematic representation of the rolling cylinder is shown in Fig. 1. The cylinders are placed at a very small distance above the wall to prevent the formation of singular elements directly beneath the cylinders. The gap height normalised by the cylinder diameter, G/D , is set to 0.005. Previous studies (Stewart et al., 2006, 2010) have shown that the simulated flow structures match the experimentally observed ones when the cylinder is actually in contact with the wall, although it is true that the lift and drag forces are sensitive to the gap ratio. At low Reynolds numbers, the drag force was more sensitive to the gap ratio than at higher flow speeds. The frequency of shedding of the wake, f , is quantified through the non-dimensional Strouhal number, $St = fD/U$. The drag coefficient (per unit width) reported here is given by $C_d = \bar{F}_d / (\frac{1}{2} \rho U^2 D)$, where \bar{F}_d is the time-averaged force experienced by the cylinder. Visualisations for all cases presented here are with flow from left to right in the frame of reference of the cylinder. Vortical structures have been visualised using a red/blue colour scheme, where red indicates negative, and blue positive vorticity, respectively. The contour levels for all figures shown are between $\pm 5U/D$.

3.1. Numerical formulation

In order to compute the flow numerically, the incompressible Navier–Stokes equations are solved in the frame of reference of the cylinder. In this inertial reference frame, the fluid moves from left to right at constant speed U . A detailed description of the numerical method and implementation is given in Thompson et al. (2006a); it has previously been employed to investigate bluff body flow dynamics for many related problems, e.g., Stewart et al. (2010), Thompson et al. (1996), Thompson et al. (2001), Leontini et al. (2007), Tan et al. (2005), Le Gal et al. (2001). The numerical method uses the spectral-element approach with the computational domain constructed from a set of quadrilateral elements with curved sides as necessary to accurately model the cylinder surface. Each element is further sub-divided by a set of internal nodes distributed according to the Gauss–Legendre–Lobatto quadrature points, with the velocity and pressure fields represented by a tensor product of Lagrangian polynomial interpolants within the elements. While the method is only continuous in the function, and not in the derivatives, across element boundaries, it has been shown to provide spectral or exponential convergence as the interpolant order is increased (Karniadakis and Sherwin, 2005). A key advantage with the method is the ability to specify the number of nodes per element $N \times N$ at runtime. The interpolant polynomial order is then given by $N - 1$. The fractional step technique is used for the time integration (Chorin, 1968; Karniadakis et al., 1991) for computing both the steady and unsteady wakes.

At the solid boundaries and the inflow and top domain boundaries, the velocity was set to the relevant known values to provide the boundary conditions there. At the outflow boundary, the pressure was set to zero together with the normal velocity gradient. The domain boundaries were placed at sufficiently large distances from the cylinder to reduce blockage to about 1%.

3.2. Linear stability analysis

The transition to three-dimensionality in the wake forms an important aspect of understanding flows over bluff bodies, not least because it precedes the transition to fully turbulent flow, and the remnants of these three-dimensional modes tend to persist into the fully turbulent regime (Williamson, 1996b; Wu et al., 1996). Flows over bodies moving close to the ground have been found to undergo transition to three-dimensionality before becoming unsteady, as shown by Stewart et al. (2010), which is noted to be similar to the three-dimensional transition for flow over a backward-facing step (Barkley et al., 2002). In order to determine the transitional values, we perform linear stability analysis by splitting the velocity and pressure fields into two-dimensional components describing the stable or unstable base flow plus three-dimensional perturbations. Mathematically, the linearised Navier–Stokes equations for the perturbation fields admit solutions based on exponential growth or decay in time, together with sinusoidal variation in the spanwise direction. In general, the full solution can be constructed as a Fourier sum of spanwise modes, each growing or decaying exponentially in time. In practice, for each Reynolds number and each spanwise wavelength (λ), the linearised equations can be integrated in time

Table 1
Variation of the time-averaged drag coefficient for $\alpha = +2$.

N	Re=20		Re=200	
	$\overline{C_d}$	Variation (%)	$\overline{C_d}$	Variation (%)
4	10.295424	-9.063091	3.920135	-2.507025
5	11.210904	-0.976885	4.027608	0.165807
6	11.281302	-0.355077	4.022211	0.031585
7	11.273864	-0.420775	4.015624	-0.132233
8	11.311096	-0.091914	4.024288	0.083239
9	11.321852	0.003091	4.021998	0.026287
10	11.321418	-0.000742	4.018557	-0.059290
11	11.321502	0	4.020941	0

Table 2
Variation of the time-averaged drag coefficient for $\alpha = -2$.

N	Re=20		Re=750	
	$\overline{C_d}$	Variation (%)	$\overline{C_d}$	Variation (%)
4	9.375690	3.380668	0.228723	-4.688425
5	9.134668	0.723049	0.241246	0.530057
6	9.087320	0.200968	0.240163	0.078759
7	9.084586	0.170822	0.240082	0.045005
8	9.072538	0.037975	0.239991	0.007084
9	9.069034	-0.000662	0.239969	-0.002084
10	9.069136	0.000463	0.239973	-0.000417
11	9.069094	0	0.239974	0

starting from a base flow perturbed with white noise. After some time, for each spanwise wavelength, only the dominant instability mode remains, since it is the one that grows fastest or decays most slowly. In fact, it is possible to extract the first few most important modes for each spanwise wavelength by using an Arnoldi decomposition of the snapshots of the evolving fields at fixed time intervals (T), typically the base flow period if the base flow is periodic (see, e.g., Barkley and Henderson, 1996; Ryan et al., 2005). In that case, the instability analysis is called Floquet analysis. The growth rate (σ) of each mode can be related to the amplification factor (μ) over time T by $\mu = e^{\sigma T}$. The critical Reynolds number (Re_c), corresponding to a maximum growth rate of $\sigma = 0$ or amplification factor $\mu = 1$, over all wavelengths, marks the transition to three-dimensional flow. For the case of rolling cylinders near a wall, the flow is steady before the onset of three-dimensionality, unlike the case of a cylinder in an unbounded flow, where three-dimensionality develops on an already unsteady periodic base flow (Thompson et al., 1996; Barkley and Henderson, 1996). More details of the theory and numerical approach can be found, e.g., in Griffith et al. (2007), Leontini et al. (2007) and Ryan et al. (2005).

3.3. Domain size and mesh resolution studies

The computational domain chosen was of similar dimensions to that used for previous work, with the inlet and outlet at $100D$ upstream and downstream of the cylinder, and the top boundary placed $150D$ from the wall. The spatial resolution is controlled by varying the number of interpolation points in each direction, N . These points are used as a basis for constructing the Lagrange interpolating polynomials over which integration is carried out, as described above. The number of points over each (two-dimensional) element was varied between $N^2 = 16$ and 121. This check was carried out for the two extreme cases of the Reynolds number at the maximum rotation rates of $\alpha = \pm 2$. Tables 1 and 2 tabulate the drag coefficient as the spatial resolution is increased. For $N=8$, the values are within 0.1% of the maximum tested resolution. Furthermore, at $N=8$, the Strouhal number at $Re=200$ and $\alpha = +2$ was well within 0.2% of that at the maximum tested resolution.

4. Results

4.1. Flow structures

Initially, we focus on the wake flow structures for different rotation rates. For moderate Reynolds numbers and for positive α , the shear layer rolls up behind the cylinder forming a strong clockwise vortex, which grows in strength prior to eventually detaching from the separating shear layer. This vortex induces the generation of vorticity of opposite sign beneath it in order to satisfy the no-slip boundary condition there. For the Reynolds number shown ($Re=180$), diffusion is

low enough to allow the secondary vorticity to be pulled away from the wall to form a vortex pair, which subsequently self-propels away from the wall through self-induction. This same scenario is observed for all positive rotation rates examined, as shown in Fig. 2. Although the parameter space was generally restricted to $\alpha = \pm 2$, some visualisations were carried out at a higher rotation rate of $\alpha = +3$. The vortex formed at the top of the cylinder rolls up in a more circular shape at higher rotation rates as compared to $\alpha = 1$, where a more oblate vortex pair is formed. Also, the increased rotation rate moves the separation point of the separating shear layer further forward. The transition from steady state to unsteady flow was found to occur at lower Reynolds numbers when increasing the rotation speed. Vortex shedding was observed at $Re=65$ at $\alpha = +2$, in contrast to unsteady flow being first observed at $Re \geq 90$ and 160 for $\alpha = +1$ and 0 , respectively. The flow at these Reynolds numbers is three-dimensional and unsteady; the flow structures have two-dimensional projections resembling the computed two-dimensional wakes shown here, but with an additional spanwise waviness (see Stewart et al., 2010).

Vortex shedding was found to occur only at higher Reynolds numbers ($Re \geq 425$) for a cylinder in clockwise rotation or reverse rolling ($\alpha = -1$) (Stewart et al., 2010). In Fig. 3, wakes are shown for $Re=750$. The vortex pairs formed in this case drifted farther away from the wall at this flow speed, compared with those at $Re=450$. On increasing the rotation speed in the clockwise direction to $\alpha = -1.25$, vortex shedding was detected only for $Re > 700$. The structure of the shear layers formed behind the cylinder resembled that at $\alpha = -1$. The frequency of shedding was far higher and the vortex structures formed were much smaller compared to those at $\alpha = -1$, and they remained closer to the wall. On further increasing the magnitude of (negative) rotation speed, the flow structure changed dramatically and vortex shedding ceased to occur for $Re \leq 750$ and $\alpha = -2$. A stand-alone run for $\alpha = -3$ showed that vortex shedding continued to be suppressed at higher negative rotation rates. For these very high reverse rotation rates, the cylinder boundary layer wraps all the way around the cylinder, almost preventing separation entirely. Note that for a rotating cylinder in a free stream, vortex shedding is briefly suppressed between rotation rates of $1.91 \leq \alpha \leq 4.34$ and beyond $\alpha \geq 4.8$ (Mittal and Kumar, 2003).

Stages of vortex shedding for $\alpha = +2$ at $Re=200$ are shown in Fig. 4 for one time period, along with the corresponding instances on the force history diagram. Points (a) and (e) both correspond to image (a). At $\tau = 165$, the vortex pair behind the rolling cylinder is about to drift away from the cylinder wall system. At a slightly later time of $\tau = 170$ [image (b)],

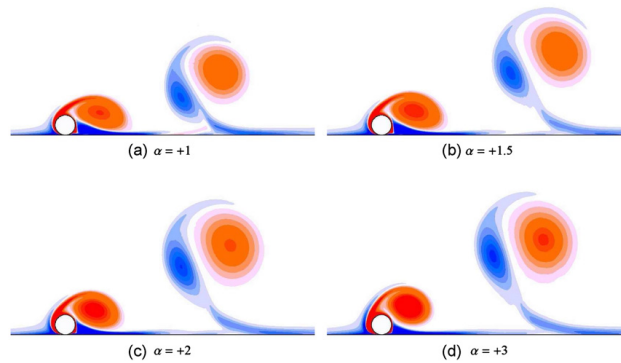


Fig. 2. Evolution of the wake for the anti-clockwise rotation of a single cylinder at $Re=180$ for the rotation rates shown. Vorticity contours and colours are the same in all images. The vortex pair for $\alpha = +3$ is the strongest. (For interpretation of the references to colour in this figure legend, the reader is referred to the web version of this article.)

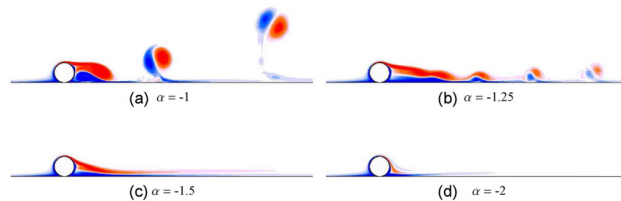


Fig. 3. Evolution of the wake for the clockwise rotation of a single cylinder at $Re=750$ for the rotation rates shown.

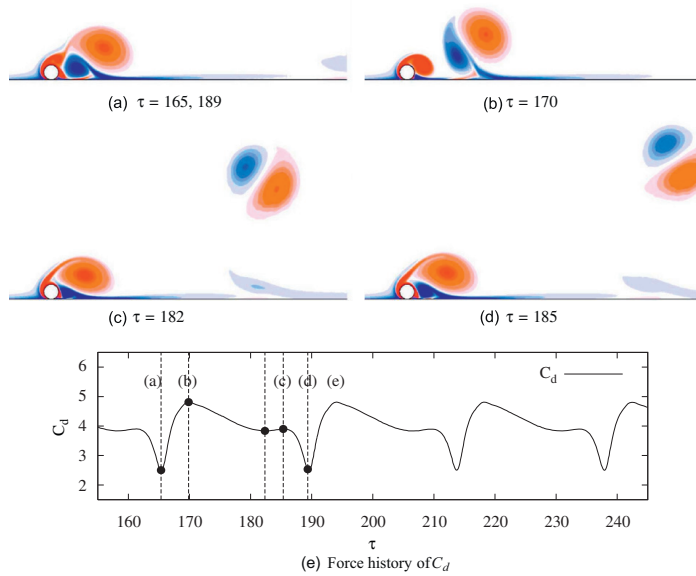


Fig. 4. (a–d) Vorticity snapshots for the single cylinder rolling at $\alpha = +2$ and $Re=200$. (e) Instantaneous drag coefficient (C_d).

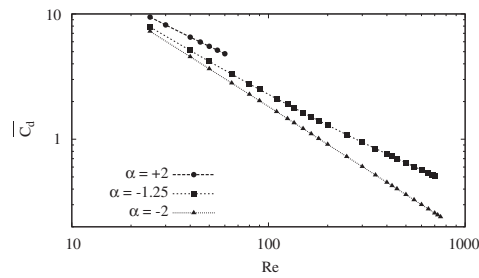


Fig. 5. Variation of the drag coefficient for different rotation rates in the steady state regime.

we observe that the drag has almost doubled, due to the low pressure caused by the rolling up of the shear layer above the cylinder. The vortex grows larger and moves away from the cylinder, leading to the recovery of pressure, thereby causing a drop in the drag force until $\tau = 182$ [image (c)]. As explained previously, the wall shear layer is also being drawn up by the much larger vortex from the top of the cylinder and leads to a slight increase in drag force [image (d)]. At a slightly later stage, the shear layer on the top of the cylinder has rolled up and has drifted further away, and a decrease in drag is observed.

4.2. Drag and Strouhal number trends

Drag coefficients for the steady and unsteady cases are shown in Figs. 5 and 6, respectively. For the steady cases, we observe that the trends vary linearly on a log–log plot. These trends are similar to those previously observed by Stewart et al. (2010) for cylinders at lower rotation rates.

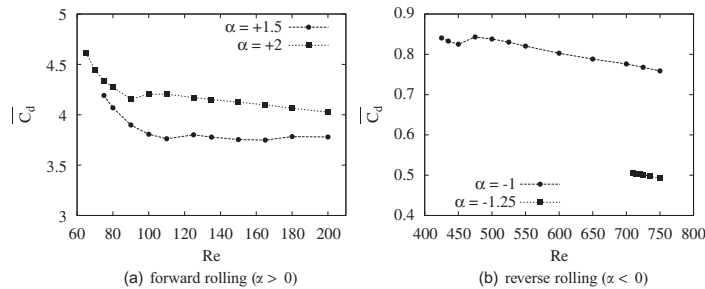


Fig. 6. Variation of the time-averaged drag coefficient with Reynolds number in the unsteady regime.

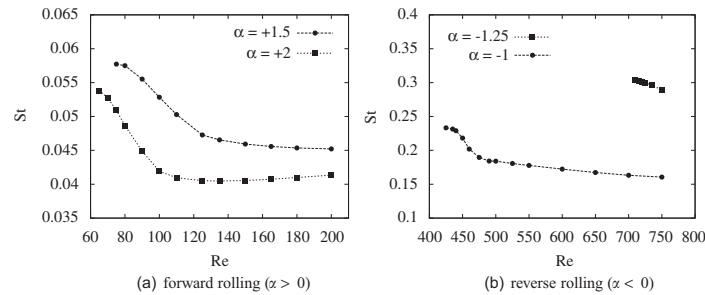


Fig. 7. Strouhal-Reynolds number relationships.

The Strouhal number variation for the higher rotation rate cases investigated is shown in Fig. 7. Strouhal numbers for the negative rotation rates are much higher compared with the positive rotation cases.

4.3. Three-dimensional transition

Stability analysis was conducted to determine the critical Reynolds number at which the flow undergoes transition to three-dimensional flow. As described above, linear stability analysis is performed based on two-dimensional steady or unsteady base flows. In practice, this amounts to determining the growth rates of the dominant modes corresponding to a range of spanwise wavelengths, for a set of Reynolds numbers. The aim is to determine the critical Reynolds number at which the growth rate first becomes zero, and the corresponding wavelength.

For the simulations conducted here, three-dimensionality is initially triggered on the steady base flow at Reynolds numbers less than the values at which unsteady flow occurs, in agreement with the findings of Stewart et al. (2010). Fig. 8 presents plots of growth rate as function of axial wavelength for different rotation rates. Fig. 9 summarises the results from the analysis of these curves: the variation of the critical Reynolds number and wavelength with rotation rate. As the rotation is increased from $\alpha = -1.5$ to $+2$, the transition Reynolds number monotonically decreases, while the critical spanwise wavelength monotonically increases.

4.4. Comparison with experimental results

Experiments were performed in a water tunnel using a cylinder driven by a stepper motor placed adjacent to a purpose-built moving floor, as described in Stewart et al. (2006, 2010). Some dye visualisations showing the two-dimensional structure of the wake for different rotation rates are shown in Figs. 10–12. Note that these images are taken just after startup, before the wake has become too three-dimensional, both from end-effects given the short aspect ratio (13:1), and the growth of the intrinsic three-dimensional instability as discussed above. The corresponding numerical simulations were conducted at slightly higher Reynolds numbers than for the experiments. This is because unsteady transition is triggered at subcritical Reynolds numbers with the current experimental setup.

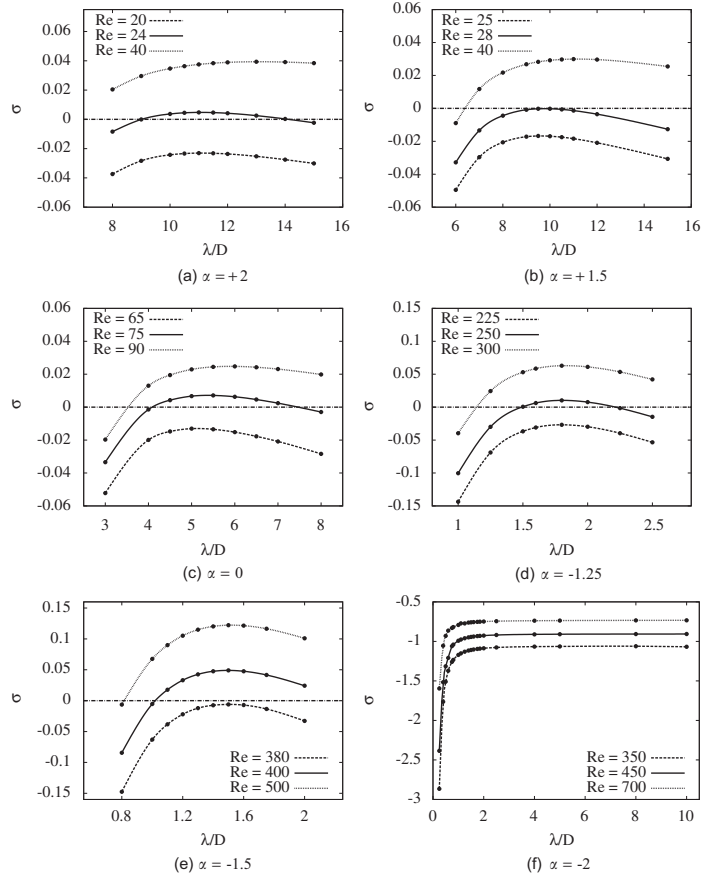


Fig. 8. Variation of growth rate for different rotation rates.

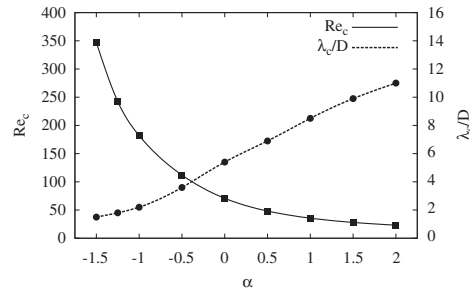


Fig. 9. Variation of the critical Reynolds number and wavelength with rotation rate, extending the work of Stewart et al. (2010).

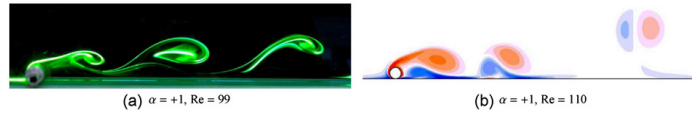


Fig. 10. Dye visualisations from the water channel (left) and vorticity contours from the numerical simulations (right).

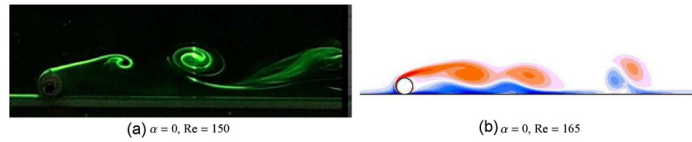


Fig. 11. Dye visualisations from the water channel (left) and vorticity contours from the numerical simulations (right).

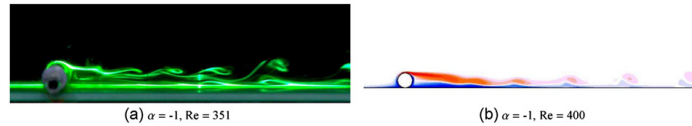


Fig. 12. Dye visualisations from the water channel (left) and vorticity contours from the numerical simulations (right).

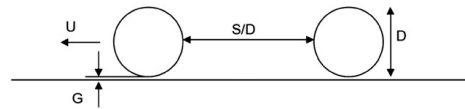


Fig. 13. Schematic representation of the tandem cylinder.

5. Tandem cylinders

The flow characteristics of a bluff body are altered when a body of similar dimension is placed in its vicinity (see, e.g., Sumner, 2010 for a recent review). Here, we consider the case of two-dimensional flow around two cylinders sliding along a plane wall without rotation ($\alpha = 0$). The trailing body is placed downstream of the first body at different normalised separation distances (S/D), measured as the dimensionless distance between the cylinders (see Fig. 13). As for the case of a single cylinder, a gap of size $G/D = 0.005$ is maintained between the cylinders and the wall. The range of Reynolds numbers for this investigation is 20–200 and the separation distance is varied between $0.1 \leq S/D \leq 10$. One motivation for this study comes from the drag reduction of the trailing or the downstream body when placed at close separation distances. At very large spacings, the cylinders effectively behave as individual entities and the flow characteristics of both should resemble those of a single cylinder.

The numerical formulation and the problem setup are very similar to that for a single cylinder. However, there is an increase in the number of macro-elements required in order to resolve the boundary layers of each cylinder and the larger region with high velocity gradients, which leads to the increase in computational effort. Mesh resolution studies were also carried out for the case of $S/D = 10$. A domain size of $50D$ (inlet) \times $50D$ (top surface) \times $100D$ (outlet) was used for the simulations, with the outlet boundary being placed $100D$ from the downstream cylinder, and a polynomial order $N = 7$. This was sufficient to capture the drag force accurately.

It may be recalled that the critical value for transition to unsteady state for a single cylinder sliding along a wall is $Re = 160$ (Stewart et al., 2010). In general for the tandem cylinder case, the flow was found to become more stable as (a) the Reynolds number decreased and (b) as the separation distance between the two cylinders decreased. For example, at $Re = 200$, the maximum Reynolds number tested, the flow was steady only for spacings $S/D \leq 4.5$. However, decreasing Re to 180, the flow remained steady out to spacings $S/D = 6$ (Fig. 14). Further decreasing the Reynolds number to $Re = 150$, unsteady flow was still detected but only for spacings greater than $S/D = 8$. Compared with the single cylinder sliding case,

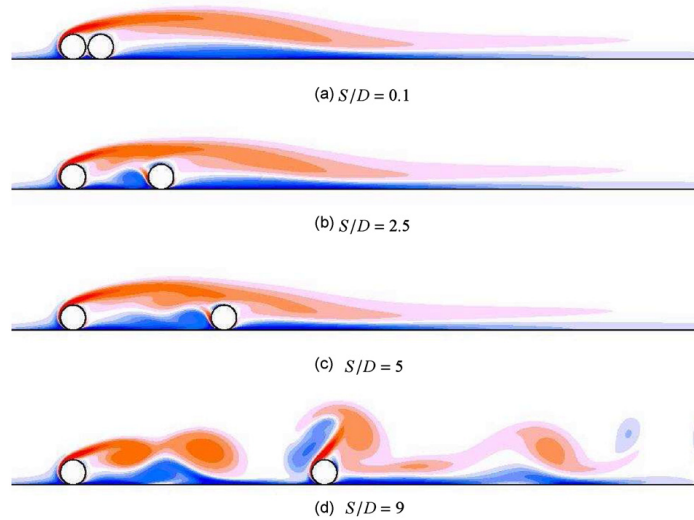


Fig. 14. Instantaneous flow structures at $Re=180$, as the spacing ratio S/D is increased. Vortex shedding is seen for $S/D=9$.

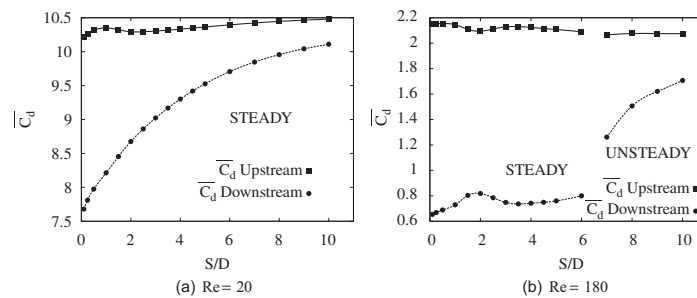


Fig. 15. Variation of the time-averaged drag coefficient with separation distance at the specified Reynolds numbers.

the presence of a downstream cylinder thus provides a stabilising effect (i.e., increases the transitional Reynolds number) on the wake for closer separation distances but destabilises the flow for greater separation distances.

The variation of the upstream and downstream cylinder drag coefficients with respect to separation distance is shown for Reynolds numbers 20 and 180 in Fig. 15. The drag on the downstream cylinder increases as the spacing between the cylinders is increased. A more rapid rise is observed for cases where the transition to unsteady state occurs. At the higher Reynolds number, the drag on the downstream cylinder for small separations is low, but remains positive. This is in contrast to the free-stream case, where the downstream cylinder experiences negative drag force at very close spacings. Fig. 16 shows the pressure distribution for the tandem cylinders at the closest spacing of $S/D=0.1$ at $Re=200$. The higher pressure near the wall on the upstream face of the downstream cylinder, together with the lower pressure on the downstream face, leads to a positive drag force.

The drag variation of the two cylinders with Reynolds number is shown in Fig. 17 for three separation distances. Only at very large spacings, the drag on the downstream cylinder approaches that of the upstream cylinder.

On increasing the separation distance, multiple circulation regions were formed in the space between the sliding cylinders, as shown for a particular case in Fig. 18.

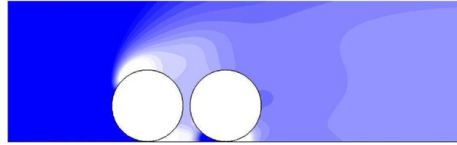


Fig. 16. Pressure distribution for cylinders separated by $S/D=0.1$ at $Re=200$. The darker shades indicate a higher pressure region, while the lighter shades indicate regions of lower pressure.

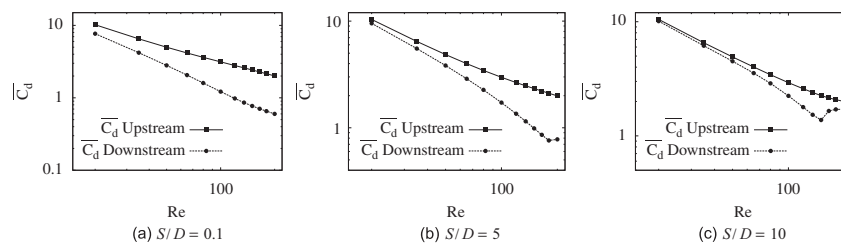


Fig. 17. Variation of the time-averaged drag coefficient with Reynolds number for the separation distances shown.

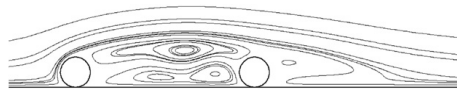


Fig. 18. Streamlines for $S/D=5$ at $Re=180$. Formation of multiple recirculation zones in the space between the two cylinders.

6. Conclusions

This paper extends the results for a single rotating cylinder close to contact with a plane wall to higher rotation rates than previously considered. For the forward rolling case, wake flow structures at rotation rates up to $\alpha = 3$ were found to be similar to those for lower rotation rates, except for the strength of the vortex pairs which self-propel away from the wall. This can be understood in terms of the velocity difference across the wake, which results in a higher flux of vorticity into the separating shear layer and subsequently stronger shed vortices. For the reverse-rotating case, the fluid boundary layer effectively remains attached as it passes over the surface of the cylinder. For $\alpha < -1.25$, vortex shedding is suppressed up to at least $Re=700$. In addition, high reverse rotation also stabilises the flow against three-dimensional instability. For both forward and reverse rotation, the drag experienced by the cylinder has been quantified. This paper also presents results for a pair of cylinders sliding along a plane wall, as a function of separation distance. Overall, the presence of the second cylinder results in the delay of transition to unsteady flow to higher Reynolds numbers. The drag on the downstream cylinder increases after the onset of unsteady flow.

Acknowledgements

The support from Australian Research Council Discovery Grants DP0877327 and DP0877517 and computing time from the National Computational Infrastructure Facility (NCI), Victorian Life Sciences Computation Initiative (VLSCI) and Monash Sungrid are gratefully acknowledged. Anirudh Rao acknowledges the support of a Monash University Departmental Postgraduate Scholarship. Bronwyn Stewart acknowledges the support of an Australian Postgraduate Award and of a Mobility Grant from the French Ministry of Higher Education and Research.

References

- Barkley, D., Gomes, M.G.M., Henderson, R.D., 2002. Three-dimensional instability in flow over a backward-facing step. *Journal of Fluid Mechanics* 473, 167–190.
- Barkley, D., Henderson, R.D., 1996. Three-dimensional Floquet stability analysis of the wake of a circular cylinder. *Journal of Fluid Mechanics* 322, 215–241.
- Beaman, P.W., Zdravkovich, M.M., 1978. Flow around a circular cylinder near a plane boundary. *Journal of Fluid Mechanics* 89, 33–47.

- Bénard, H., 1908. The formation of gyration centres at the back of a moving obstacle. *Comptes Rendus Hebdomadaires des Séances de l'Académie des Sciences* 147, 839.
- Cheng, M., Luo, L.S., 2007. Characteristics of two-dimensional flow around a rotating circular cylinder near a plane wall. *Physics of Fluids* 19, 063601.
- Chorin, A.J., 1968. Numerical solution of the Navier–Stokes equations. *Mathematics of Computation* 22, 745–762.
- Griffith, M.D., Thompson, M.C., Leweke, T., Hourigan, K., Anderson, W.P., 2007. Wake behaviour and instability of flow through a partially blocked channel. *Journal of Fluid Mechanics* 582, 319–340.
- Huang, W.X., Sung, H.J., 2007. Vortex shedding from a circular cylinder near a moving wall. *Journal of Fluids and Structures* 23, 1064–1076.
- von Kármán, T., 1911. Über den Mechanismus des Widerstandes, den ein bewegter Körper in einer Flüssigkeit erfährt. *Göttinger Nachrichten Mathematisch-Physikalische Klasse* 12, 509–517.
- Karniadakis, G.E., Israeli, M., Orszag, S.A., 1991. High-order splitting methods for the incompressible Navier–Stokes equations. *Journal of Computational Physics* 97, 414–443.
- Karniadakis, G.E., Sherwin, S.J., 2005. *Spectral/hp Methods for Computational Fluid Dynamics*. Oxford University Press, Oxford.
- Lawrence, M.B., Springer, T.A., 1991. Leukocytes roll on a selectin at physiologic flow rates: distinction from and prerequisite for adhesion through integrins. *Cell* 65, 859–873.
- Le Gal, P., Nadim, A., Thompson, M., 2001. Hysteresis in the forced Stuart–Landau equation: application to vortex shedding from an oscillating cylinder. *Journal of Fluids and Structures* 15, 445–457.
- Lei, C., Cheng, L., Armfield, S., Kavanagh, K., 2000. Vortex shedding suppression for flow over a circular cylinder near a plane boundary. *Ocean Engineering* 27, 1109–1127.
- Leontini, J.S., Thompson, M.C., Hourigan, K., 2007. Three-dimensional transition in the wake of a transversely oscillating cylinder. *Journal of Fluid Mechanics* 577, 79–104.
- Mahir, N., 2009. Three-dimensional flow around a square cylinder near a wall. *Ocean Engineering* 36, 357–367.
- Mittal, S., Kumar, B., 2003. Flow past a rotating cylinder. *Journal of Fluid Mechanics* 476, 303–334.
- Nishino, T., Roberts, G.T., Zhang, 2007. Vortex shedding from a circular cylinder near a moving ground. *Physics of Fluids* 19, 025103.
- Norberg, C., 2003. Fluctuating lift on a circular cylinder: review and new measurements. *Journal of Fluids and Structures* 17, 57–96.
- Ryan, K., Thompson, M.C., Hourigan, K., 2005. Three-dimensional transition in the wake of bluff elongated cylinders. *Journal of Fluid Mechanics* 538, 1–29.
- Stewart, B.E., Hourigan, K., Thompson, M.C., Leweke, T., 2006. Flow dynamics and forces associated with a cylinder rolling along a wall. *Physics of Fluids* 18, 111701.
- Stewart, B.E., Thompson, M.C., Leweke, T., Hourigan, K., 2010. The wake behind a cylinder rolling on a wall at varying rotation rates. *Journal of Fluid Mechanics* 648, 225–256.
- Sumner, D., 2010. Two circular cylinders in cross-flow: a review. *Journal of Fluids and Structures* 26, 849–899.
- Tan, B.T., Thompson, M.C., Hourigan, K., 2005. Evaluating fluid forces on bluff bodies using partial velocity data. *Journal of Fluids and Structures* 20 (1), 5–24.
- Taneda, S., 1965. Experimental investigation of vortex streets. *Journal of the Physical Society of Japan* 20, 1714–1721.
- Thompson, M.C., Hourigan, K., Cheung, A., Leweke, T., 2006a. Hydrodynamics of a particle impact on a wall. *Applied Mathematical Modelling* 30, 1356–1369.
- Thompson, M.C., Hourigan, K., Ryan, K., Sheard, G.J., 2006b. Wake transition of two-dimensional cylinders and axisymmetric bluff bodies. *Journal of Fluids and Structures* 22, 793–806.
- Thompson, M.C., Hourigan, K., Sheridan, J., 1996. Three-dimensional instabilities in the wake of a circular cylinder. *Experimental Thermal and Fluid Science* 12, 190–196.
- Thompson, M.C., Leweke, T., Williamson, C.H.K., 2001. The physical mechanism of transition in bluff body wakes. *Journal of Fluids and Structures* 15, 607–616.
- Wagner, D.D., Frenette, P.S., 2008. The vessel wall and its interactions. *Blood* 111, 5271–5281.
- Williamson, C.H.K., 1996a. Three-dimensional wake transition. *Journal of Fluid Mechanics* 328, 345–407.
- Williamson, C.H.K., 1996b. Vortex dynamics in the cylinder wake. *Annual Review of Fluid Mechanics* 28, 477–539.
- Wu, J., Sheridan, J., Welsh, M.C., Hourigan, K., 1996. Three-dimensional vortex structures in a cylinder wake. *Journal of Fluid Mechanics* 312, 201–222.

Chapter 5

Flow past tandem cylinders sliding along a wall

5.1 Overview

This chapter is an extension of the previous study, where an identical body is placed downstream of the original body in the near wake region. While the case of tandem cylinders was investigated with respect to flow stabilisation and drag reduction in chapter 4, a detailed study is presented here. Flows past tandem cylinders in freestream have been investigated by several researchers (Biermann & Herrnstein 1933; Igarashi 1981; Mizushima & Suehiro 2005; Meneghini *et al.* 2001); where different regimes of flow were identified based on the longitudinal separation distance (S/D). The three-dimensional stability over a range of spacings was investigated by Papaioannou *et al.* (2005) and Carmo *et al.* (2010), where modes with similar spatio-temporal symmetries as those of mode A and B were observed at different spacings. Very few studies have investigated the flow dynamics for multiple cylinders near a wall. Bhattacharyya & Dhinakaran (2008) performed numerical simulations for square cylinders in a linear shear flow at $Re = 200$ at $G/D = 0.5$, where vortex shedding was observed at large cylinder spacings. Recent numerical simulations by Harichandan & Roy (2012) for circular cylinders show the onset of vortex shedding at high Reynolds numbers and large cylinder spacings and higher gap heights.

Here, two-dimensional simulations are performed for circular cylinders translating along a wall for $0.1 \leq S/D \leq 10$ and $Re \leq 200$ to investigate the flow structures and to quantify the forces. Linear stability analysis is then performed for these cases to investigate the onset of three-dimensionality. As the separation distance is increased from small spacings, the critical Reynolds number increases until $S/D \simeq 4.5$. For $4.5 \leq$

$S/D \leq 6$, flow first transitions to three-dimensionality at a lower Reynolds number and on increasing Reynolds number, the flow stabilises prior to becoming unstable for a second time at much higher Reynolds numbers. For $S/D > 6$, the critical Reynolds numbers for the onset of three-dimensionality is similar to an isolated cylinder sliding along a wall. Three-dimensional simulations carried out at $Re = 200$ indicate the rapid transition to chaotic flow for a wide range of cylinder spacings.

5.2 Flow dynamics of tandem cylinders sliding along a wall

The following article was submitted in 2012 to *Journal of Fluid Mechanics*. This work was co-authored by M. C. Thompson, T. Leweke and K. Hourigan, and is entitled, “*Dynamics and stability of the wake behind tandem cylinders sliding along a wall*”. The paper is reproduced in this thesis directly from the version submitted to the editor for review.

Declaration for manuscript included in PhD Thesis

Monash University

Declaration for Thesis Chapter 5

Declaration by candidate

In the case of Chapter 5, the nature and extent of my contribution to the work was the following:

Nature of contribution	Extent of contribution (%)
Conceived ideas, initiated the paper, performed numerical simulations, analysed the data, wrote the manuscript	80

The following co-authors contributed to the work. Co-authors who are students at Monash University must also indicate the extent of their contribution in percentage terms:

Name	Nature of contribution	Extent of contribution (%) for student co-authors only
Prof. M.C. Thompson	Co-wrote manuscript	N. A.
Prof. T. Leweke	Co-wrote manuscript	N. A.
Prof. K. Hourigan	Co-wrote manuscript	N. A.

Candidate's Signature	<i>[Handwritten Signature]</i>	Date	20 June 2012
-----------------------	--------------------------------	------	--------------

Declaration by co-authors

The undersigned hereby certify that:

- 1) the above declaration correctly reflects the nature and extent of the candidate's contribution to this work, and the nature of the contribution of each of the co-authors.
- 2) they meet the criteria for authorship in that they have participated in the conception, execution, or interpretation, of at least that part of the publication in their field of expertise;
- 3) they take public responsibility for their part of the publication, except for the responsible author who accepts overall responsibility for the publication;
- 4) there are no other authors of the publication according to these criteria;
- 5) potential conflicts of interest have been disclosed to (a) granting bodies, (b) the editor or publisher of journals or other publications, and (c) the head of the responsible academic unit; and
- 6) the original data are stored at the following location(s) and will be held for at least five years from the date indicated below:

Location(s)	Dept. Of Mechanical and Aerospace Engineering, Monash University, Clayton
-------------	---

Signature 1	<i>[Handwritten Signature]</i> (K. HOURIGAN)	Date	20/6/2012
Signature 2	<i>[Handwritten Signature]</i> (for M.C. THOMPSON & T. LEWEKE)	Date	20/6/2012
Signature 3			

Dynamics and stability of the wake behind tandem cylinders sliding along a wall

A. Rao¹, M. C. Thompson¹, T. Leweke^{2†} and K. Hourigan^{1,3}

¹Fluids Laboratory for Aeronautical and Industrial Research (FLAIR), Department of Mechanical and Aerospace Engineering, Monash University, Melbourne, Victoria 3800, Australia

²Institut de Recherche sur les Phénomènes Hors Équilibre (IRPHE),

UMR 7342 CNRS, Aix-Marseille Université, F-13384 Marseille CEDEX 13, France

³Division of Biological Engineering, Monash University, Melbourne, Victoria 3800, Australia

(Received 4 July 2012)

The dynamics and stability of the flow past two cylinders sliding along a wall in a tandem configuration is studied numerically at low to intermediate Reynolds numbers (Re). For cylinders at close separations, the onset of unsteady two-dimensional flow is delayed to higher Re compared to the case of a single sliding cylinder, while at larger separations, this transition occurs earlier. For Reynolds numbers above the threshold, shedding from both cylinders is periodic and locked. At intermediate separation distances, the wake frequency shifts to the subharmonic of the leading-cylinder shedding frequency, which appears to be due to a feedback cycle whereby shed leading-cylinder vortices interact strongly with the downstream cylinder to influence subsequent leading-cylinder shedding two cycles later. In addition to the shedding frequency, the drag coefficients for the two cylinders are quantified for the steady and unsteady regimes. The three-dimensional stability of the flow is also investigated. It is found that, when increasing the Reynolds number at intermediate separations, an initial three-dimensional instability develops, which disappears at higher Re . The new two-dimensional steady flow again becomes unstable, but with a different three-dimensional instability mode. At very close spacings, when the two cylinders are effectively seen by the flow as a single body, and at very large spacings, when the cylinders form independent wakes, the flow characteristics are similar to those of a single cylinder sliding along a wall.

Key words: wakes, vortex shedding, vortex streets

1. Introduction

The wakes behind generic bluff bodies such as cylinders and spheres placed in a free stream have been widely investigated. Williamson (1996) summarises the behaviour of the flow around a circular cylinder in the laminar and transition regimes. For Reynolds numbers (Re , based on the cylinder diameter D and free-stream velocity U) below 47, the wake is steady. Above this value, and up to $Re \simeq 180$, laminar vortex shedding is observed, which, in the absence of end effects, is periodic and two-dimensional. The three-dimensional transition regime, found in the range $180 \lesssim Re \lesssim 300$, was first described in detail by Williamson (1988). The initial three-dimensional shedding mode (*Mode A*) involves a spanwise waviness of the shed vortices, with a wavelength of approximately four cylinder diameters, and a discontinuity in the evolution of the shedding frequency. It can be related to an elliptic instability of the vortex cores (Thompson *et al.* 2001). A second mode (*Mode B*) appears at higher Reynolds numbers ($Re \gtrsim 230$), with

† Email address for correspondence: Thomas.Leweke@irphe.univ-mrs.fr

a smaller spanwise wavelength of approximately one diameter. It involves the amplification of secondary streamwise vortices in the strain-dominated braid regions between the shed vortices. Initially, the two modes co-exist, with a subsequent gradual shift to a pure *Mode B*, accompanied by a second discontinuity in the frequency relation. The characteristics of the two instability modes, including the associated vortex structures, were documented numerically by a number of authors (Barkley & Henderson 1996; Zhang *et al.* 1995; Mittal & Balachandar 1995; Thompson *et al.* 1996; Henderson 1997).

The presence of a second bluff body of similar dimensions in close proximity influences the wakes behind each body, and also the forces experienced by each of them. Critical parameters for categorising the flow regimes for a particular Reynolds number are based on the separation distance and the magnitudes of lift and drag forces experienced by the cylinders. Biermann & Herrstein (1933), in their investigation of streamlined struts and cylinders, found that the drag on the upstream cylinder is not greatly influenced by the presence of the downstream cylinder, however the drag on the rear cylinder was greatly reduced by the upstream cylinder. They also found that the wake from the upstream cylinder was not fully developed in the presence of another body at close separation distances. Igarashi (1981) carried out an experimental study for cylinders in a tandem configuration at $Re \approx 10^4$ and classified the flow based on the separation distance. A similar study was conducted by Zdravkovich (1987), who recorded the force variations for cylindrical arrays of tubes in various configurations such as in-line, side by side, and staggered. The broad classification based on the longitudinal separation distance S is as follows:

- $0.1 \leq S/D \leq 0.2 - 0.8$, a regime of close spacing, where the shear layers shed from the upstream cylinder do not reattach to the downstream cylinder. The two cylinders behave as a single extended body and vortices are formed from the detached shear layers of the downstream cylinder.
- $0.2 - 0.8 \leq S/D \leq 2.4 - 2.8$, an intermediate regime, where the shear layers shed from the upstream cylinder reattach onto the downstream cylinder and shedding takes place behind the downstream cylinder. Also observed in this regime is the intermittent vortex formation behind the upstream cylinder.
- $S/D \geq 2.8$, a regime of large spacing, where vortices are shed from both cylinders.

The critical separation distance (2.5 – 3 cylinder diameters) for the onset of vortex shedding from both cylinders has been identified by many researchers (Liang *et al.* 2008; Didier 2007; Mussa *et al.* 2009; Zhou & Yiu 2005), both numerically and experimentally, for a wide range of Reynolds numbers. The two-dimensional numerical simulations by Liang *et al.* (2008) showed a sharp increase of the drag coefficient and Strouhal number ($St = fD/U$, where f is the vortex shedding frequency), once this critical spacing was exceeded.

Mizushima & Suehiro (2005) concluded that the flow behind the upstream body is greatly stabilised by the presence of the downstream body and the transition to unsteady flow for spacings of $S/D = 1$ and $S/D = 3$ occurred at $Re = 68$ and $Re = 78.5$, respectively. This is much higher than the critical value observed for an isolated single cylinder ($Re = 47$). It was also shown that for a spacing of $S/D = 1$, the transition was supercritical, and subcritical at $S/D = 3$. For large spacing ratios ($S/D \geq 3$), the downstream cylinder experienced large lift and drag forces. The amplitude of the lift on the downstream cylinder was observed to be approximately four times that of the upstream cylinder.

Meneghini *et al.* (2001) performed numerical simulations for cylinders in tandem and side-by-side arrangement in a free stream for $Re \leq 200$. They quantified the forces on the two cylinders and the shedding frequency. For close spacings, the Strouhal number was 65% lower than for a single cylinder in a free stream. Also, the drag on the downstream cylinder was negative for spacings $S/D \leq 2$.

Two- and three-dimensional numerical simulations were performed by Deng *et al.* (2006) for $Re \geq 220$ and different separation distances. In their two-dimensional simulations at $Re = 220$

for $S/D \leq 2.5$, vortex shedding does not take place between the two cylinders, while for $S/D \geq 3$, each cylinder produces a vortex wake. However, in their three-dimensional simulations, three-dimensionality was observed for $S/D \geq 2.5$, but not for smaller spacings. For the critical spacing of $S/D = 2.5$, the transition to three-dimensionality occurs at $Re = 250$. Similar computations have been performed by Papaioannou *et al.* (2005) for tandem cylinder cases. Their simulations show an increase in three-dimensionality of the wake as the critical spacing distance was approached. At close spacings, the primary vortices were unable to roll up and form strong vortex cores, which reduces the sensitivity to three-dimensional effects and thereby stabilises the flow.

Stability analysis for a tightly packed cylinder array was performed by Kevlahan (2007) for cylinders spaced by $S/D = 1.5$, and for the array being in line with, or at an angle of 45° to, the flow. For the inline cylinders, periodic flow was detected beyond $Re = 119$ and three-dimensional flow set in at $Re \simeq 132$, with the formation of *Mode A* type structures of spanwise wavelength $3D$. He further reports that the *Mode B* type structures are absent in cylinder arrays, since the braid structures are suppressed by the tight packing. At $Re = 200$, the growth rates of the three-dimensional modes were higher for the angled array than for the inline array.

Recent numerical investigations by Carmo *et al.* (2010) of the flow around isolated tandem cylinders, showed the existence of three new modes at various separation distances for $Re \geq 200$. For small separations, the onset of three-dimensionality occurs via a *Mode T1*, whose spatio-temporal symmetry resembles that of the *Mode B* instability of an isolated cylinder at higher Reynolds numbers. This mode has a spanwise wavelength of $\sim 2D$. Two other modes were observed when the cylinders were spaced in the range $0.8 \leq S/D \leq 1.5$. The physical mechanism of the *Mode T2* instability is believed to be centrifugal, while *Mode T3* has similar characteristics to *Mode A* of the single-cylinder wake. *Mode T2* has a spanwise wavelength of $\sim 3D$, while *Mode T3* has a wavelength of $\sim 4.6D$ at onset. At large separations, the *Mode A* instability is followed by the *Mode B* instability, akin to the case of an isolated cylinder in a free stream.

Flow features behind a single cylinder near a wall have been discussed by several researchers (Mahir 2009; Stewart *et al.* 2006, 2010b; Rao *et al.* 2011; Huang & Sung 2007). The case of cylinders sliding along a wall with rotation effects was investigated numerically by Stewart *et al.* (2006, 2010b) for $Re \leq 500$. The transition to unsteady flow was delayed to higher Reynolds numbers ($Re \simeq 160$) relative to isolated cylinders, and three-dimensional flow was detected at much lower Reynolds numbers ($Re \geq 71$). Experiments performed in a closed-loop water tunnel were consistent with the flow structures observed numerically.

Very few studies have considered the flow features of multiple bodies moving along a wall. Bhattacharyya & Dhinakaran (2008) conducted numerical simulations for a pair of tandem square cylinders in a linear shear flow at $G/D = 0.5$, where G is the distance between the cylinder and the wall. Below $Re = 125$, the shear layers separating from the two sides, are unable to interact and cause vortex shedding. At a spacing of $S/D \leq 2$, the two cylinders effectively behave as one body at $Re \leq 200$. For $2 < S/D < 3$, vortices are shed from the downstream cylinder only. Above this range, vortices are shed from both cylinders, and at even larger separation distances, the shedding frequency recorded for both cylinders match that of a single cylinder under similar flow conditions. The height above the wall and the separation distance both influence the shear layer interaction responsible for the formation of vortices. Harichandan & Roy (2012) performed numerical investigations for circular cylinders in tandem close to a wall at Reynolds numbers $Re = 100$ and 200 for separation distances of $S/D = 1$ and 4 . The bodies were placed at $0.5D$ and $1D$ above the stationary wall. They observed that the variation of the separation distance has a stronger influence on the flow stability than changes in the gap to the wall. Vortex shedding occurred when the gap heights and the separation distance were both large.

The present numerical work focuses on the wake and drag characteristics of two circular cylinders sliding along a wall, as function of the separation distance and the Reynolds number. The

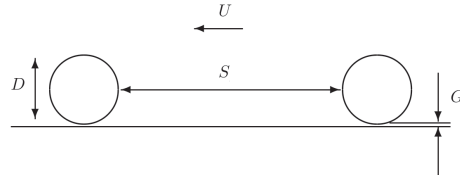


Figure 1: Schematic representation of the tandem cylinder problem showing key parameters.

transitions to unsteady and three-dimensional flow are examined by stability analyses, and we attempt to characterise these different transition regimes in terms of the flow physics as the control parameters are varied. We first describe the numerical method and stability analysis techniques, and provide domain size and resolution studies. We then present the observations and analysis of the transition behaviour in two chapters, one dealing with the transition to unsteady two-dimensional flow, and one with the transition to three-dimensional (steady or unsteady) flow. Finally, we use Direct Numerical Simulations (DNS) to investigate some fully developed three-dimensional wakes, for Reynolds numbers such that multiple three-dimensional linear modes are known to be unstable.

2. Numerical methods

2.1. Problem definition

Figure 1 shows a schematic of the flow problem under consideration. We investigate the flow over two identical tandem cylinders of diameter D , separated by a distance S , sliding to the left along a wall at constant speed U . A small gap of size G is maintained between the cylinders and the wall to prevent the high-order mesh elements from becoming degenerate directly underneath. The gap ratio G/D is held fixed at 0.005 for both cylinders, after verifying that the effect on the downstream flow is negligible, in line with previous studies for single cylinders and spheres (Zeng *et al.* 2005; Stewart *et al.* 2006, 2010a,b; Rao *et al.* 2011). The fluid is assumed to be Newtonian and incompressible. For computational convenience, we employ a uniformly translating frame of reference attached to the cylinders, with the origin at the centre of the first cylinder. In this frame, the cylinders appear stationary, with both the far fluid and the wall moving to the right at uniform speed U . In the following, all quantities are non-dimensionalized with the cylinder diameter D and the free stream velocity U .

2.2. Numerical scheme

The numerical approach is based on a spectral-element formulation to discretise the unsteady incompressible Navier-Stokes equations in two dimensions. The domain consists of a collection of quadrilateral elements with a higher element density in regions of high velocity gradients near the cylinders and in the wake regions. These quadrilateral (or macro-) elements are further subdivided internally into $N \times N$ nodes. The nodes correspond to Gauss-Legendre-Lobatto quadrature points, and the velocity and pressure fields are represented by tensor products of Lagrangian polynomial interpolants of order $N-1$ within elements. The resolution can be set at runtime by selecting the number of internal node points. The method exhibits exponential convergence as N is increased (Karniadakis & Sherwin 2005), consistent with global spectral methods.

The unsteady discretised Navier-Stokes equations are then solved using a time-splitting approach, originally developed by Chorin (1968), where the advection, pressure and diffusion terms

are solved using different time-stepping schemes to ensure stability of the solver. A more detailed explanation of the numerical procedure can be found in various articles (Ryan *et al.* 2005; Thompson *et al.* 2006a; Leontini *et al.* 2007). It has been previously used to investigate related problems such as flows past cylinders in a free stream (Thompson *et al.* 2001, 1996; Leontini *et al.* 2007; Thompson *et al.* 2006b) or around bodies near a wall (Stewart *et al.* 2006; Thompson *et al.* 2007; Stewart *et al.* 2010b; Rao *et al.* 2011).

2.3. Linear stability analysis

Linear stability analysis is used here to determine the stability of the flow with respect to spanwise perturbations. The numerical approach is similar to that employed by Barkley & Henderson (1996), Blackburn & Lopez (2003), Sheard *et al.* (2003), Leontini *et al.* (2007), Griffith *et al.* (2009), and others. The Navier-Stokes equations are used to derive linearised equations for the velocity and pressure perturbation fields about a two-dimensional base flow, which are explicitly dependent on the spanwise coordinate. Because of the linearity and lack of spanwise dependence of the base flow, the spanwise dependence of the perturbation fields can be represented as a combination of Fourier modes, each of which can grow or decay exponentially in time. In practice, to determine stability, the linearised Navier-Stokes equations for the perturbation fields are marched forward in time until the fastest-growing or slowest-decaying Fourier mode dominates the solution. Alternatively a Krylov subspace method can be used with Arnoldi decomposition to extract more of the most dominant modes (see, e.g., Mamun & Tuckerman 1995). The evolution (growth or decay) of a given perturbation mode depends on its spanwise wavelength λ and the Reynolds number. The growth rate σ can be evaluated from the amplitude ratio at two instants in time, separated by a time interval T : $|A(t = t_0 + T)|/|A(t = t_0)| = \exp(\sigma T) = \mu$. For $\sigma > 0$ (or $|\mu| > 1$), the perturbations grow and three-dimensionality develops, while for $\sigma < 0$ (or $|\mu| < 1$), the perturbations die out. Neutral stability occurs for $\sigma = 0$ or $|\mu| = 1$. For periodic base flows, the time period for monitoring the growth is set to the base flow period, a process known as Floquet analysis, with μ being the Floquet multiplier. For flow past a single cylinder near a wall, three-dimensional flow usually occurs in the steady flow regime, prior to the onset of periodic flow (Stewart *et al.* 2010b; Rao *et al.* 2011). For periodic flows, the three-dimensional modes may also have a periodicity different to the oscillatory base flow, in which case the Floquet multipliers are complex. Such methods have been used previously to resolve subharmonic modes in the wake behind rings (Sheard *et al.* 2005, 2003) and other bluff bodies (Blackburn & Lopez 2003).

2.4. Effect of domain size

The domain is defined in terms of the location of the inlet, top and outlet boundaries relative to the cylinders. Several meshes were constructed with their boundaries placed at different distances from the cylinders. For these investigations, the simulations were run at $Re = 200$ with a polynomial order of $N = 7$ for the cylinders separated by the maximum distance considered of $S/D = 10$. The inlet and the lateral/top boundaries were placed between $25D$ and $100D$ from the leading cylinder, and the outlet boundary between $50D$ and $200D$ downstream of the trailing cylinder. The simulations were run for the same time interval and the forces on the cylinders were monitored. The time-averaged drag coefficient of the downstream cylinder was computed from the force histories. Periodic flow was observed for this case and the Strouhal number was also computed. Based on the results, the values $50D$, $100D$ and $50D$ were chosen for the inlet and outlet distances and the domain height, respectively. With this choice, the mean drag coefficient and the Strouhal number differed by less than 0.5% and 0.6%, respectively, from the values obtained with the largest domain.

Table 1: Variation of the time-averaged drag coefficient (\overline{C}_d) and shedding frequency (St) for $S/D = 10$ at the specified Reynolds numbers (Re).

N^2	$Re = 20$		$Re = 200$		$Re = 200$	
	\overline{C}_d	% variation	\overline{C}_d	% variation	St	% variation
5^2	10.097389	0.1398206	1.732380	-2.035431	0.090208	-0.898475
6^2	10.102081	0.0934181	1.708033	-0.601417	0.089602	-0.220676
7^2	10.110580	0.0093655	1.704390	-0.386848	0.089509	-0.116657
8^2	10.111458	0.0006824	1.700441	-0.154256	0.089451	-0.051785
9^2	10.111456	0.0007021	1.699990	-0.127693	0.089447	-0.047311
10^2	10.111518	0.0000890	1.698354	-0.031334	0.089417	-0.013757
11^2	10.111527	0	1.697822	0	0.089407	0

2.5. Effect of mesh resolution

The number of macroelements varies with the separation distance and is significantly higher than that required for previous single cylinder studies. One advantage of the spectral-element method is the ability to specify the number N of internal node points on each edge, and therefore the resolution, at run time. Once a reasonable macroelement distribution is established, the resolution can then be further controlled by varying N . The maximum separation distance ($S/D = 10$) was chosen in order to test the value of N required to resolve the flow correctly. The number of node points in each macroelement was varied between $N^2 = 5^2$ and $N^2 = 11^2$, and tests were performed at two Reynolds numbers of 20 and 200. The resolution of $N^2 = 4^2$ was insufficient to capture the flow characteristics, while $N^2 = 12^2$ proved to be computationally expensive with a strong (Courant) restriction on the time-step. The simulations for the grid resolution study used a fixed non-dimensional time-step of $\Delta\tau = 0.001$. Table 1 shows the variation of the time-averaged drag coefficient \overline{C}_d of the downstream cylinder and the Strouhal number, as the resolution is varied. For $N^2 = 7^2$, the variation in \overline{C}_d and St is less than 0.5% and 0.15%, respectively, relative to the most resolved case. Computations at $Re = 20$ showed a variation of less than 0.1% at $N^2 = 7^2$ compared with the highest resolution tested. Thus an inter-element resolution of $N^2 = 7^2$ was chosen for all computations, since it provided an acceptable accuracy for a reasonable computational effort.

3. Two-dimensional flow

3.1. Flow structures

The flow past a single cylinder sliding along a wall was investigated by Stewart *et al.* (2006, 2010*b*). Two recirculation zones form in the near wake of the cylinder, whose lengths vary linearly with Reynolds number. The recirculation zones extend to a maximum of approximately $8D$ downstream of the cylinder at $Re = 150$, above which unsteady periodic flow occurs. The shear layer moving over the cylinder and the induced wall boundary layer form vortex pairs, which drift downstream of the cylinder. The flow features associated with two tandem cylinders *rolling* along a wall were previously investigated by Rao *et al.* (2011). At large separation distances, unsteady flow was encountered at high Reynolds numbers, while steady flow was found at low

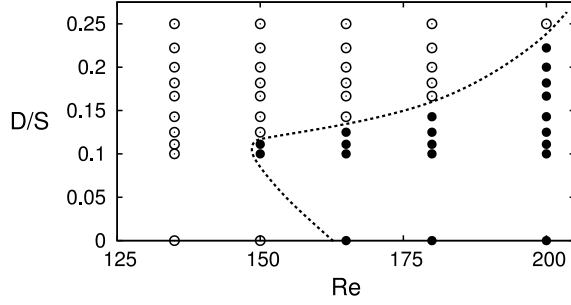


Figure 2: Transition diagram showing the onset of unsteady state with Reynolds number (Re) for $0 \leq D/S \leq 0.25$. The steady flow regime is marked by open symbols (\circ) and the unsteady flow regime is marked by closed symbols (\bullet). Steady flow was observed for all spacings at $Re = 135$. The dashed line shows the approximate demarcation between the steady and unsteady flow regimes.

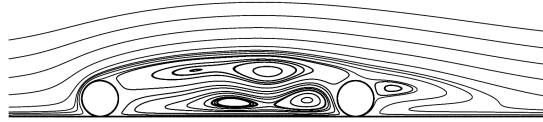


Figure 3: Streamlines of the flow past tandem cylinders for $S/D = 6$ at $Re = 180$. Multiple recirculation zones are observed in the space between the cylinders. The cylinders are translating from right to left.

Reynolds numbers. In a similar way, we here investigate the onset of periodic flow for *sliding* tandem cylinders, in the range of spacings $4 \leq S/D \leq 10$ for $Re \leq 200$.

Figure 2 presents the transition map, showing the onset of unsteady flow as the Reynolds number and cylinder spacing are varied. In this plot, the inverse of the separation distance, D/S , is used, in order to include the isolated cylinder case ($D/S = 0$). Unsteady flow is observed at $Re = 150$ for cylinders with $S/D = 9$ and 10 . This is marginally below the critical Reynolds number for the transition to the unsteady regime for an isolated cylinder sliding along a wall ($Re_c \simeq 160$, Stewart *et al.* 2010*b*). At higher Reynolds numbers, unsteady flow occurs at smaller spacings, as predicted by Rao *et al.* (2011). At the maximum Reynolds number tested, $Re = 200$, unsteady flow was observed at a separation distance as low as $S/D = 4.5$.

As mentioned above, the steady wake of a single cylinder near a wall comprises two recirculation zones. For two cylinders at very close spacings, a similar wake structure is found behind the downstream cylinder. As the spacing is increased, multiple recirculation zones are observed in the gap between the cylinders (figure 3), which remain steady even at higher Reynolds numbers. These zones are similar to what Igarashi (1981) described as quasi-stationary vortices, which occur in the range $1 \leq S/D \leq 2.5$ for cylinders in a free stream, prior to the onset of unsteady flow.

The process of vortex shedding, found in the unsteady periodic regime, is illustrated in figure 4, showing a sequence of vorticity distributions in the near wake during one shedding cycle for $S/D = 9$ and $Re = 200$. In the first snapshot, the separating shear layer from the top of

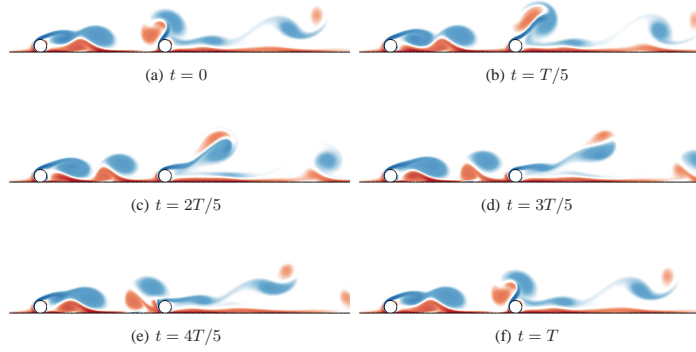


Figure 4: Instantaneous vorticity fields at $Re = 200$, for $S/D = 9$. Time t is expressed in terms of the shedding period T . The cylinders are translating from right to left, and vorticity contours cover the range $\pm 5U/D$.

the upstream cylinder is beginning to roll up. The presence of this primary vorticity induces secondary vorticity at the wall underneath it. This secondary vorticity is pulled away from the wall between two successive primary vortex structures. In later images, the previously shed primary vortex and the rolled-up secondary vorticity combine into a non-symmetrical vortex pair, which impinges on the downstream cylinder and subsequently moves away from that cylinder at an oblique angle due to self-induction. Since the primary vorticity is stronger, and because it is also supplemented by more vorticity separating from the second cylinder, the combined structure moves closer to the wall as it travels downstream. At about $10D$ downstream of the second cylinder, the remaining clockwise vorticity again induces secondary vorticity at the wall, which is pulled away from the wall to combine with the primary vorticity to form a new vortex pair. This reformed pair then moves away from the wall through self-induction as the structure advects further downstream (not shown).

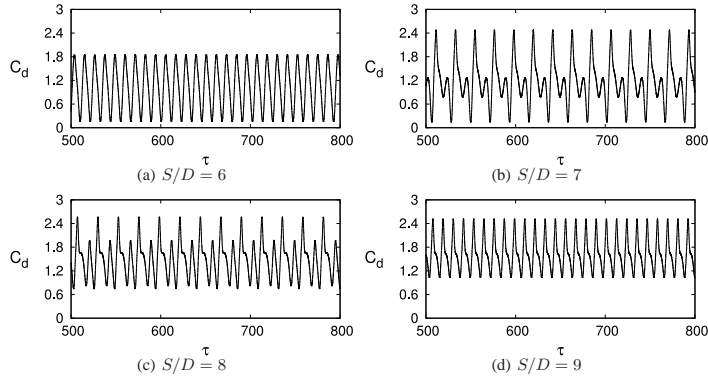
3.2. Strouhal numbers

The drag coefficient was monitored for several hundred units of non-dimensional time τ ($= tU/D$), in order to compute the shedding frequency. Table 2 shows the variation of the Strouhal number with separation distance for the parameter range studied, along with the results of Stewart *et al.* (2010b), where an isolated cylinder near a wall was investigated at similar Reynolds numbers. Their case is denoted by $S/D = \infty$, implying that the trailing cylinder is at a very large distance. The transition diagram (figure 2) shows that for $S/D \simeq 10$ the flow becomes unsteady at Reynolds numbers lower than the limit for an isolated cylinder near a wall. Presumably this can be attributed to the complex flow upstream of the second cylinder due to the presence of the first cylinder (figure 3). Shedding is synchronous from both cylinders, and a single frequency is detected from the Fourier spectra of the drag histories. At $Re = 150$ and 165 , a slight decrease in St is observed as the spacing is increased.

The time histories of the drag coefficient for the downstream cylinder at $Re = 200$, for the separation distances in the range $6 \leq S/D \leq 9$ are shown in figure 5, and the corresponding frequency spectra in figure 6. At $S/D = 7$ and 8 , the waveform of the drag history clearly

Table 2: Variation of St with S/D at the specified Re . The data for $S/D = \infty$ is taken from Stewart *et al.* (2010b)

S/D	$Re = 150$		$Re = 165$		$Re = 180$		$Re = 200$	
	St_1	St_1	St_1	St_2	St_1	St_2	St_1	St_2
4.5	—	—	—	—	0.0887	—	—	—
5	—	—	—	—	0.0871	—	—	—
5.5	—	—	—	—	0.0880	—	—	—
6	—	—	—	—	0.0884	—	—	—
7	—	—	0.0895	0.0447	0.0461	0.0922	—	—
8	—	0.0889	0.0879	—	0.0875	0.0437	—	—
9	0.0892	0.0877	0.0878	—	0.0878	—	—	—
10	0.0877	0.0872	0.0888	—	0.0893	—	—	—
∞	—	0.1004	0.0982	—	0.0983	—	—	—

Figure 5: Time histories of the drag coefficient for the downstream cylinder at $Re = 200$ for the specified separation distances.

indicates the presence of two dominant frequencies, which were found to be integer multiples of each other. For $S/D = 7$, the dominant Strouhal number St_1 (in terms of power spectral density) is one half of the second strongest frequency St_2 , while at a slightly larger spacing of $S/D = 8$, the value of the dominant Strouhal number is twice St_2 . At $Re = 180$, the drag history for $S/D = 7$ also contains two frequencies, while for spacings below or above this value only a single strong frequency component is observed.

The reason for the commensuration of frequencies can be seen by visualising the wake for different separation distances using vorticity contours. Shown in figure 7 is the sequence of im-

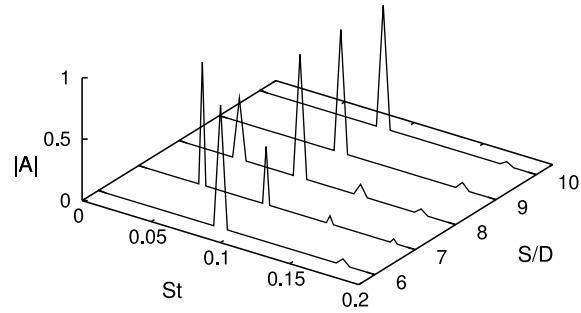


Figure 6: Fourier spectra for different spacings at $Re = 200$. Multiple peaks are found for $S/D = 7$ and $S/D = 8$.

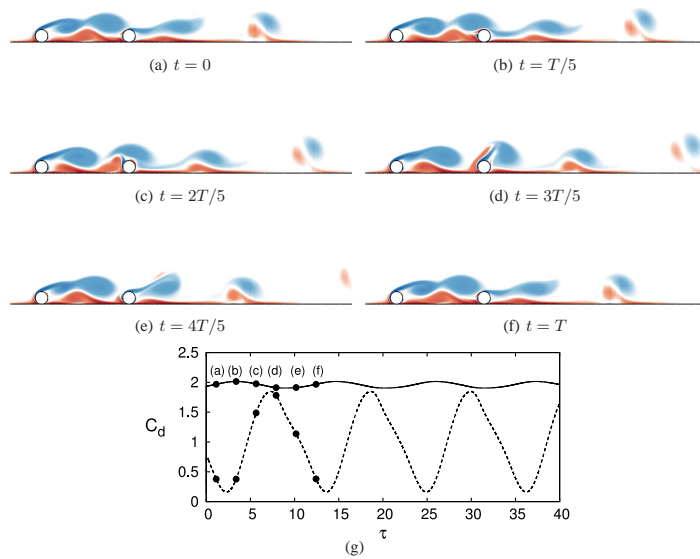


Figure 7: (a)-(f) Instantaneous vorticity contours at $Re = 200$ for $S/D = 6$. (g) Drag histories for the upstream (solid line) and downstream (dashed line) cylinders, showing the times corresponding to (a)-(f).

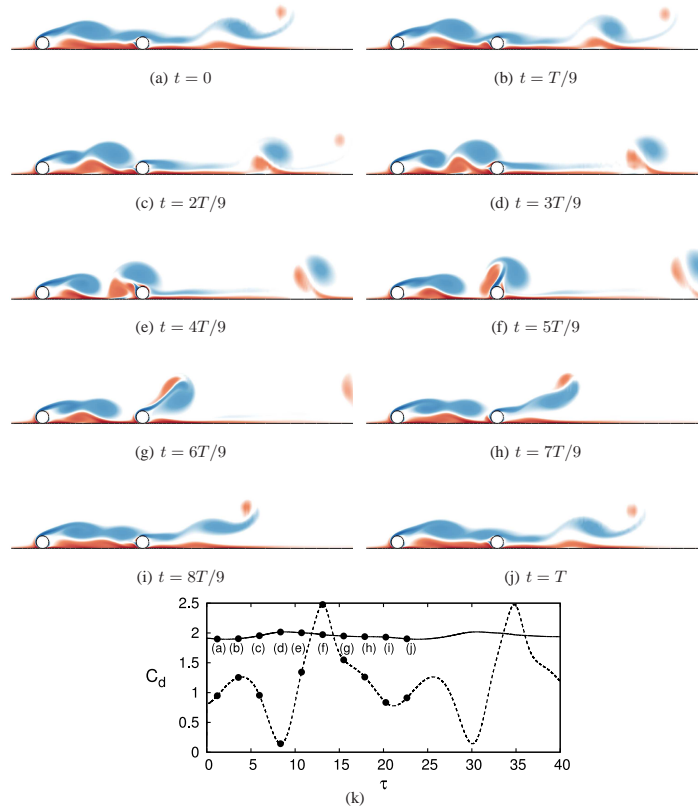


Figure 8: Same as figure 7 for $S/D = 7$. The period T of the flow oscillations is now twice the shedding period of the leading cylinder.

ages over one cycle of shedding for $S/D = 6$, where a single peak is observed in the frequency spectrum. We observe that the shear layer (blue) separating from the upstream cylinder rolls up into a vortex which generates and lifts up a wall boundary layer (red) before striking the downstream cylinder. The rolled-up shear layer convects further downstream, where it draws more opposite-signed boundary layer vorticity from the wall to form a vortex pair, which then advects away from the wall through self-induction. At a slightly larger separation distance of $S/D = 7$, stronger and weaker vortex structures are formed alternately from the shear layer separating from the first cylinder. This behaviour is clearly evident in the sequence of images in figure 8. Com-

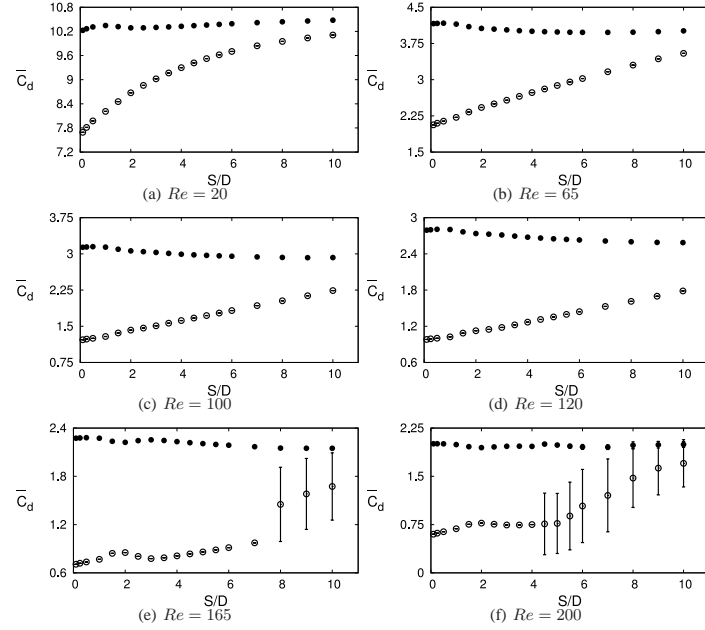


Figure 9: Drag trends at the specified Reynolds numbers. The filled circles (\bullet) and the open circles (\circ) indicate the time-averaged drag coefficient on the upstream and downstream cylinders, respectively. The vertical error bars represent one standard deviation of the instantaneous force coefficients.

paring figures 8(c) and 8(h), the structure of the separated shear layer between the cylinders is distinctly different. In the first case, the second rolled-up clockwise vortex structure of the shear layer is considerably stronger. The vortex draws the secondary vorticity from the boundary to form a vortex pair, which collides with the second cylinder before moving obliquely away from it. In the second case, the clockwise vorticity is weaker and does not draw boundary layer vorticity into the main flow. The clockwise vorticity merges smoothly with the shear layer separating from the second cylinder. The result is a very different behaviour between the two halves of the cycle. The period of shedding is approximately twice that observed for $S/D = 6$. This phenomenon is similar to the lock-in phenomenon observed in the wakes of elongated bluff bodies, where the timing of leading-edge vortices passing the trailing edge (equivalent to the second cylinder in the present configuration) controls the roll-up and shedding of further leading-edge vortices (Hourigan *et al.* 2001). For $S/D = 8$, the behaviour is similar to that for $S/D = 7$, while for $S/D = 9$ (see figure 4), the system period corresponds again to a single shedding cycle of the leading cylinder (rather than two leading-cylinder shedding cycles as for $S/D = 7$ or 8).

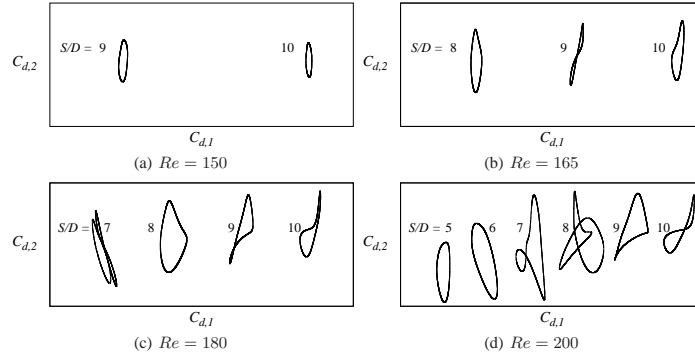


Figure 10: Phase plots showing the variation of the drag coefficient of the upstream ($C_{d,1}$) and downstream ($C_{d,2}$) cylinders at the specified Reynolds numbers.

3.3. Drag trends

The forces experienced by the cylinders were quantified by the direct summation of the pressure and viscous forces on the cylinders. The variation of the drag coefficient for the upstream and downstream cylinders is shown in figure 9 at different Reynolds numbers. The drag on the downstream cylinder was found to be much lower than that on the upstream cylinder for close spacings, as the upstream cylinder experiences a considerably larger pressure force than the downstream cylinder. However, at all spacings investigated here, the drag on both cylinders is positive. This can be attributed to the cylinders being close to the wall, where a higher pressure force acts on the upstream face of each cylinder. As expected, the drag coefficient on the downstream cylinder increases, as the spacing between the cylinders grows. When the cylinders are placed further apart, they behave increasingly as individual bodies. At higher Reynolds numbers, the flow is unsteady, and higher mean drag is experienced by the downstream cylinder. At $Re = 200$, the drag coefficient on the downstream cylinder approaches that experienced by the upstream cylinder. The vertical error-bars indicate one standard deviation from the mean value for the unsteady flow cases.

Shown in figure 10 are phase plots for the drag coefficients of the upstream and downstream cylinders in the unsteady regime for the specified separation distances. They show the complex phase relationships between the forces acting on the two cylinders, in particular for the cases discussed above, where two dominant frequencies are present in the drag histories.

4. Three-dimensional stability

In this section, we investigate the stability of the two-dimensional base flow obtained in the previous section with respect to three-dimensional perturbations. Linear stability analysis is initially performed for the steady-state regime to detect the initial three-dimensional modes that grow at low Reynolds number. We employ the Arnoldi method based on a Krylov subspace to obtain the growth rate of the first few dominant modes, which can be either real or complex. For a single cylinder sliding along a wall, the flow undergoes a transition to three-dimensionality, with a spanwise wavelength $\lambda/D = 5.5$, at $Re = 71$ (Stewart *et al.* 2010b), which is below the threshold for the transition to unsteadiness of the two-dimensional flow at $Re = 160$.

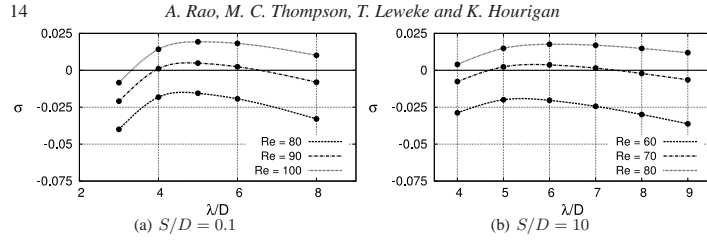


Figure 11: Growth rate curves for (a) small and (b) large spacing, about the critical Reynolds numbers for three-dimensional transition.

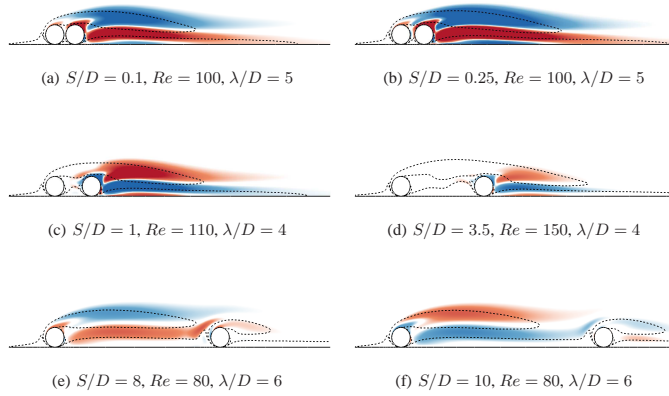


Figure 12: Spanwise perturbation vorticity contours for different separation distances at the specified Reynolds numbers and wavelengths. Vorticity contours cover the range $\pm 0.1D/U$, and base flow vorticity contour levels $\pm 1D/U$ are overlaid.

4.1. Steady base flow

Simulations were performed in the steady flow regime for the entire range of separation distances investigated previously. Examples of growth rate curves are given in figure 11 for a small and a large spacing between cylinders. Growth rates (σ) are shown as function of the perturbation wavelength for different Reynolds numbers, illustrating how the corresponding modes shift from stable ($\sigma < 0$) to unstable ($\sigma > 0$) as Re is increased.

Figure 12 shows perturbation vorticity contours for different separation distances. For small S/D , large amplitudes occur downstream of the trailing cylinder, while in the gap region the amplitude is small. When the separation distance between the two cylinders is large, the maximum mode amplitudes occur inside the gap. The perturbation field resembles that of an isolated

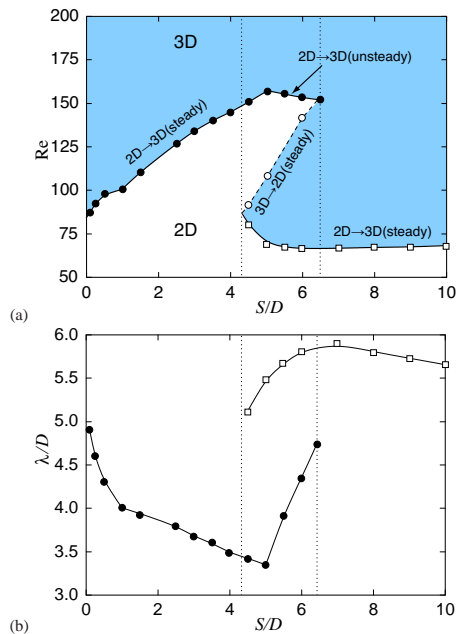
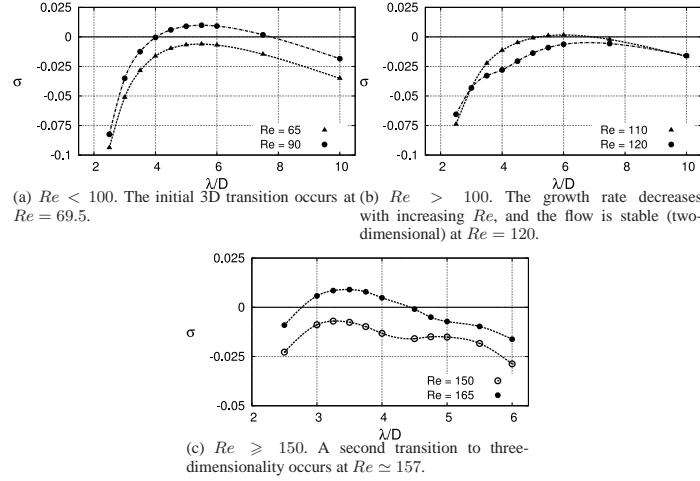
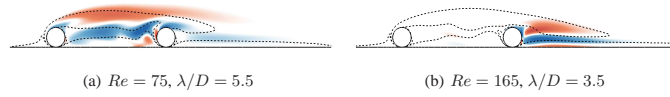


Figure 13: Variation with S/D of (a) the critical Reynolds number(s) and (b) the critical wavelength(s) for three-dimensional transition. Data concerning the same transition are represented by identical symbols.

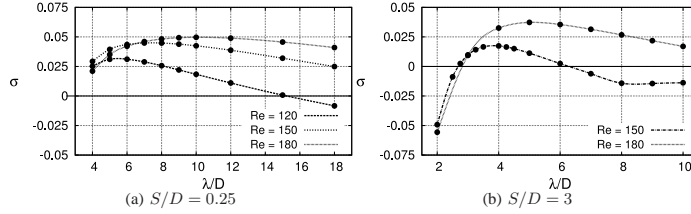
sliding cylinder near a wall (Stewart *et al.* 2010*b*). The Floquet multiplier for the cases shown is real and positive.

Figure 13 shows the variation with separation distance of the critical Reynolds numbers for the three-dimensional transition and the corresponding instability wavelength. The critical values were obtained by polynomial interpolation from the growth rate curves at Reynolds numbers above and below the critical values. For large spacings ($S/D \geq 7$), these values are quite close to those observed for a single sliding cylinder.

The transition to three-dimensionality for intermediate spacings occurs in a more complex way. For $4.5 \leq S/D \leq 6.5$, an initial transition to three-dimensionality occurs at low Reynolds number, followed by a re-stabilisation of the flow to a two-dimensional state as the Reynolds number is increased. Increasing the Reynolds number further, the flow once again undergoes a transition to a new three-dimensional state, involving either a steady or an unsteady mode (see below). This surprising sequence of stable two-dimensional and unstable three-dimensional regimes is further illustrated in figure 14, where growth rate curves for the case with $S/D = 5$ are shown. In figure 14(a), the growth rates for $Re < 100$ illustrate the first three-dimensional transition at $Re = 69.5$. Increasing the Reynolds number to 110, the maximum growth rates decrease, and at $Re = 120$ the flow is found to be stable (i.e., two-dimensional) again (figure 14b). Further increasing Re , a second transition to three-dimensional flow is found at $Re \approx 157$ for a signifi-

Figure 14: Growth rate curves for $S/D = 5$.Figure 15: Spanwise perturbation vorticity for (a) the first and (b) the second transition to three-dimensionality for $S/D = 5$. Contour shading as in figure 12.Figure 16: Spanwise perturbation vorticity for (a) the first and (b) the second transition to three-dimensionality for $S/D = 6$. Contour shading as in figure 12.

cantly smaller wavelength of $\lambda/D = 3.4$ (figure 14c), i.e., involving a different instability mode. Spanwise perturbation vorticity is plotted for $S/D = 5$ in figure 15 for both three-dimensional transitions. For the first transition, three-dimensionality develops in the space between the two cylinders, while for the second one, the growth of perturbations occurs downstream of the trailing cylinder.

Figure 17: Growth rate curves at higher Reynolds numbers for lower S/D .Figure 18: Spanwise perturbation vorticity contours for lower S/D . Contour shading as in figure 12.

For comparison, the case with $S/D = 6$, which also exhibits two successive 3D transitions, is illustrated in figure 16. In this case, both modes have high amplitudes within the gap region between the cylinders, although the perturbation vorticity patterns are quite distinct. However, the growth rate for the second transition has a non-zero imaginary part, indicating that the flow is periodic, while for the first transition the growth rate is purely real.

As mentioned above, the two-stage instability scenario occurs for spacings in the range $4.5 \leq S/D \leq 6.5$. A further investigation was undertaken by carrying out stability analysis at higher Reynolds numbers for separation distances on either side of this range. Shown in figure 17 are the growth rate curves at two smaller separation distances of $S/D = 0.25$ and 3. At higher Reynolds numbers, the growth rate curves shift to higher values and the flow is more unstable to perturbations with longer spanwise wavelengths. The growth rate curve clearly broadens as the Reynolds number is increased from $Re = 150$ to 180 for $S/D = 3$ (figure 17b). The corresponding perturbation vorticity contours are shown in figure 18. Comparing figures 17(a) and 12(b), we observe that the three-dimensional modes possess identical structure, although at $Re = 150$ the length of the recirculation zone is longer than at $Re = 100$. The perturbation fields are broadly similar to the single cylinder case, so that the two cylinders are effectively acting as a single extended body.

In figure 19, streamwise perturbation vorticity contours are shown for almost touching cylinders ($S/D = 0.1$) at $Re = 150$. The structure of the perturbation contours bears a close resemblance to that of figure 22(b) in Stewart *et al.* (2010b), although the Reynolds number in this case is much higher, indicating that the three-dimensional modes involved are effectively identical.

Figure 20(a,b) shows the growth rate curves for larger separations, $S/D = 7$ and 8. We observe that the growth rate decreases at higher Reynolds numbers; however, positive growth is still maintained prior to the unsteady two-dimensional transition. The maximum growth shifts to slightly longer wavelengths. This is similar to the trend for the range $4.5 \leq S/D \leq 6.5$, although the mode does not restabilise. At $S/D = 9$ and 10, the growth rates increase with increasing Reynolds numbers (figure 20c,d).

The perturbation modes for higher S/D are depicted in figure 21. Their shape is clearly dif-

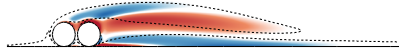


Figure 19: Streamwise perturbation vorticity contours for $S/D = 0.1$ at $Re = 150$, with $\lambda/D = 8$. Contour shading as in figure 12.

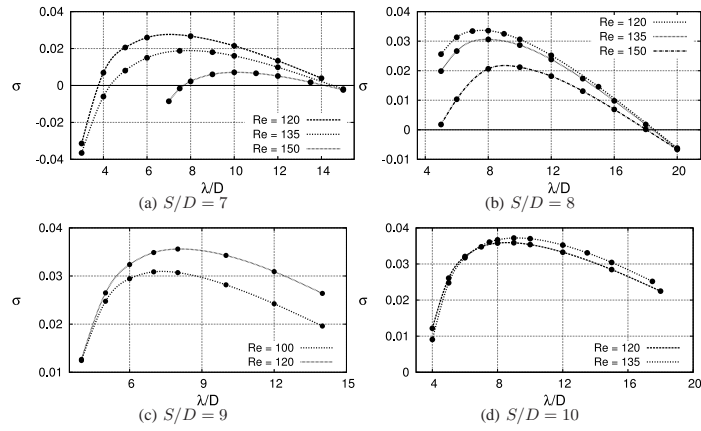


Figure 20: Growth rate curves at higher Reynolds numbers for higher S/D .

ferent from the mode structure for smaller separations. The strong flow within the gap and the significant streamline curvature, with strong localised recirculations towards the second cylinder, modifies the unstable three-dimensional mode shape. This effect is less pronounced at larger separations, where once again the perturbation field tends towards the one for a single cylinder.

For the case with $S/D = 7$, $Re = 165$ represents the highest Reynolds number at which the two-dimensional flow remains steady. For this parameter combination, the flow was found to be unstable to two different three-dimensional modes. The growth rate of the longer-wavelength mode, as a function of Reynolds number, was given in figure 20(a). Figure 22 shows that this mode still remains unstable at $Re = 165$; however, a shorter-wavelength mode is now even more unstable. The maximum growth rates of these two modes occur at $\lambda/D \simeq 4.5$ and 12, respectively (figure 22). The short-wavelength mode is periodic, with a complex growth rate, while the long-wavelength mode is stationary (purely real growth rate). The perturbation vorticity contours of these two modes can be seen in figure 23.

4.2. Periodic base flow

In the preceding section, the three-dimensional stability analysis was performed in the regime where the two-dimensional base flow is steady. To further explore the three-dimensional flow behaviour in the unsteady state, a Floquet stability analysis was performed at $Re = 200$ for

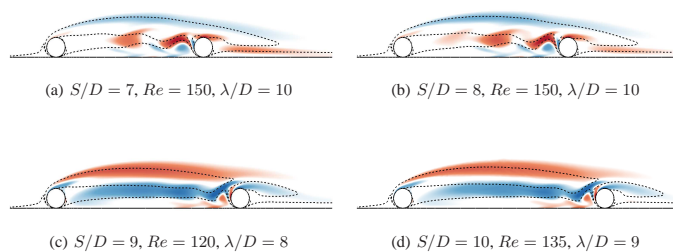


Figure 21: Spanwise perturbation vorticity contours for higher S/D . Contour shading as in figure 12.

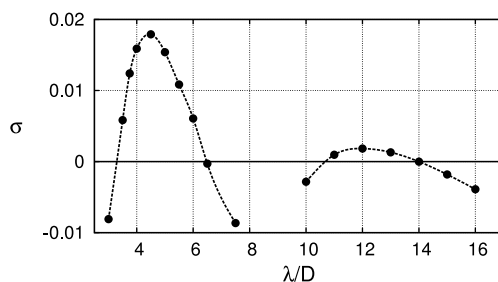


Figure 22: Growth rate curves for $S/D = 7$ at $Re = 165$. Two modes are present at this Reynolds number, including the one decaying as Re increases shown in figure 20(a).



Figure 23: Spanwise perturbation vorticity contours for $S/D = 7$ at $Re = 165$ for the two instability modes at the specified wavelengths. Contour shading as in figure 12.

the cylinders at the maximum separation distance of $S/D = 10$. Figure 24 shows the growth rate curves obtained by perturbing the two-dimensional base flow at different wavelengths. Four distinct modes (labelled I to IV) can be discerned, with their peaks at $\lambda/D = 2.6, 5.5, 6.0$ and 12 , the fastest growing mode having the shortest wavelength. Shown in figure 25 are the spanwise perturbation contours for these modes. Inspection of the corresponding Floquet multipliers shows that Modes I, III and IV are oscillating at frequencies incommensurate with the one of the base flow, leading to a quasi-periodic total flow, whereas Mode II was found to be subharmonic (negative real Floquet multiplier), oscillating with a period twice that of the base flow.

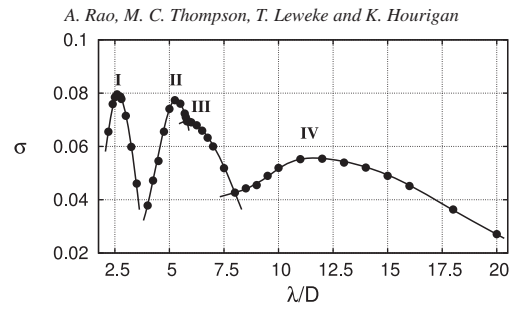


Figure 24: Growth rate curves for the cylinders separated by $S/D = 10$, $Re = 200$. Four distinct modes are visible, Mode III being partially masked by Mode II. The fastest growing mode has a maximum growth rate at $\lambda/D = 2.6$.

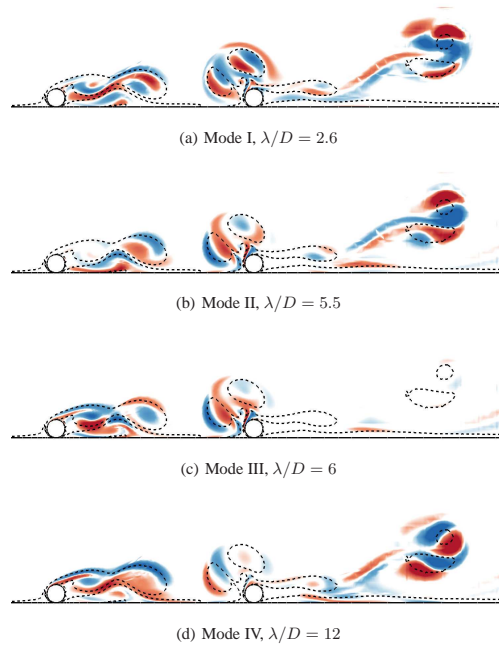


Figure 25: Spanwise perturbation vorticity contours for $S/D = 10$ at $Re = 200$ for the specified wavelengths. Contour shading as in figure 12.

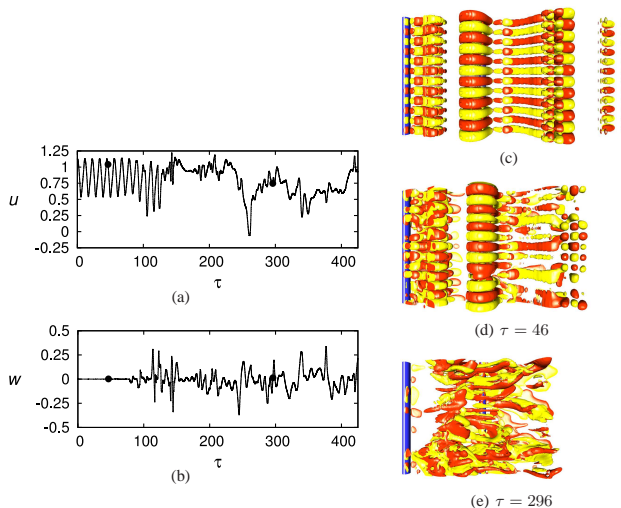


Figure 26: DNS results for the tandem cylinders sliding along a wall with $S/D = 10$ at $Re = 200$. Left: The time histories of the streamwise (u) and spanwise (w) velocity components for a location midway between the cylinders. Right: Visualisations using streamwise vorticity isosurfaces viewed from above. (c) Mode II with $\lambda/D = 2.4$ from linear stability analysis; (d) perturbation field obtained from DNS at $\tau = 46$; (e) the same field at $\tau = 296$.

5. Direct Numerical Simulation

At Reynolds numbers not too far above the threshold for three-dimensional transition, it appears that a number of linear modes become unstable, as shown e.g. in figure 24. To investigate the nonlinear interaction between these modes, a three-dimensional Direct Numerical Simulation (DNS) was performed. A three-dimensional version of the computational code employing a Fourier expansion in the spanwise direction (Thompson *et al.* 1996; Karniadakis & Triantafyllou 1992; Ryan *et al.* 2005; Leontini *et al.* 2007) was used, with the two-dimensional solution for $S/D = 10$ and $Re = 200$ as initial condition. A spanwise domain length of 16 cylinder diameters with 96 Fourier planes was chosen to capture the wake dynamics. Low-intensity white noise was added to trigger three-dimensional flow. The spanwise extent of the domain could contain respectively six and three wavelengths of the two fastest growing modes shown in figure 24. Figures 26(a) and 26(b) give time traces of the streamwise and spanwise velocity components at a point midway between the cylinders. Figure 26(c) represents the most unstable mode from linear stability analysis, using isosurfaces of positive and negative streamwise vorticity to indicate the wake structure. This should be compared with the DNS isosurfaces shown in figure 26(d), corresponding to $\tau = 46$, while the mode is still undergoing exponential amplification. Figure 26(e) shows the complex nature of the wake at a later time ($\tau = 296$), after the wake has become highly non-linear. As indicated above, in this state even the remnants of periodicity in the u velocity component are lost. Also, there does not appear to be a clearly dominant spanwise wavelength. Hence the flow shows signs of a rapid transition to a chaotic state.

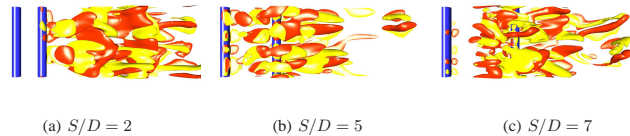


Figure 27: The final wake states at $Re = 200$ for the cylinders sliding along a wall at various spacings. These images can be compared to figure 26(e), where the flow eventually becomes chaotic.

Figure 27 shows similar visualisations of the wake for tandem cylinders with $S/D = 2, 5$ and 7 at $Re = 200$. Starting from the respective two-dimensional solutions, the simulations were run for approximately 300 time units. For this set of simulations, the spanwise distance was set to eight cylinder diameters. For $S/D = 2$, the flow is three-dimensional and unsteady, and the long-wavelength instability is the dominant three-dimensional mode, while for $S/D = 5$ and 7 , the final wake state is chaotic, similar to that observed in figure 26(e). In any case, the two-dimensional base flow is clearly no longer an adequate model of the real flow in this regime.

6. Conclusions

The flow past two tandem cylinders sliding along a wall has been investigated via stability analyses and Direct Numerical Simulations. Two-dimensional calculations were used to investigate the transition from two-dimensional steady to two-dimensional unsteady flow, when the Reynolds number is increased, as function of the cylinder spacing. Steady flow involves multiple recirculation zones, with complicated streamline patterns arising in the gap between the cylinders for intermediate spacings. For very small and very large spacings, both steady and unsteady wakes resemble those of a single sliding body. Whereas at low Reynolds numbers in the unsteady regime, the wakes behind both cylinders oscillate at the same frequency, for larger Re an intermediate spacing range exists, where a period doubling is observed. This can be explained by a feedback mechanism, where the vortex shed from the first cylinder impacting on the second one triggers shedding of a new vortex from the first cylinder at slightly different conditions. The same phenomenon is known to occur in flow around elongated bluff bodies, where vortices are shed from both the leading and trailing edges. The drag forces acting on both cylinders in two-dimensional flow were determined for the steady and periodic regimes up to $Re = 200$ and separations up to 10 cylinder diameters.

Three-dimensional stability analysis of the two-dimensional flows showed that, for all parameter combinations, the flow becomes unstable at Reynolds number well below the threshold for unsteadiness in two dimensions. Again, for vanishing and very large cylinder separations, the unstable modes are similar to those found previously for a single sliding cylinder. In an intermediate spacing range around 5-6 cylinder diameters, a sequence of alternating regimes of three-dimensional instability and stability is observed for increasing Reynolds numbers. Whereas outside this interval the unstable three-dimensional modes are steady, the second transition within part of this range occurs through the amplification of an unsteady three-dimensional mode. Three-dimensional instability persists at higher Reynolds numbers, where the two-dimensional base flow is periodic. A Floquet stability analysis at $Re = 200$ for a large cylinder separation revealed the existence of at least four unstable modes at various wavelengths and frequencies. Direct Numerical Simulation of this flow with a spanwise domain size allowing for the growth

of several of these modes showed their non-linear interaction, leading rapidly to a disordered chaotic state.

The fact that the first transition of flow around tandem cylinders sliding along a wall involves three-dimensional steady modes, makes the results from the analysis of the transition from steady to unsteady two-dimensional flow appear less relevant for the description of realistic flows in this configuration. A similar situation was previously encountered in the study of the transitions of the wake of an isolated circular cylinder. The characteristics of the three-dimensional *Mode B* were determined through a Floquet stability analysis of the two-dimensional periodic flow (Barkley & Henderson 1996), even though in reality the wake is already highly three-dimensional when *Mode B* is first observed. In that case, although the critical Reynolds number is overpredicted, the predicted wavelength and spatio-temporal symmetry of *Mode B* carry across to the real flow. For the sliding tandem cylinders examined here, the onset of three-dimensional flow is likely to alter the critical Reynolds numbers for the unsteady transition. Other observed characteristics, such as Strouhal numbers and average two-dimensional flow structures, may nevertheless remain at least roughly similar to the prediction obtained from a two-dimensional base flow. The full analysis of the unsteady transition for three-dimensional wakes is a substantial computational problem, and will form the basis of a future study.

The support from Australian Research Council Discovery Grants DP0877327 and DP0877517 and computing time from the National Computational Infrastructure (NCI), Victorian Life Sciences Computation Initiative (VLSCI) and Monash Sungrid are gratefully acknowledged. A. R. also acknowledges the support of a Monash University Departmental Postgraduate Scholarship.

REFERENCES

- BARKLEY, D. & HENDERSON, R. D. 1996 Three-dimensional Floquet stability analysis of the wake of a circular cylinder. *J. Fluid Mech.* **322**, 215–241.
- BHATTACHARYYA, S. & DHINAKARAN, S. 2008 Vortex shedding in shear flow past tandem square cylinders in the vicinity of a plane wall. *J. Fluids Struct.* **24**, 400–417.
- BIERMANN, D. & HERRNSTEIN, W. H. 1933 The interference of struts in various combinations. *Tech. Rep.* 468. National Advisory Committee for Aeronautics.
- BLACKBURN, H. M. & LOPEZ, J. M. 2003 On three-dimensional quasi-periodic Floquet instabilities of two-dimensional bluff body wakes. *Phys. Fluids* **15**, L57–L60.
- CARMO, B. S., MENEGHINI, J. R. & SHERWIN, S. J. 2010 Secondary instabilities in the flow around two circular cylinders in tandem. *J. Fluid Mech.* **644**, 395–431.
- CHORIN, A. J. 1968 Numerical solution of the Navier-Stokes equations. *Math. Comp.* **22**, 745–762.
- DENG, J., REN, A.-L., ZOU, J.-F. & SHAO, X.-M. 2006 Three-dimensional flow around two circular cylinders in tandem arrangement. *Fluid Dyn. Res.* **38**, 386–404.
- DIDIER, E. 2007 Simulation de l'écoulement autour de deux cylindres en tandem. *C. R. Mécanique* **335**, 696–701.
- GRIFFITH, M. D., LEWEKE, T., THOMPSON, M. C. & HOURIGAN, K. 2009 Pulsatile flow in stenotic geometries: Flow behaviour and stability. *J. Fluid Mech.* **622**, 291–320.
- HARICHANDAN, A. B. & ROY, A. 2012 Numerical investigation of flow past single and tandem cylindrical bodies in the vicinity of a plane wall. *J. Fluids Struct.* doi:10.1016/j.jfluidstructs.2012.04.006, published online by Elsevier Ltd. 7 June 2012.
- HENDERSON, R. D. 1997 Non-linear dynamics and pattern formation in turbulent wake transition. *J. Fluid Mech.* **352**, 65–112.
- HOURIGAN, K., THOMPSON, M. C. & TAN, B. T. 2001 Self-sustained oscillations in flows around long flat plates. *J. Fluids Struct.* **15**, 387–398.
- HUANG, W.-X. & SUNG, H. J. 2007 Vortex shedding from a circular cylinder near a moving wall. *J. Fluids Struct.* **23**, 1064–1076.
- IGARASHI, T. 1981 Characteristics of flow around two circular cylinders arranged in tandem. *Bull. JSME* **24**, 323–331.

- KARNIADAKIS, G. E. & SHERWIN, S. J. 2005 *Spectral/hp Methods for Computational Fluid Dynamics*. Oxford: Oxford University Press.
- KARNIADAKIS, G. E. & TRIANTAFYLLOU, G. S. 1992 Three-dimensional dynamics and transition to turbulence in the wake of bluff objects. *J. Fluid Mech.* **238**, 1–30.
- KEVLAHAN, N. K. R. 2007 Three-dimensional Floquet stability analysis of the wake in cylinder arrays. *J. Fluid Mech.* **592**, 79–88.
- LEONTINI, J. S., THOMPSON, M. C. & HOURIGAN, K. 2007 Three-dimensional transition in the wake of a transversely oscillating cylinder. *J. Fluid Mech.* **577**, 79–104.
- LIANG, C., PAPADAKIS, G. & LUO, X. 2008 Effect of tube spacing on the vortex shedding characteristics of laminar flow past an inline tube array: a numerical study. *Comput. Fluids* **38**, 950–964.
- MAHIR, N. 2009 Three-dimensional flow around a square cylinder near a wall. *Ocean Eng.* **36**, 357–367.
- MAMUN, C. K. & TUCKERMAN, L. S. 1995 Asymmetry and Hopf-bifurcation in spherical Couette flow. *Phys. Fluids* **7**, 80–91.
- MENEGHINI, J. R., SALTARA, F., SIQUEIRA, C. L. R. & FERRARI, J. A. 2001 Numerical simulation of flow interference between two circular cylinders in tandem and side-by-side arrangements. *J. Fluids Struct.* **15**, 327–350.
- MITTAL, R. & BALACHANDAR, S. 1995 Generation of streamwise vortical structures in bluff body wakes. *Phys. Rev. Lett.* **75**, 1300–1303.
- MIZUSHIMAA, J. & SUEHIRO, N. 2005 Instability and transition of flow past two tandem circular cylinders. *Phys. Fluids* **17**, 104107.
- MUSSA, A., ASINARI, P. & LUO, L.-S. 2009 Lattice Boltzmann simulations of 2d laminar flows past two tandem cylinders. *J. Comput. Phys.* **228**, 983–999.
- PAPAIANOANNOU, G. V., YUE, D. K. P., TRIANTAFYLLOU, M. S. & KARNIADAKIS, G. E. 2005 Three-dimensional flow around two circular cylinders in tandem arrangement. *J. Fluid Mech.* **558**, 387–413.
- RAO, A., STEWART, B. E., THOMPSON, M. C., LEWEKE, T. & HOURIGAN, K. 2011 Flows past rotating cylinders next to a wall. *J. Fluids Struct.* **27**, 668–679.
- RYAN, K., THOMPSON, M. C. & HOURIGAN, K. 2005 Three-dimensional transition in the wake of bluff elongated cylinders. *J. Fluid Mech.* **538**, 1–29.
- SHEARD, G. J., THOMPSON, M. C. & HOURIGAN, K. 2003 From spheres to circular cylinders: The stability and flow structures of bluff ring wakes. *J. Fluid Mech.* **492**, 147–180.
- SHEARD, G. J., THOMPSON, M. C. & HOURIGAN, K. 2005 Subharmonic mechanism of the mode C instability. *Phys. Fluids* **17**, 111702.
- STEWART, B. E., HOURIGAN, K., THOMPSON, M. C. & LEWEKE, T. 2006 Flow dynamics and forces associated with a cylinder rolling along a wall. *Phys. Fluids* **18**, 111701.
- STEWART, B. E., THOMPSON, M. C., LEWEKE, T. & HOURIGAN, K. 2010a Numerical and experimental studies of the rolling sphere wake. *J. Fluid Mech.* **643**, 137–162.
- STEWART, B. E., THOMPSON, M. C., LEWEKE, T. & HOURIGAN, K. 2010b The wake behind a cylinder rolling on a wall at varying rotation rates. *J. Fluid Mech.* **648**, 225–256.
- THOMPSON, M. C., HOURIGAN, K., CHEUNG, A. & LEWEKE, T. 2006a Hydrodynamics of a particle impact on a wall. *Appl. Math. Mod.* **30**, 1356–1369.
- THOMPSON, M. C., HOURIGAN, K., RYAN, K. & SHEARD, G. J. 2006b Wake transition of two-dimensional cylinders and axisymmetric bluff bodies. *J. Fluids Struct.* **22**, 793–806.
- THOMPSON, M. C., HOURIGAN, K. & SHERIDAN, J. 1996 Three-dimensional instabilities in the wake of a circular cylinder. *Exp. Therm. Fluid Sci.* **12**, 190–196.
- THOMPSON, M. C., LEWEKE, T. & HOURIGAN, K. 2007 Sphere-wall collisions: vortex dynamics and stability. *J. Fluid Mech.* **575**, 121–148.
- THOMPSON, M. C., LEWEKE, T. & WILLIAMSON, C. H. K. 2001 The physical mechanism of transition in bluff body wakes. *J. Fluids Struct.* **15**, 607–616.
- WILLIAMSON, C. H. K. 1988 The existence of two stages in the transition to three-dimensionality of a cylinder wake. *Phys. Fluids* **31**, 3165–3168.
- WILLIAMSON, C. H. K. 1996 Vortex dynamics in the cylinder wake. *Annu. Rev. Fluid Mech.* **28**, 477–539.
- ZDRAVKOVICH, M. M. 1987 The effects of interference between circular cylinders in cross flow. *J. Fluids Struct.* **1**, 239–261.
- ZENG, L., BALACHANDAR, S. & FISCHER, P. 2005 Wall-induced forces on a rigid sphere at finite Reynolds number. *J. Fluid Mech.* **536**, 1–25.
- ZHANG, H. Q., NOACK, B. R., KÖNIG, M. & ECKELMANN, H. 1995 On the transition of the cylinder wake. *Phys. Fluids* **7**, 779–793.

ZHOU, Y. & YIU, M. W. 2005 Flow structure, momentum and heat transport in a two-tandem-cylinder wake. *J. Fluid Mech.* **548**, 17–48.

Chapter 6

The sinuous mode in the wake of a rolling sphere

6.1 Overview

The preceding chapters have discussed the effects of rotation for a circular cylinder near a wall. This chapter deals with the flow dynamics of a spherical body, which is given a fixed rotation rate as it translates along a wall. The flow dynamics for a sphere rolling along a wall have been previously investigated by Stewart *et al.* (2010a) for $-1 \leq \alpha \leq +1$, both experimentally and numerically. For the forward rolling sphere, the Reynolds number for the onset of periodic flow occurred at lower values as the rotation rate was increased. The shedding was characterised by the formation of hairpin vortices which moved away from the wall and convected downstream. This was observed at the highest tested Reynolds number of 200 for $\alpha = +1$. Recent experimental findings of Bolnot *et al.* (2011) showed the lateral displacement of these hairpin vortices on either side of the wake centreline at $Re = 230$.

To examine the sinuous structure of the wake numerically, simulations are undertaken using a two-dimensional computational domain rotated azimuthally to obtain a cylindrical volume with the sphere at the centre. The journal article presented in this chapter elucidates the numerical findings for the wake of a rolling sphere for $\alpha = +1$ and $Re \leq 500$. As Reynolds number is increased from low values, the flow transitions to the periodic state at $Re \simeq 140$, and at a higher Reynolds number of $Re \simeq 192$, the wake no longer retains its planar symmetry. The nature of these transitions is investigated by the Stuart-Landau model. Following the second transition, the flow then locks onto a $7 : 3$ resonance, prior to the onset of chaotic flow at higher Reynolds number, while retaining the sinuous structure. Using frequency spectra, phase plots and Poincaré

maps, the chaotic nature of this flow is established. Furthermore, the tracer particle visualisations from the numerical simulations are in excellent agreement with the dye visualisations from the experiments.

6.2 Transition to chaotic flow in the wake of a rolling sphere

The following article was published in 2012 in *Journal of Fluids Mechanics*. This work was co-authored by P.-Y. Passaggia, H. Bolnot, M. C. Thompson, T. Leweke and K. Hourigan, and is entitled, “*Transition to chaos in the wake of a rolling sphere*”. The paper is reproduced in this thesis directly from the version published online.

Declaration for manuscript included in PhD Thesis

Monash University

Declaration for Thesis Chapter 6

Declaration by candidate

In the case of Chapter 6, the nature and extent of my contribution to the work was the following:

Nature of contribution	Extent of contribution (%)
Initiated the paper, performed numerical simulations, analysed the data, wrote the manuscript, revised the manuscript	65

The following co-authors contributed to the work. Co-authors who are students at Monash University must also indicate the extent of their contribution in percentage terms:

Name	Nature of contribution	Extent of contribution (%) for student co-authors only
P-Y. Passagia	Performed experiments	5
H. Bolnot	Performed experiments	5
Prof. M.C. Thompson	Co-wrote the manuscript	N. A.
Prof. T. Leweke	Co-wrote the manuscript	N. A.
Prof. K. Hourigan	Co-wrote the manuscript	N. A.

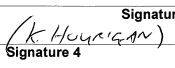
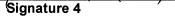
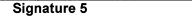
Candidate's Signature  Date 20 JUNE 2012

Declaration by co-authors

The undersigned hereby certify that:

- ^L 1) the above declaration correctly reflects the nature and extent of the candidate's contribution to this work, and the nature of the contribution of each of the co-authors.
- ^L 2) they meet the criteria for authorship in that they have participated in the conception, execution, or interpretation, of at least that part of the publication in their field of expertise;
- ^L 3) they take public responsibility for their part of the publication, except for the responsible author who accepts overall responsibility for the publication;
- ^L 4) there are no other authors of the publication according to these criteria;
- ^L 5) potential conflicts of interest have been disclosed to (a) granting bodies, (b) the editor or publisher of journals or other publications, and (c) the head of the responsible academic unit; and
- ^L 6) the original data are stored at the following location(s) and will be held for at least five years from the date indicated below.

Location(s)

Signature 1  Signature 2  Date 20/6/2012
Signature 3  Signature 4  Signature 5 

K Hourigan (For P-Y. PASSAGIA, H. BOLNOT, M.C. THOMPSON, T. LEWEKE) 20/6/2012

Transition to chaos in the wake of a rolling sphere

A. Rao^{1†}, P.-Y. Passaglia², H. Bolnot², M. C. Thompson¹, T. Leweke²
and K. Hourigan^{1,3}

¹ Fluids Laboratory for Aeronautical and Industrial Research (FLAIR), Department of Mechanical and Aerospace Engineering, Monash University, Melbourne, VIC 3800, Australia

² Institut de Recherche sur les Phénomènes Hors-Équilibre (IRPHE), CNRS/Aix-Marseille Université, 13384 Marseille CEDEX 13, France

³ Division of Biological Engineering, Monash University, Melbourne, VIC 3800, Australia

(Received 6 September 2011; revised 18 December 2011; accepted 31 December 2011;
first published online 22 February 2012)

The wake of a sphere rolling along a wall at low Reynolds number is investigated numerically and experimentally. Two successive transitions are identified in this flow, as the Reynolds number is increased. The first leads to the periodic shedding of planar symmetric hairpin vortices. The second and previously unknown transition involves a loss of planar symmetry and a low-frequency lateral oscillation of the wake, exhibiting a surprising 7:3 resonance with the hairpin vortex shedding. The two transitions are characterized by dye visualizations and quantitative information obtained from numerical simulations, such as force coefficients and wake frequencies (Strouhal numbers). Both transitions are found to be supercritical. Further increasing the Reynolds number, the flow becomes progressively more disorganized and chaotic. Overall, the transition sequence for the rolling sphere is closer to the one for a non-rotating sphere in a free stream than to that of a non-rotating sphere close to a wall.

Key words: chaos, vortex shedding, wakes

1. Introduction

We here investigate the first transitions in the flow generated by a forward rolling sphere on a solid surface, as the Reynolds number is increased from the initially steady regime. Motivation for this study comes, for example, from the modelling of wall effects in fluid–particle systems, or from biological applications such as cells moving and rolling along blood vessel walls, even though the Reynolds numbers in the latter class are often much lower. Indeed, with rolling near-spherical bodies being ubiquitous in nature (e.g. sand or dust in wind, rocks in avalanches) and in sports (e.g. football, bowls, billiards, pétanque), it seems surprising that the dynamics and transitions of their wakes have been largely unexplored until only recently (Stewart *et al.* 2010a).

The case of a non-rotating sphere in a uniform free stream has been studied extensively. This flow undergoes a transition at $Re \simeq 212$ (Johnson & Patel 1999)

† Email address for correspondence: anirudh.rao@monash.edu

from a steady axisymmetric state to a steady non-axisymmetric flow with planar symmetry: the ‘double-threaded wake’ (Magarvey & Bishop 1961*a,b*), consisting of two trailing counter-rotating vortices. Beyond $Re = 272$, these threads interact during formation, leading to the shedding of vortex loops (or ‘hairpins’). From analysis of direct simulations, both transitions have been shown to be supercritical (Ghidersa & Dušek 2000; Thompson, Leweke & Provansal 2001*a*), obeying the Landau model as the flow saturates. Numerical simulations indicate that the planar symmetry is broken at $Re \simeq 345$ (Mittal 1999), which is in line with experimental investigations of Sakamoto & Haniu (1990). They suggested that a transitional regime exists for $420 \leq Re \leq 480$, wherein the hairpin vortices are intermittently displaced to either side of the wake centreline.

Direct numerical simulations were performed by Zeng, Balachander & Fisher (2005) for a sphere moving parallel to a wall. Their study showed that as the sphere was moved closer to the wall, the transition to the unsteady state occurred at Reynolds numbers lower than for the free stream case ($Re < 272$), with a sudden increase observed for the closest tested distance of $0.25D$. The effect of free rotation was also studied. This group (Zeng *et al.* 2009) also performed direct numerical simulations for a stationary spherical particle close to a plane wall in a linear shear flow. They present results for gap ratios between $0.005 \leq G/D \leq 3.5$, using a symmetry plane. The double-threaded wake is observed at $Re = 200$ for larger gap ratios, while a toroidal structure engulfing the particle is observed for lower Reynolds numbers. These findings are similar to the results of Stewart *et al.* (2010*a*), where the transition to an unsteady state for the non-rotating sphere was in excess of $Re = 300$. Furthermore, they propose empirical relationships for the lift and drag coefficient variation with distance from the wall.

Previous studies by Stewart *et al.* (2010*a*) investigated the wake dynamics of a sphere moving next to a wall, under conditions of forward rolling, sliding or reverse rotation. For the forward-rolling case, which is of interest here, the wake is attached and steady for $Re < 125$. The wake structure shows some similarities to the two-tailed wake of a non-rotating isolated sphere, except that the trailing counter-rotating vortex pair loses strength more quickly with downstream distance due to the damping effect of the wall. Between $125 < Re < 150$, the wake becomes unsteady, periodically shedding vortex loops. The structure is initially symmetric with respect to the vertical plane passing through the sphere and wake. Note that the rotation and the presence of the wall reduces the critical Reynolds number of unsteady flow transition from $Re_c \simeq 212$ (Johnson & Patel 1999; Ghidersa & Dušek 2000; Thompson *et al.* 2001*a*) for the isolated sphere wake. Initial experiments and direct simulations indicated that the wake mirror symmetry is maintained until approximately $Re = 200$, which was the highest Reynolds number reported. Stewart *et al.* (2010*a*) also examined the reverse-rolling case. They observed the development of a transverse sinusoidal oscillation of the wake at $Re = 200$, and recorded a transverse force as the unsteady wake advected downstream. In their simulations at $Re = 300$, initialized from a zero velocity state, it was found that the wake retained mirror symmetry with respect to the wake centreline for a long time. The addition of noise was required to initiate the transition to the asymmetric mode, although this is presumably due to the low growth rate of the instability. The steady double-threaded wake formed downstream of the sphere developed a sinusoidal oscillation, which advected with the flow. Similar sinuous oscillations of the otherwise steady flow were also observed for a translating (sliding) sphere at $Re \geq 300$ in the experiments.

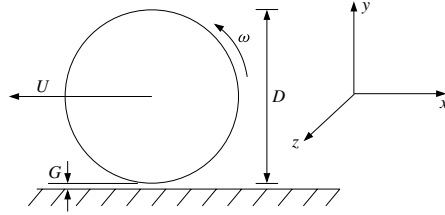


FIGURE 1. Schematic of the configuration. For a forward-rolling sphere, $\omega = 2U/D$.

A first experimental visualization of the transition to an asymmetric rolling sphere wake $Re_c \simeq 200$ was shown in Bolnot *et al.* (2011). The present paper quantifies the transition sequence in this flow determining the critical Reynolds numbers and sub/super-criticality, investigates and characterizes the intriguing high-order resonance between the modes, and quantifies the rapid progression to fully chaotic flow.

2. Problem definition and methodology

A schematic of the rolling sphere setup is shown in figure 1. A dimensionless rotation rate of the sphere, α , can be defined by

$$\alpha = \frac{D\omega}{2U}. \quad (2.1)$$

Here, the sphere diameter is D , the velocity of the sphere centroid is U and ω is the angular velocity. For the situation examined in this paper, α is set to +1. This corresponds to prograde non-slip rolling.

For computational efficiency, the reference frame is attached to the centre of the sphere. Relative to this moving frame of reference, the fluid and the lower wall move with the same speed U , directed to the right. The other key governing parameter is the Reynolds number $Re = UD/\nu$, where ν is the kinematic viscosity of the fluid. The force on the sphere consists of viscous and pressure contributions and can be split into streamwise (F_x), vertical (F_y) and lateral (F_z) components. These are non-dimensionalized in the standard way: $C_{x,y,z} = 8F_{x,y,z}/(\rho U^2 \pi D^2)$, with ρ the fluid density. Finally, the non-dimensional shedding frequency is given by the Strouhal number $St = fD/U$, where f is the shedding frequency.

2.1. Numerical formulation and validation

The time-dependent incompressible Navier–Stokes equations are solved in cylindrical polar coordinates (r, θ, z) . The numerical scheme employs a three-step time-splitting approach (Chorin 1968), with the sub-steps accounting for the advection, diffusion and pressure terms in the Navier–Stokes equations. Previous studies have shown that the implementation achieves second-order temporal accuracy. In terms of spatial discretization, the spectral element method is used for the r – z discretization and a Galerkin Fourier approach for the azimuthal dependence. The method/implementation has previously been used to simulate flows past bluff bodies such as cylinders, spheres and rings both in the free stream (Thompson, Leweke & Williamson 2001b; Sheard, Thompson & Hourigan 2003; Schouveiler *et al.* 2004; Ryan, Thompson & Hourigan 2005; Leontini, Thompson & Hourigan 2007) and also close to a surface (Thompson,

Leweke & Hourigan 2007; Stewart *et al.* 2010*b*). Details of the numerical method are provided in Thompson *et al.* (2006).

Because quadrilateral elements are used to build the mesh, the sphere is placed slightly above the wall at a distance G in order to prevent degeneracy of nodes for the elements directly underneath the sphere. A gap ratio of $G/D = 0.005$ is typically used for the simulations. By varying this distance, it was found that the flow structures in the wake were not affected, although the (lift) force on the sphere does vary slightly with increasing gap height (Stewart *et al.* 2010*a*).

The computational domain consisted of 320 macro-elements in the r - z plane. This was extended into three dimensions using N_θ Fourier planes in the azimuthal direction. The origin of the cylindrical polar coordinate system was taken as the point on the wall directly below the sphere with the polar axis passing through the sphere. Each quadrilateral (spectral) element employs $N \times N$ internal node points. These internal node points correspond to the Gauss–Legendre–Lobatto quadrature points with the velocity and pressure fields represented by a tensor product of Lagrangian polynomial interpolants of order $N - 1$ within elements. The macro-elements are concentrated around the sphere and decrease in concentration with increasing distance from it. The top boundary is located $150D$ away from the lower wall while the lateral boundaries are $100D$ away; thus, blockage is negligible. During resolution testing, the interpolant order was varied between $N - 1 = 4$ and 7, with up to 256 Fourier planes. It was found that at $Re = 300$ for $N = 6$ and $N_\theta = 128$, convergence of the drag force is better than 0.5%, with the Strouhal number resolved to better than 0.1%.

2.2. Experimental setup

Previous experiments by Stewart *et al.* (2010*a*) were undertaken in a closed circuit water tunnel with a moving floor and the sphere mounted on a motor-driven axle parallel to the moving floor. In addition, the upstream boundary layer was sucked off prior to the moving floor section to improve the quality of the entry flow. This setup allowed the sphere to be rotated independently of the wall motion. In the current set of experiments, that extra flexibility was not required and a simpler, less invasive setup was employed. The experimental apparatus consisted of a water-filled tank, with an inclined Plexiglas plate used as a false floor. Steel spheres of diameters 4.7 and 6.5 mm were first coated with fluorescein dye, slowly lowered into the water using a glass pipe and allowed to roll down the incline. The angle between the horizontal and the plate surface was of the order of 0.5° and could be precisely controlled to obtain the desired terminal velocity of the sphere, and hence set the Reynolds number. A 1 mm groove in the inclined surface ensured the sphere rolled along a straight path. The fluid in the tank was illuminated in volume using an argon ion laser, allowing the wake behind the sphere to be visualized and photographed. One distinct advantage of the current setup is the removal of the driven axle, which slightly modifies the flow, and reduced vibration, even though it was necessary to add the groove to ensure passage along a straight path. With the current setup, it was also easy to coat the sphere with dye prior to immersing it and beginning the experimental runs. The velocity of the sphere and thus the Reynolds number was easy to determine accurately from its position in video images.

Various authors (Chhabra & Ferreira 1999; Verekar & Arakeri 2010) have previously studied the distance required to effectively reach the terminal velocity for a sphere rolling down an incline. Chhabra & Ferreira (1999) established an approximate relationship for $Re < 500$ in terms of the density ratio. For the case here using steel spheres, this shows that the terminal velocity is reached within approximately

13 sphere diameters. For the experiments reported in this paper, data were recorded for $120D$ after the sphere had travelled $30D$ from its initial position.

3. Results

3.1. Flow structures

The flow behind the wake of a rolling sphere has been visualized by Stewart *et al.* (2010a), both experimentally by dye visualization in a water channel and also numerically using the method of Jeong & Hussain (1999). In those investigations, steady flow was observed for $Re \leq 125$. The visualizations of the flow structures showed the wake is displaced away from the wall at low Reynolds numbers and the formation of a double threaded wake is observed, similar to that behind a non-rotating sphere in unbounded flow for $212 < Re < 272$ (Johnson & Patel 1999). Similar structures were observed in our simulations for $Re \leq 135$. However, at $Re = 140$, periodic fluctuations in the time histories were observed for the streamwise and wall normal components of force. The kinking of the double-threaded wake, as described by Magarvey & Bishop (1961a,b) and Thompson *et al.* (2001a), was observed, and hairpin vortices formed behind the sphere advected downstream and moved away from the wall. On further increasing the Reynolds number, the amplitude of the fluctuations increased, while no variation was observed in the lateral component of force, indicating a planar symmetry about the wake centreline. The studies of Stewart *et al.* (2010a) show that the symmetry was maintained until $Re = 200$, with the shedding frequency remaining approximately constant at $St \simeq 0.125$ across the unsteady range.

In the current study, numerical simulations at $Re > 195$ showed the growth of the lateral component of the force C_z , whose frequency of oscillation was approximately (but not exactly) twice that of the shedding period for the streamwise direction. The amplitude of the lateral component of force grew with increasing flow speeds beyond $Re = 195$. Tracer particles injected into the flow showed small displacements about the wake centreline at flow speeds near the transition. However, at slightly higher Reynolds numbers, the vortex cores were displaced alternately on either side. The injected dye was drawn into these vortex cores, making it easier to visualize them in the water tank experiments.

Shown in figure 2 are the vortex structures before and after this transition. Figure 2 shows the comparison between the dye visualizations from the experiments (a,b) and analogous numerical visualizations (c,d) obtained by injecting tracer particles from a location just above the surface of the sphere. Note that the wake became increasingly chaotic beyond $Re = 220$. This is indicated by the force time traces showing irregular fluctuations, and is discussed in further detail in the following sections.

3.2. Nature of the transitions

The Stuart–Landau model for flow supercritical transitions predicts that, close to the critical Reynolds number, the square of the amplitude at saturation should vary linearly with the Reynolds number increment above the critical value (e.g. Provansal, Mathis & Boyer 1987; Dušek, Le Gal & Fraunié 1994; Le Gal, Nadim & Thompson 2001; Thompson & Le Gal 2004). Here, the amplitude can be any flow quantity that is zero prior to transition. For the current flow system, the initial transition is from a steady two-threaded wake to an unsteady wake. In that case, an appropriate measure is the amplitude of the oscillatory component of the drag force coefficient. The second transition corresponds to the breaking of mirror symmetry of the wake as

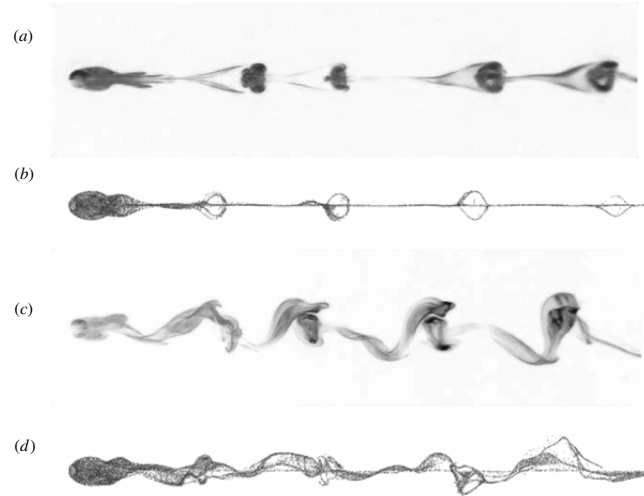


FIGURE 2. Comparison of experimental dye visualizations (*a,c*, negative image) and numerically obtained tracer particle images (*b,d*). (*a,b*) $Re = 190$; (*c,d*) $Re = 230$.

viewed from above. In that case, the amplitude of the side force coefficient can be used as a suitable measure. Figure 3 shows plots of the amplitude squared against Reynolds numbers for both transitions determined using data from direct numerical simulations. The unsteady transition occurs at $Re_{c1} = 138.9$ and the mirror symmetry breaking transition occurs at $Re_{c2} = 191.6$. Previously, the critical Reynolds number for the first transition had only been determined to lie in the range $125 < Re_{c1} < 150$, while the second transition was unobserved (Stewart *et al.* 2010*a*). Both plots show that the functional behaviour close to transition is well represented by straight lines, confirming the supercritical (non-hysteretic) nature of both transitions. In terms of the mathematics underlying the Landau model, this means that the real component of the cubic amplitude term in the amplitude evolution equation is negative, meaning that term is responsible for limiting the initial linear growth once the critical Reynolds number is exceeded.

3.3. Behaviour of the lateral component

To the knowledge of the authors, the mirror-symmetry breaking transition has not been seen previously in either experiments or numerical simulations. That transition can be further analysed by taking a Fourier transform of the time series of the force coefficients. Power spectra corresponding to the lift and side force components are shown in figure 4 for a range of Reynolds numbers near the lateral transition. At $Re = 200$, just above the transition Reynolds number of $Re = 191.6$, both spectra show peaks at the Strouhal numbers corresponding to the shedding of vortex loops ($St_{x,y} = 0.1167$) and the lateral oscillation ($St_z = 0.05$). These are identified in the spectra. In addition, nonlinear interaction frequency peaks are clearly seen. Some of these have also been marked. As the Reynolds number is increased further to $Re = 240$, the characteristic shedding or lateral oscillation frequency is still present as

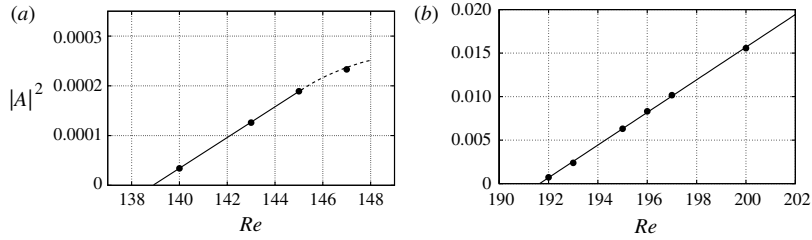


FIGURE 3. Linear fits of the square of the amplitude against Re using data obtained from numerical simulations for the first two transitions. The critical values for the transitions are obtained by extrapolating the straight line fits to zero amplitude. See text for further details. (a) First transition (steady to unsteady); (b) second transition (loss of planar symmetry).

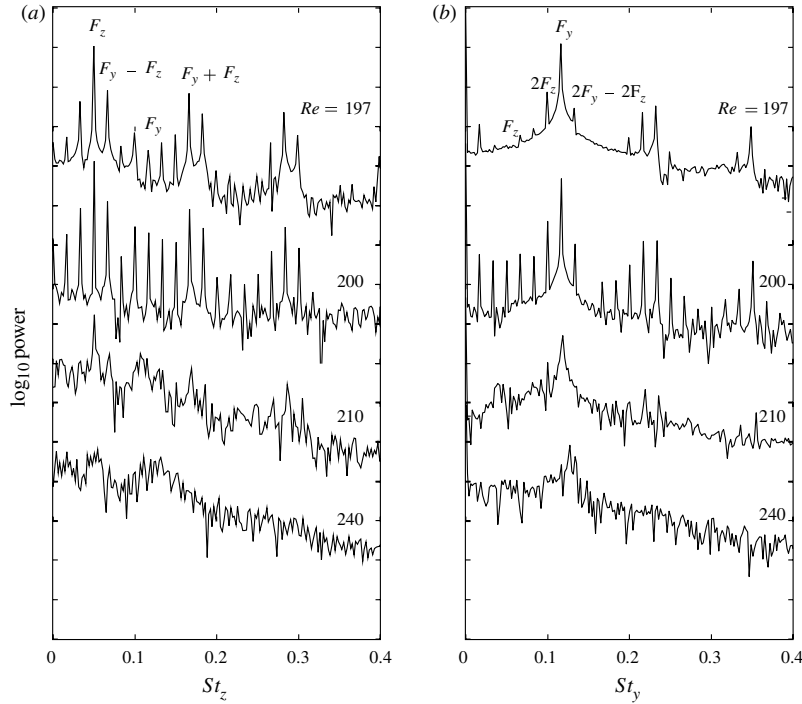


FIGURE 4. Power spectra showing the change in frequency content as a function of Reynolds number. (a) The frequency decomposition for the side force (C_z), (b) the same for the lift force. Some peaks corresponding to the nonlinear interactions have been labelled.

a broad feature in the C_y and C_z spectra, respectively, but overall the spectra do not show a set discrete set of peaks, indicating a richer frequency content consistent with the evolution towards a chaotic state.

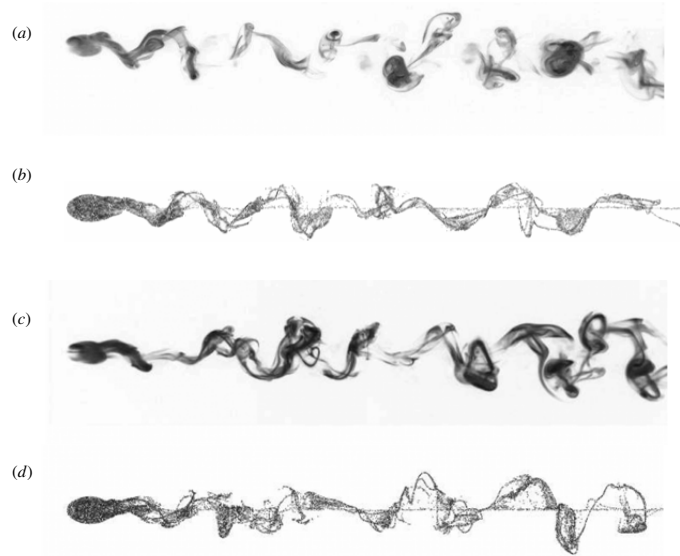


FIGURE 5. Comparison of experimental dye visualizations (*a,c*, negative image) and numerically obtained tracer particle images (*b,d*), for two higher Reynolds numbers. (*a,b*) $Re = 328$; (*c,d*) $Re = 415$.

3.4. Wake behaviour at higher Reynolds number

Experimental visualizations of the wake show irregular shedding at higher Reynolds numbers. As indicated previously, the wake structures are visualized with dye in the experiments, and for the computations, visualization is undertaken with massless tracer particles originating near the surface of the sphere. Figure 5 shows the visual comparisons in plan view at Reynolds numbers above transition. For the two cases shown, the wakes are clearly asymmetric about the wake centreline and vortex shedding is irregular. The cross-stream extent of the wake increases as the Reynolds number increases. The wake structures obtained appear similar to those in the wake of a non-rotating sphere placed in a free stream at $Re > 650$ (Mittal & Najjar 1993).

3.5. Force histories

Sample force histories of the streamwise C_x and lateral C_z components are shown in figure 6 for $Re = 200$ and 300 . The lower Reynolds number is just above transition, so the variation of the force components is close to sinusoidal. The C_x component predominantly shows the wake signal corresponding to the formation and shedding of the vortex loops. There is a small degree of modulation due to the cross-stream oscillation. This oscillation in the cross-stream component chiefly corresponds to the post-transition symmetry-breaking sinuous spanwise oscillation, but in turn it is modulated by the vortex-loop formation/shedding signal. At $Re = 200$, the Strouhal numbers of these dominant components are $St_{x,y} = 0.117$ and $St_z = 0.050$.

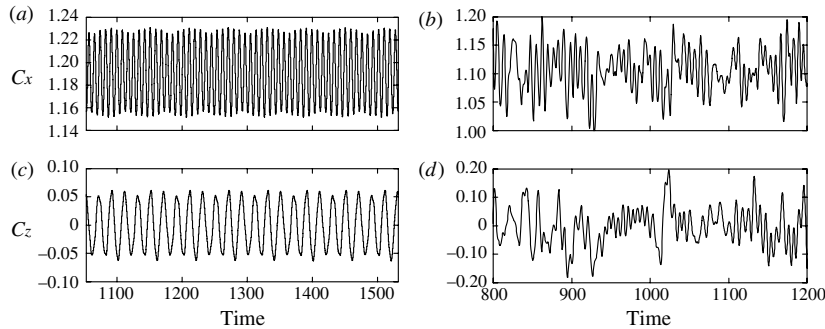


FIGURE 6. Evolution of the drag coefficient C_x (a,b), and the lateral force coefficient C_z (c,d). (a,c) $Re = 200$; (b,d) $Re = 300$.

At the higher Reynolds number of $Re = 300$, the time signals of the force coefficients are very irregular, although the underlying signal corresponding to the shedding of vortex loops is still clearly visible.

Figure 7 shows the variation of the force coefficients with Reynolds numbers. The streamwise component (C_x) decreases, as does the magnitude of the lift coefficient, noting that the force is towards the wall. The lateral component (C_z) fluctuates beyond the transition point. The force coefficients vary smoothly across the transition from the steady to unsteady state. This figure also shows the Strouhal number variation with Reynolds number (7d) corresponding to the drag and lateral force components. After the second transition, there is a sudden shift upwards in the St_x curve. Intriguingly the Strouhal number ratio, St_x/St_z , appears locked to a 7:3 resonance post-transition for $Re_{c2} \leq Re \leq 205$. This is seen clearly in figure 7(e), which shows this ratio close to the transition. A phase space plot ($C_x(t)$ against $C_y(t-1)$) is displayed in figure 8(a). (Note that the time lag is to make the trajectory more circular so that the individual orbits can be seen more easily.) The boxed region of this subfigure for $Re = 200$ is magnified in figure 8(b). This shows that the trajectory repeats after every 7 orbits for $Re = 200$. Approximately 100 orbits are plotted in this figure. To investigate the apparent resonance further, a simulation was performed at $Re = 215$ with planar symmetry enforced. This gave a Strouhal number consistent with extrapolating the sub-critical St_x curve (see figure 7d), which is quite different to the measured Strouhal number without the restriction. Thus, it does appear that the frequency of the hairpin shedding alters substantially when the lateral oscillation mode is present in order to lock onto the 7:3 resonance. If Re is increased to 220, the phase plot shows that the trajectory is no longer closed with individual orbits broadly following a mean orbit, but with a significant spread. By $Re = 250$, the orbits appear to fill a closed region of phase space, indicating the rapid progression to chaotic behaviour. The broad spectral content at higher frequencies shown in figure 4 supports this conclusion.

A variant of Poincaré surfaces of section was used to investigate this further. These maps are obtained by plotting the streamwise (or lateral) force coefficient against its value one complete lateral (or streamwise) cycle previously, as explained below.

- (a) The streamwise and lateral force coefficients were recorded for 400 time units. This corresponds to approximately 20 cycles in the lateral direction and 50 cycles in the streamwise direction.

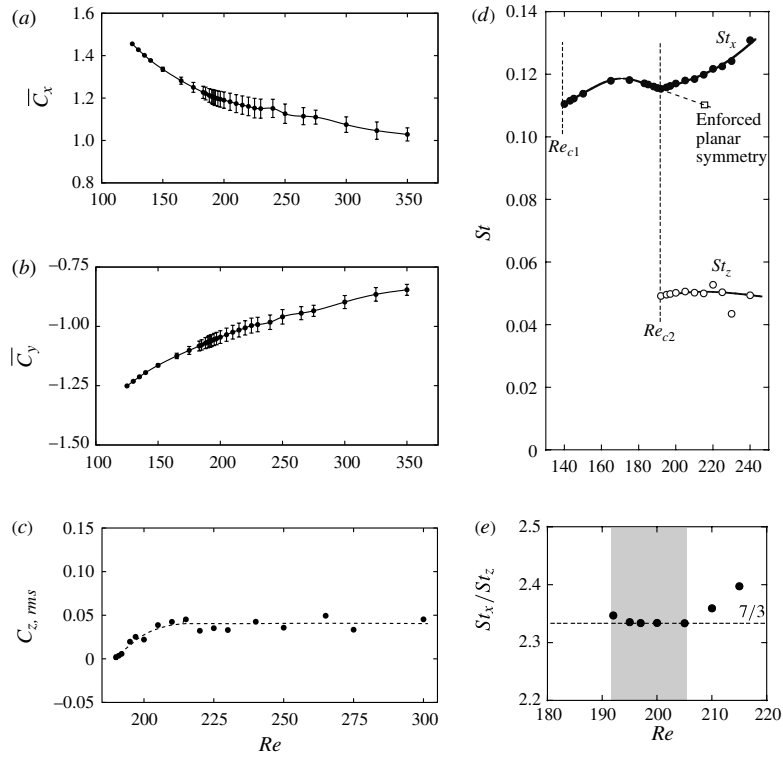


FIGURE 7. Variation of force coefficients and Strouhal numbers with Reynolds number. (a) Mean drag coefficient \overline{C}_x ; (b) mean wall-normal force coefficient \overline{C}_y ; and (c) the r.m.s. of the lateral force coefficient $C_{z,rms}$. Error bars represent one standard deviation. (d) Strouhal numbers for the drag (St_x) and lateral force (St_z) corresponding to the shedding of hairpin vortices and asymmetric wake oscillations, respectively. (e) Strouhal number ratio, St_x/St_z , against Reynolds number near the second critical Reynolds number.

- (b) The mean value of the coefficient C_x (or C_z) was subtracted from the values of each coefficient.
- (c) For every complete cycle of C_x (or C_z), the corresponding value of C_z (or C_x) was recorded.
- (d) $C_{z(n)}$ (or $C_{x(n)}$) was plotted against $C_{z(n-1)}$ (or $C_{x(n-1)}$).

These maps are shown in figure 9. The Poincaré maps are first plotted for $Re = 200$, which is slightly above the critical value of lateral symmetry-breaking transition and in the regime where the flow locks onto the 7:3 resonance. From the two Poincaré maps shown in figure 9(a,b), we observe that the points lie on a discrete set of fixed points on the surface of section for both the C_x and C_z maps, with the first showing only 3 nodes and the second showing 7 nodes, as required by the 7:3 resonance. These fixed points represent the intersection points of the limit cycle. At $Re = 210$, (figure 9c,d) the maps show some similarity to those at $Re = 200$, but with the

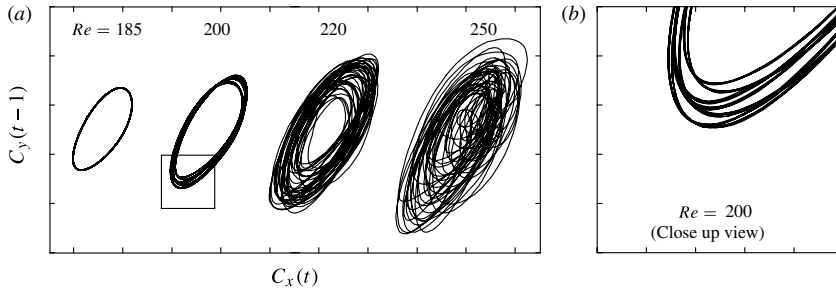


FIGURE 8. (a) Qualitative evolution of the phase trajectories of the drag and lift coefficients. Mean values are adjusted, and C_y is plotted with a lag of one time unit for better visual clarity. Tick marks are separated by 0.02 on both axes. (b) Close-up of the boxed region for $Re = 200$, showing the trajectory in C_x/C_y space.

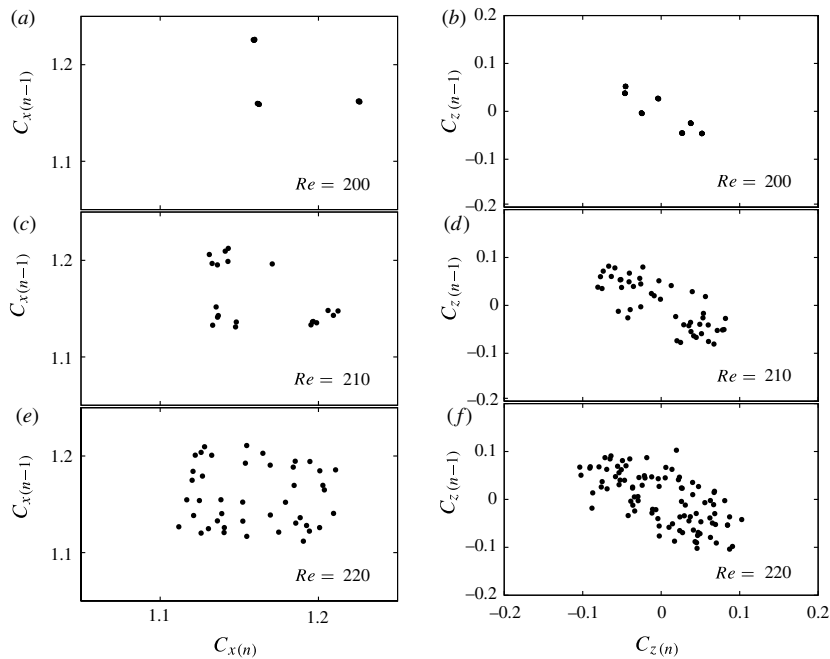


FIGURE 9. ‘Poincaré’ maps for C_x and C_z , taken for each cycle of C_z and C_x , respectively, at $Re = 200$ (a,b), 210 (c,d) and 220 (e,f).

intersection points instead now clustered around the fixed points. For the C_x map (figure 9c) it appears that the points broadly lie in three sets mostly distributed around the three fixed points. While there are insufficient data to be definitive, it appears that this clustering provides evidence of (the disruption of) KAM tori centred on the

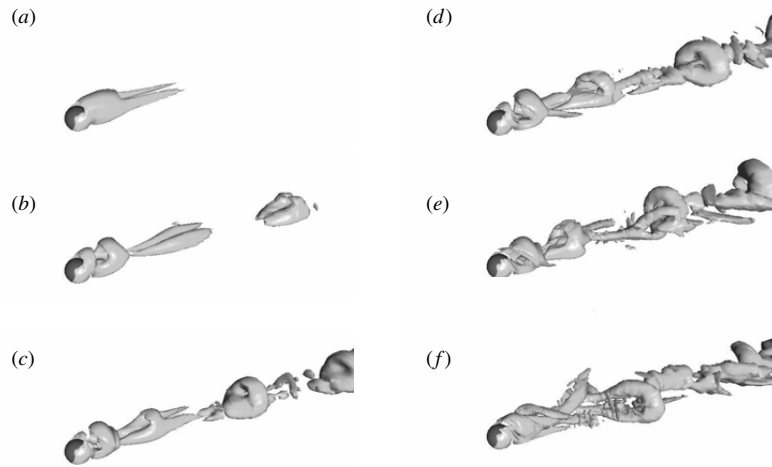


FIGURE 10. Predicted vortical structure of the rolling sphere wake, for increasing Re , visualized using the approach of Jeong & Hussain (1999). The sphere is rolling from right to left. (a) $Re = 125$, (b) $Re = 150$, (c) $Re = 175$, (d) $Re = 200$, (e) $Re = 230$, (f) $Re = 265$.

fixed points, on the route to chaos. This is less clear from the C_z map (figure 9d), although it does appear that the points are not yet space-filling at this stage. A clearer picture might be obtained from longer time series, but the simulation times required are very long. At the higher Reynolds number of $Re = 220$ (figure 9ef), the Poincaré sections show that the intersection points of the orbits are no longer restricted to lie on or near only fixed points, with the points now appearing randomly distributed over a large region. This shows that the remnants of the 7:3 resonance have disappeared and the governing periods are incommensurate. Together with phase portraits and the frequency spectra, this indicates that the system is undergoing a transition to temporal chaos.

The wake structures in the different flow regimes are summarized in figure 10 for $125 \leq Re \leq 265$. These images show (a) the double-threaded wake, (b) the initiation of unsteadiness, (c) formation of strong vortex loops, (d) breaking of planar symmetry, (e) the development of a lateral oscillation and (f) the progression towards a chaotic wake state.

4. Conclusions

The flow around a rolling sphere has been investigated in detail both numerically and experimentally, including new low background noise level experiments, and a new symmetry breaking transition has been discovered. After the first transition, from a steady to unsteady wake at $Re_{c1} \simeq 139$, the wake remains strictly periodic. Above the second transition at $Re_{c2} \simeq 192$, the two governing frequencies are approximately $St = 0.117$ (for the C_x and the C_y force components) and 0.050 (for the C_z force component). The corresponding oscillations vary in time nearly sinusoidally, each modulated by the other mode, but with these two quite different frequencies. The frequency ratio St_x/St_z appears to lock to 7:3 post-transition up to $Re = 205$, even

though the natural frequencies need to adjust considerably for this resonance to occur. By $Re = 250$, the power spectrum shows broad frequency content, and a plot of C_x versus C_y shows the trajectory starting to fill a closed region of phase space; both are consistent with the rapid progression to chaotic flow.

The wake transition sequence matches that for a non-rotating sphere in a free stream, but not a non-rotating sphere sliding along a wall. In the latter case, the first transition to the double-threaded wake is the sinusoidal cross-oscillation rather than the periodic shedding of loops. For the non-rotating sphere on the wall, fluid can flow freely over the top but not directly underneath. The addition of positive rotation presumably assists the transport of fluid around the underside of the sphere, which counteracts the blockage effect and makes the downstream flow closer to that of an isolated sphere. However, the presence of the wall does reduce the critical Reynolds numbers considerably: from $Re_{c1} = 272$ –139 for the unsteady transition, and from $Re_{c2} = 345$ –192 for breaking of mirror symmetry. Finally, it is observed that the wake structure shown in figure 10 for $Re = 265$ (and higher) resembles closely that of an isolated non-rotating sphere wake at $Re = 650$ (figure 2c of Mittal & Najjar 1993).

Acknowledgements

The authors acknowledge computing-time support from the Victorian Life Sciences Computation Initiative (VLSCI), the National Computational Infrastructure (NCI) and Monash Sungrid. A.R. also acknowledges financial support from the Australian Research Council, under grant no. DP0877328.

REFERENCES

- BOLNOT, H., PASSAGGIA, P.-Y., LEWEKE, T. & HOURIGAN, K. 2011 Wake transition of a rolling sphere. *J. Vis.* **14**, 1–2.
- CHHABRA, R. P. & FERREIRA, J. M. 1999 An analytical study of the motion of a sphere rolling down a smooth inclined plane in an incompressible Newtonian fluid. *Powder Technol.* **104** (2), 130–138.
- CHORIN, A. J. 1968 Numerical solution of the Navier–Stokes equations. *Math. Comput.* **22**, 745–762.
- DUŠEK, J., LE GAL, P. & FRAUNIE, P. 1994 A numerical and theoretical study of the first Hopf bifurcation in a cylinder wake. *J. Fluid Mech.* **264**, 59–80.
- GHIDERSA, B. & DUŠEK, J. 2000 Breaking of axisymmetry and onset of unsteadiness in the wake of a sphere. *J. Fluid Mech.* **423**, 33–69.
- JEONG, J. & HUSSAIN, F. 1999 On the identification of a vortex. *J. Fluid Mech.* **285**, 69–94.
- JOHNSON, T. A. & PATEL, V. C. 1999 Flow past a sphere up to a Reynolds number of 300. *J. Fluid Mech.* **378**, 19–70.
- KARNIADAKIS, G. E. & SHERWIN, S. J. 2005 *Spectral/hp Methods for Computational Fluid Dynamics*. Oxford University Press.
- LE GAL, P., NADIM, A. & THOMPSON, M. 2001 Hysteresis in the forced Stuart–Landau equation: application to vortex shedding from an oscillating cylinder. *J. Fluids Struct.* **15**, 445–457.
- LEONTINI, J. S., THOMPSON, M. C. & HOURIGAN, K. 2007 Three-dimensional transition in the wake of a transversely oscillating cylinder. *J. Fluid Mech.* **577**, 79–104.
- MAGARVEY, R. H. & BISHOP, R. L. 1961a Transition ranges for three-dimensional wakes. *Can. J. Phys.* **39**, 1418–1422.
- MAGARVEY, R. H. & BISHOP, R. L. 1961b Wakes in liquid-liquid systems. *Phys. Fluids* **4**, 800–805.
- MITTAL, R. 1999 Planar symmetry in the unsteady wake of a sphere. *AIAA J.* **37**, 388–390.
- MITTAL, R. & NAJJAR, F. M. 1993 Vortex dynamics in the sphere wake. *AIAA Paper* 99-3806.

- PROVANSAL, M., MATHIS, C. & BOYER, L. 1987 Bénard–von Kármán instability: transient and forced regimes. *J. Fluid Mech.* **182**, 1–22.
- RYAN, K., THOMPSON, M. C. & HOURIGAN, K. 2005 Three-dimensional transition in the wake of bluff elongated cylinders. *J. Fluid Mech.* **538**, 1–29.
- SAKAMOTO, H. & HANIU, H. 1990 A study of vortex shedding from spheres in a uniform flow. *Trans. ASME: J. Fluids Engng* **112**, 386–392.
- SCHOUVEILER, L., BRYDON, A., LEWEKE, T. & THOMPSON, M. C. 2004 Interaction of the wakes of two spheres placed side by side. *Eur. J. Mech. B* **23**, 137–145.
- SHEARD, G. J., THOMPSON, M. C. & HOURIGAN, K. 2003 From spheres to circular cylinders: the stability and flow structures of bluff ring wakes. *J. Fluid Mech.* **492**, 147–180.
- STEWART, B. E., THOMPSON, M. C., LEWEKE, T. & HOURIGAN, K. 2010a Numerical and experimental studies of the rolling sphere wake. *J. Fluid Mech.* **648**, 225–256.
- STEWART, B. E., THOMPSON, M. C., LEWEKE, T. & HOURIGAN, K. 2010b The wake behind a cylinder rolling on a wall at varying rotation rates. *J. Fluid Mech.* **643**, 137–162.
- THOMPSON, M. C., HOURIGAN, K., CHEUNG, A. & LEWEKE, T. 2006 Hydrodynamics of a particle impact on a wall. *Appl. Math. Model.* **30**, 1356–1369.
- THOMPSON, M. C. & LE GAL, P. 2004 The Stuart–Landau model applied to wake transition revisited. *Eur. J. Mech. B* **23**, 219–228.
- THOMPSON, M. C., LEWEKE, T. & HOURIGAN, K. 2007 Sphere–wall collision: vortex dynamics and stability. *J. Fluid Mech.* **575**, 121–148.
- THOMPSON, M. C., LEWEKE, T. & PROVANSAL, M. 2001a Kinematics and dynamics of a sphere wake transition. *J. Fluids Struct.* **15**, 575–585.
- THOMPSON, M. C., LEWEKE, T. & WILLIAMSON, C. H. K. 2001b The physical mechanism of transition in bluff body wakes. *J. Fluids Struct.* **15**, 607–616.
- VEREKAR, P. K. & ARAKERI, J. H. 2010 Sphere rolling down an incline submerged in a liquid. In *Proceedings of the 37th International and 4th International Conference on Fluid Mechanics and Fluid Power, 16–18 December, 2010, IIT Madras, Chennai, India*, pp. 1–9.
- ZENG, L., BALACHANDER, S. & FISHER, P. 2005 Wall-induced forces on a rigid sphere at finite Reynolds number. *J. Fluid Mech.* **536**, 1–25.
- ZENG, L., NAJJAR, F., BALACHANDAR, S. & FISCHER, P. 2009 Forces on a finite-sized particle located close to a wall in a linear shear flow. *Phys. Fluids* **21**, 033302.

Chapter 7

Conclusions

7.1 Conclusions

In this study, we have examined the flow dynamics and stability of bluff bodies in isolation and near a wall by two- and three-dimensional numerical simulations. Experimental visualisations have been used for comparative purposes. The main findings are summarised below.

The first of these studies explored the onset of three-dimensionality for a spinning cylinder in freestream for $\alpha \leq 2.5$, $Re \leq 350$, extending the findings of Akoury *et al.* (2008) who observed that the onset of the mode A instability was delayed to higher Reynolds numbers as compared to that of a non-rotating cylinder. Using linear stability analysis, the onset of the three-dimensional flow was investigated at other rotation rate. Our studies were found to be consistent with the findings of Akoury *et al.* (2008), where the onset of modes A and B showed a monotonic increase in Reynolds number for $\alpha \leq 1$. At higher rotation rates, the wake no longer retains its symmetry across the centreline, leading to the possibility of three-dimensional modes other than A and B. At $\alpha = 1.5$, mode C was the first three-dimensional mode to become unstable, while mode A occurred at higher Reynolds numbers, the mode C instability decayed. At higher rotation rates, mode C was found to persist alongside other three-dimensional modes. In the unsteady regime, two new modes were found to be unstable at rotation rates higher than $\alpha = 1.8$. A long wavelength mode, mode G first became unstable at $\alpha = 1.85$, $Re \gtrsim 280$, while mode D was observed in the high frequency shedding region of $\alpha \simeq 1.9$. At rotation rates $\alpha > 2.1$, vortex shedding was suppressed for $Re \leq 400$ in the parameter space investigated. In this steady regime, two three-dimensional modes were observed, of which one had an associated spanwise frequency, while the other was a real mode, similar to the spatio-temporal characteristics of the mode D instability.

Mode	λ/D	Nature of μ	Base flow	Symmetry
A	$\simeq 4$	Real and positive	Unsteady	$u(x, y, z, t) = u(x, y, z + n\lambda, t + T)$
B	$\simeq 0.8$	Real and positive	Unsteady	$u(x, y, z, t) = u(x, y, z + n\lambda, t + T)$
C	$\simeq 1$	Real and negative	Unsteady	$u(x, y, z, t) = u(x, y, z + n\lambda, t + 2T)$
D	$\simeq 1.9$	Real and positive	Unsteady	$u(x, y, z, t) = u(x, y, z + n\lambda, t + T)$
E	$\simeq 1.8$	Real and positive	Steady	$u(x, y, z, t) = u(x, y, z + n\lambda)$
F	$\simeq 0.4$	Complex	Steady	$u(x, y, z, t) = u(x, y, z + n\lambda, t + T_{3D})$
G	$\simeq 18$	Real and positive	Unsteady	$u(x, y, z, t) = u(x, y, z + n\lambda, t + T)$

TABLE 7.1: Summary of the modes showing the characteristic wavelength, nature of the Floquet multiplier (μ), the periodicity of the two-dimensional base flow and the spatial symmetries of these modes with respect to the streamwise velocity, u .

The spatio-temporal symmetries of these modes have been described in table 7.1.

The studies of non-rotating cylinders in freestream occurred in the unsteady regime of flow, while for bodies near a wall, the flow undergoes transition in the steady regime at Reynolds numbers lower than the predicted onset of periodic flow (Stewart *et al.* 2010b). The variation of this transition as the body was brought closer to the wall has been investigated from $G/D = \infty$ (freestream) to $G/D = 0$ (near a wall) for $Re \leq 200$. Over this parameter range, the force coefficients and shedding frequencies have been quantified. The onset of three-dimensionality has been determined by linear stability analysis. For $G/D > 0.28$, the three-dimensional transition occurred in the unsteady regime, while for $G/D < 0.28$, flow undergoes transition in the steady regime. Furthermore, the critical values at onset were obtained. Stability analysis for the circular cylinder near the wall at higher Reynolds numbers indicate multiple modes being unstable to the perturbations. Three-dimensional investigations undertaken to study the non-linear interactions of these modes indicate that the flow rapidly descends into a chaotic state.

For a circular cylinder near a wall, the influence of the rotation rate parameter on the flow characteristics was investigated for $Re \leq 750$. On increasing the rotation rate to positive values of α (forward or prograde rolling), the vortex pairs which resulted from the combination of the shear layers over the cylinder and the wall were larger and less oblate, while on decreasing the rotation rate to negative values of α (reverse or retrograde rolling), vortex shedding was delayed to higher values and suppressed for $\alpha \leq -1.5$. The critical Reynolds number for the onset of three-dimensional flow was

lowered for $\alpha > 0$, while three-dimensionality was suppressed for $\alpha = 2$. The critical spanwise wavelength at the onset was found to decrease monotonically as the rotation rate was decreased.

These studies were further extended to investigate the influence of an identical body placed in the wake of the original body. Flow stabilisation was achieved at higher Reynolds numbers, where steady flow was observed for bodies closely separated. For spacings of $S/D \leq 4$, the flow remained steady compared to the onset of unsteady flow for an isolated cylinder near a wall at $Re \simeq 160$ (Stewart *et al.* 2010b). The drag force on the downstream cylinder was much lower compared to the upstream cylinder in the steady regime, while in the unsteady regime, the drag force increased on both bodies. At small and large spacings, three-dimensional onset of flow occurred at Reynolds numbers lower than that observed at intermediate spacings. For a range of spacings ($4.5 \leq S/D \leq 6$), the two-dimensional flow became unstable to three-dimensional perturbations and then at higher Reynolds numbers, the flow returned to a two-dimensional state. At much higher Reynolds numbers, the flow returned to a three-dimensional state for the second time. Three-dimensional simulations at $Re = 200$, over a range of separation distances, showed the flow to be chaotic akin to the isolated cylinder near a wall.

The wake of a rolling sphere was investigated at higher Reynolds numbers. The experimental findings of Bolnot *et al.* (2011) showed the onset of a sinuous mode in the wake for $Re \simeq 230$ from an otherwise laterally symmetric wake which was observed at lower Reynolds numbers. Previous numerical and experimental investigations by Stewart *et al.* (2010a) showed the formation of hairpin vortices at $Re = 200$ for a forward rolling sphere. In our investigations, the rolling sphere wake is extended to $Re = 500$. The first transition to a periodic state was found to occur at $Re_{c1} \simeq 140$, followed by a second transition at $Re_{c2} \simeq 192$, where the hairpin vortices were displaced alternately across the wake centreline, thereby giving a sinuous structure. Both transitions were found to be supercritical by Landau modelling. For Reynolds numbers past the secondary transition, the wake is locked into a 7 : 3 resonance for $Re_{c2} < Re \lesssim 205$. Beyond this range, the wake is irregular and at higher values of Reynolds numbers, the flow was found to be chaotic. The transition to chaotic flow was investigated by analysing the streamwise and lateral force histories by Fourier analysis, phase plots and Poincaré maps. At the maximum tested Reynolds number of 500, the

wake was chaotic and retained its sinuous structure. Furthermore, the numerical tracer visualisations were in good agreement with the dye visualisation from the experiments.

7.2 Future directions

This thesis investigates several studies where flow control and stabilisation has been achieved in the low Reynolds number regime by varying control parameters such as α , G/D and S/D over wide ranges in the parameter space. However, there remains scope for future work within the current set of parameters and some suggestions are listed below:

- For the spinning cylinders in freestream, full three-dimensional simulations would provide a clear picture of the dominant three-dimensional structures at higher Reynolds numbers. The non-linear interactions in the wake where multiple three-dimensional modes are unstable could be investigated. Furthermore, the parameter space could be extended to higher rotation rates, where previous studies (Mittal 2004; Kumar *et al.* 2011; Meena *et al.* 2011) have identified the dominance of centrifugal instabilities along the span of the cylinder.
- Experimental investigations for a spinning cylinder in freestream have not focussed on the three-dimensional aspects at low Reynolds numbers. These investigations could be undertaken to demarcate regions of instability for each mode identified from the stability analysis.
- For bodies near a wall, three-dimensional simulations indicate the onset of chaotic flow at higher Reynolds numbers where the flow no longer retains the flow structures observed in the two-dimensional simulations. Three-dimensional simulations, albeit computationally expensive, will provide a better understanding of the transition to chaotic flow. This could also be extended to rotating cylinders and to cylinders sliding in tandem along a wall, where three-dimensionality occurs at low Reynolds numbers prior to the onset of periodic flow.
- For cylinders sliding in tandem, the studies could be extended to other rotation rates and their stability to three-dimensional perturbations could be investigated.
- For a forward rolling sphere, the onset of the symmetry breaking transition occurs at higher Reynolds numbers as the rotation rate is decreased from $\alpha = +1$ to

+0.5. This could be extended to other rotation rates. The experimental studies of Stewart *et al.* (2010a) showed undulations in the double threaded wake of a sliding sphere at $Re = 330$, while the maximum tested Reynolds number in their numerical simulations was 300, where the steady wake was observed. The parameter range could be extended to higher Reynolds number to observe this transition. For the reverse rolling sphere ($\alpha < 0$), the nature of the transitions can be investigated by performing simulations in the vicinity of the predicted values.

These studies can further be extended to investigate the flow dynamics of a freely suspended bluff body near a wall when a flow is impulsively started. The induced forces and moments would impart body rotation, and/or a possible displacement away from the wall. This continuous particle-wall interactions could be investigated over a range of Reynolds numbers using numerical solvers similar to those used here. Furthermore, the interaction between multiple particles and their associated wake dynamics would lead to fluid mixing in the vicinity of a wall, which is an important aspect of many industrial applications. While the current study investigates particle-wall interactions in various scenarios; several studies have been suggested for further exploration.

References

- AKOURY, R. E., BRAZA, M., PERRIN, R., HARRAN, G. & HOARAU, Y. 2008 The three-dimensional transition in the flow around a rotating cylinder. *Journal of Fluid Mechanics* **607**, 1–11.
- BADR, H., DENNIS, S. & YOUNG, P. 1989 Steady and unsteady flow past a rotating circular cylinder at low Reynolds numbers. *Computers and Fluids* **17** (4), 579–609.
- BADR, H. M., COUTANCEAU, M., DENNIS, S. C. R. & MENARD, C. 1990 Unsteady flow past a rotating circular cylinder at Reynolds numbers 10^3 and 10^4 . *Journal of Fluid Mechanics* **220**, 459–484.
- BARKLEY, D. & HENDERSON, R. D. 1996 Three-dimensional Floquet stability analysis of the wake of a circular cylinder. *Journal of Fluid Mechanics* **322**, 215–241.
- BAYLY, B. J. 1988 Three-dimensional centrifugal-type instabilities in inviscid two-dimensional flows. *Physics of Fluids* **31**, 56–64.
- BEARMAN, P. W. & ZDRAVKOVICH, M. M. 1978 Flow around a circular cylinder near a plane boundary. *Journal of Fluid Mechanics* **89** (01), 33–47.
- BÉNARD, H. 1908 The formation of gyration centres at the back of a moving obstacle. *Comptes Rendus Hebdomadaires des Séances de l'Académie des Sciences* **147**, 839.
- BHATTACHARYYA, S. & DHINAKARAN, S. 2008 Vortex shedding in shear flow past tandem square cylinders in the vicinity of a plane wall. *Journal of Fluids and Structures* **24**, 400–417.
- BIERMANN, D. & HERRNSTEIN, W. H. 1933 The interference between struts in various combinations. *NACA Report 468* pp. 1–12.
- BLACKBURN, H. M. & LOPEZ, J. M. 2003 On three-dimensional quasi-periodic Floquet instabilities of two-dimensional bluff body wakes. *Physics of Fluids* **15** (8), L57–L60.
- BLACKBURN, H. M., MARQUES, F. & LOPEZ, J. M. 2005 Symmetry breaking of two-dimensional time-periodic wakes. *Journal of Fluid Mechanics* **552**, 395–411.

- BOLNOT, H., PASSAGGIA, P.-Y., LEWEKE, T. & HOURIGAN, K. 2011 Wake transition of a rolling sphere. *Journal of Visualization* **14** (1), 1–2.
- CARMO, B. S., MENEGHINI, J. R. & SHERWIN, S. J. 2010 Secondary instabilities in the flow around two circular cylinders in tandem. *Journal of Fluid Mechanics* **644**, 395–431.
- CHEN, Y.-M., OU, Y.-R. & PEARLSTEIN, A. J. 1993 Development of the wake behind a circular cylinder impulsively started into rotatory and rectilinear motion. *Journal of Fluid Mechanics* **253**, 449–484.
- CHEW, Y. T., CHENG, M. & LUO, S. C. 1995 A numerical study of flow past a rotating circular cylinder using a hybrid vortex scheme. *Journal of Fluid Mechanics* **299**, 35–71.
- DENG, J., REN, A.-L., ZOU, J.-F. & SHAO, X.-M. 2006 Three-dimensional flow around two circular cylinders in tandem arrangement. *Fluid Dynamics Research*. **38**, 386–404.
- DIDIER, E. 2007 Simulation de l'écoulement autour de deux cylindres en tandem. *C. R. Mécanique* **335**.
- GHIDERSA, B. & DUŠEK, J. 2000 Breaking of axisymmetry and onset of unsteadiness in the wake of a sphere. *Journal of Fluid Mechanics* **423**, 33–69.
- HARICHANDAN, A. & ROY, A. 2012 Numerical investigation of flow past single and tandem cylindrical bodies in the vicinity of a plane wall. *Journal of Fluids and Structures* **33** (0), 19 – 43.
- HENDERSON, R. D. 1997 Non-linear dynamics and pattern formation in turbulent wake transition. *Journal of Fluid Mechanics* **352**, 65–112.
- HUANG, W.-X. & SUNG, H. J. 2007 Vortex shedding from a circular cylinder near a moving wall. *Journal of Fluids and Structures* **23** (7), 1064 – 1076.
- IGARASHI, T. 1981 Characteristics of flow around two circular cylinders arranged in tandem. *Japan Society of Mechanical Engineering* **24** (188), 323–331.
- INGHAM, D. 1983 Steady flow past a rotating cylinder. *Computers and Fluids* **11** (4), 351–366.
- JOHNSON, T. A. & PATEL, V. C. 1999 Flow past a sphere up to a Reynolds number of 300. *Journal of Fluid Mechanics* **378**, 19–70.
- KANG, S. M., CHOI, H. C. & LEE, S. 1999 Laminar flow past a rotating circular cylinder. *Physics of Fluids* **11** (11).

- VON KÁRMÁN, T. 1911 Über den Mechanismus des Widerstandes, den ein bewegter Körper in einer Flüssigkeit erfährt. *Göttinger Nachrichten Mathematisch-Physikalische Klasse* **12**, 509–517.
- KARNIADAKIS, G. E. & TRIANTAFYLLOU, G. S. 1992 Three-dimensional dynamics and transition to turbulence in the wake of bluff objects. *Journal of Fluid Mechanics* **238**, 1–30.
- KUMAR, S., CANTU, C. & GONZALEZ, B. 2011 Flow past a rotating cylinder at low and high rotation rates. *Journal of Fluids Engineering* **133** (4), 041201.
- LEI, C., CHENG, L., ARMPFIELD, S. & KAVANAGH, K. 2000 Vortex shedding suppression for flow over a circular cylinder near a plane boundary. *Ocean Engineering* **27** (10), 1109 – 1127.
- MAHIR, N. 2009 Three-dimensional flow around a square cylinder near a wall. *Ocean Engineering* **36** (5), 357 – 367.
- MEENA, J., SIDHARTH, G. S., KHAN, M. H. & MITTAL, S. 2011 Three dimensional instabilities in flow past a spinning and translating cylinder. In *IUTAM Symposium on Bluff Body Flows*.
- MENEGHINI, J. R., SALTARA, F., SIQUEIRA, C. L. R. & FERRARI, J. A. 2001 Numerical simulation of flow interference between two circular cylinders in tandem and side-by-side arrangements. *Journal of Fluids and Structures* **15** (2), 327 – 350.
- MITTAL, R. 1999 Planar symmetry in the unsteady wake of a sphere. *AIAA J.* **37** (3), 388–390.
- MITTAL, R. & NAJJAR, F. M. 1993 Vortex dynamics in the sphere wake. *AIAA* **3806**.
- MITTAL, S. 2004 Three-dimensional instabilities in flow past a rotating cylinder. *Journal of Applied Mechanics* **71** (1), 89–95.
- MITTAL, S. & KUMAR, B. 2003 Flow past a rotating cylinder. *Journal of Fluid Mechanics* **476**, 303–334.
- MIZUSHIMAA, J. & SUEHIRO, N. 2005 Instability and transition of flow past two tandem circular cylinders. *Physics of Fluids* **17**, 104107–1–104107–11.
- NORBERG, C. 2003 Fluctuating lift on a circular cylinder: review and new measurements. *Journal of Fluids and Structures* **17** (1), 57 – 96.
- PAPAIOANNOU, G. V., YUE, D. K. P., TRIANTAFYLLOU, M. S. & KARNIADAKIS, G. E. 2005 Three-dimensionality effects in flow around two tandem cylinders. *Journal of Fluid Mechanics* **558**, 387–413.

- PRALITS, J. O., BRANDT, L. & GIANNETTI, F. 2010 Instability and sensitivity of the flow around a rotating circular cylinder. *Journal of Fluid Mechanics* **650**, 513–536.
- PRANDTL, L. 1925 Application of the “Magnus effect” to the wind propulsion of ships.
- PRICE, S. J., SUMNER, D., SMITH, J. G., LEONG, K. & PAÏDOUSSIS, M. P. 2002 Flow visualization around a circular cylinder near to a plane wall. *Journal of Fluids and Structures* **16** (2), 175–191.
- ROBICHAUX, J., BALACHANDAR, S. & VANKA, S. P. 1999 Three-dimensional Floquet instability of the wake of a square cylinder. *Physics of Fluids* **11** (3), 560–578.
- SAKAMOTO, H. & HANIU, H. 1990 A study of vortex shedding from spheres in a uniform flow. *Journal of Fluids Engineering* **112**, 386 – 392.
- SHEARD, G. J. 2011 Wake stability features behind a square cylinder: Focus on small incidence angles. *Journal of Fluids and Structures* **27** (5-6), 734 – 742.
- SHEARD, G. J., FITZGERALD, M. J. & RYAN, K. 2009 Cylinders with square cross-section: wake instabilities with incidence angle variation. *Journal of Fluid Mechanics* **630**, 43–69.
- SHEARD, G. J., THOMPSON, M. C. & HOURIGAN, K. 2003 From spheres to circular cylinders: The stability and flow structures of bluff ring wakes. *Journal of Fluid Mechanics* **492**, 147–180.
- SHEARD, G. J., THOMPSON, M. C. & HOURIGAN, K. 2005a Subharmonic mechanism of the mode C instability. *Physics of Fluids* **17** (11), 1–4.
- SHEARD, G. J., THOMPSON, M. C., HOURIGAN, K. & LEWEKE, T. 2005b The evolution of a subharmonic mode in a vortex street. *Journal of Fluid Mechanics* **534**, 23–38.
- STEWART, B. E., HOURIGAN, K., THOMPSON, M. C. & LEWEKE, T. 2006 Flow dynamics and forces associated with a cylinder rolling along a wall. *Physics of Fluids* **18** (11), 111701–1–111701–4.
- STEWART, B. E., THOMPSON, M. C., LEWEKE, T. & HOURIGAN, K. 2010a Numerical and experimental studies of the rolling sphere wake. *Journal of Fluid Mechanics* **643**, 137–162.
- STEWART, B. E., THOMPSON, M. C., LEWEKE, T. & HOURIGAN, K. 2010b The wake behind a cylinder rolling on a wall at varying rotation rates. *Journal of Fluid Mechanics* **648**, 225–256.
- STOJKOVIĆ, D., BREUER, M. & DURST, F. 2002 Effect of high rotation rates on the laminar flow around a circular cylinder. *Physics of Fluids* **1** (9).

- STOJKOVIĆ, D., SCHÖN, P., BREUER, M. & DURST, F. 2003 On the new vortex shedding mode past a rotating circular cylinder. *Physics of Fluids* **15** (5), 1257–1260.
- THOMPSON, M. C., HOURIGAN, K. & SHERIDAN, J. 1996 Three-dimensional instabilities in the wake of a circular cylinder. *Experimental Thermal and Fluid Science* **12**, 190–196.
- THOMPSON, M. C., LEWEKE, T. & PROVANSAL, M. 2001 Kinematics and dynamics of sphere wake transition. *Journal of Fluids and Structures* **15**, 575–585.
- WILLIAMSON, C. H. K. 1988a Defining a universal and continuous Strouhal-Reynolds number relationship for the laminar vortex shedding of a circular cylinder. *Physics of Fluids* **31**, 2742–2744.
- WILLIAMSON, C. H. K. 1988b The existence of two stages in the transition to three-dimensionality of a cylinder wake. *Physics of Fluids* **31**, 3165–3168.
- WILLIAMSON, C. H. K. 1996a Three-dimensional wake transition. *Journal of Fluid Mechanics* **328**, 345–407.
- WILLIAMSON, C. H. K. 1996b Vortex dynamics in the cylinder wake. *Annual Review of Fluid Mechanics* **28**, 477–539.
- YOON, H., LEE, J. & CHUN, H. 2007 A numerical study on the fluid flow and heat transfer around a circular cylinder near a moving wall. *International Journal of Heat and Mass Transfer* **50** (17–18), 3507 – 3520.
- YOON, H., LEE, J., SEO, J. & PARK, H. 2010 Characteristics for flow and heat transfer around a circular cylinder near a moving wall in wide range of low Reynolds number. *International Journal of Heat and Mass Transfer* **53** (23–24), 5111 – 5120.
- ZDRAVKOVICH, M. M. 1987 The effects of interference between circular cylinders in cross flow. *Journal of Fluids and Structures* **1**, 239–261.
- ZENG, L., BALACHANDAR, S. & FISCHER, P. 2005 Wall-induced forces on a rigid sphere at finite Reynolds number. *Journal of Fluid Mechanics* **536**, 1–25.
- ZENG, L., NAJJAR, F., BALACHANDAR, S. & FISCHER, P. 2009 Forces on a finite-sized particle located close to a wall in a linear shear flow. *Physics of Fluids* **21**, 033302–1–033302–18.
- ZHANG, H.-Q., FEY, U., NOACK, B. R., KÖNIG, M. & ECKELMANN, H. 1995 On the transition of the cylinder wake. *Physics of Fluids* **7** (4), 779–793.